

A Model to Examine the Outer Blood-Retinal Barrier in Rodents

Von der Naturwissenschaftlichen Fakultät
der Gottfried Wilhelm Leibniz Universität Hannover

zur Erlangung des Grades
Doktor der Naturwissenschaften
Dr. rer. nat.

genehmigte Dissertation
von

Dipl.-Biol. Mark Ivan Melhorn
geboren am 08. Dezember 1979, in Hannover.

2012

Referent:

Professor Dr. Anaclet Ngezahayo

Institut für Biophysik

Gottfried Wilhelm Leibniz Universität Hannover

Koreferent:

Professor Dr. Ali Hafezi-Moghadam

Department of Radiology - Center for Excellence in Functional and Molecular Imaging

Brigham and Women's Hospital and Harvard Medical School

Tag der Promotion: 16. Februar 2012

Abstract

In the eye, the main contributor to the outer blood-retinal barrier (BRB) is the intact retinal pigment epithelium (RPE). A breakdown of the barrier can occur naturally, caused by advanced age due to related diseases such as age-related macular degeneration (AMD) or diabetic retinopathy (DR). Current treatment methods target disease progression using anti-angiogenic factors and steroids. Current research focuses on cell culture with the associated limitation that the RPE cells develop in the absence of their physiologic partner, the retinal photo receptors.

To gain a better understanding of the complex circumstances that lead to compromises in the outer BRB, this project established a new approach based on existing Ussing chamber systems for the use of rat tissue. The Ussing chamber examines the transepithelial electrical resistance (TEER) of the excised tissue and allows changes in the transepithelial transport to be measured. Furthermore, the Ussing chamber allows the applying and testing of diverse substances on the TEER and the resulting effect on transepithelial transport. In the adult rat, the RPE developed in its natural environment and rat eyes are large enough to harvest intact RPE tissue that allows for the mechanical removal of sclera.

The results presented in this thesis show stable TEER values with little variance when using the RPE in its complex including retina and sclera (RRS sample). The stability of RRS recommends its use for future research projects, especially when the barrier function of aged animals is studied. Its TEER was measured for a period of 100 minutes and established to be $152 \pm 12 \Omega \cdot \text{cm}^2$ (n=12) with a decrease of 11% over this time period. After the mechanical removal of sclera and retina (RPE-tissue), the TEER of RPE decreased by 25% after 80 minutes. This constellation reveals that the RPE without retina is not a suitable model for studying its physiology. TEER values of the RPE-choroid tissue were established at $133 \pm 7 \Omega \cdot \text{cm}^2$ (n=32). Significantly greater TEER values than RRS or RPE were observed for RPE including retina but devoid of sclera (RR sample; $209 \pm 13 \Omega \cdot \text{cm}^2$; n=9). TEER measurements of sclera ($7 \pm 2 \Omega \cdot \text{cm}^2$; n=9) and retina ($19 \pm 2 \Omega \cdot \text{cm}^2$; n=7) showed their contribution to the TEER of the RPE complex, while the RR measurements showed that these values are not simply additive. Sodium-fluorescein (332 Da) was added to the apical bathing solution to study the transepithelial transport of a small non-ionic compound in the tissues described. Among the RPE-bearing explants, the RR complex demonstrated the greatest amount of fluorescein transport from apical to basal.

The results indicate that this Ussing chamber assay presents a newly established method for studying the outer blood-retinal barrier. They reveal that the disruption of the RPE-retina complex by retinal removal changes the RPE's barrier function and that the presence of the RPE-retina complex may be essential for the functionality and vitality of the RPE.

Zusammenfassung

Das retinale Pigmentepithel (RPE) ist der Hauptbestandteil der äußeren Blut-Retina-Schranke (BRS). Mit zunehmendem Alter entwickeln sich häufig Augenkrankheiten wie altersbedingte Makuladegeneration (AMD) oder diabetische Retinopathie (DR), welche die BRB beeinträchtigen.

Derzeitige Therapieansätze bedienen sich antiangiogener Substanzen und Steroiden, die den Krankheitsverlauf von vielen Patienten eindämmen können.

Um die Umstände, die zu der Beeinträchtigung der äußeren BRS führen, besser untersuchen zu können, wurde in dieser Arbeit ein auf einer Ussing-Kammer basierender neuer Ansatz etabliert. Die Kammer ist darauf spezialisiert den transepithalen elektrischen Widerstand (TEER) und den transepithalen Transport von adulter Ratten-RPE zu bestimmen. Darüber hinaus erlaubt es diese Methode, die Auswirkungen verschiedener Substanzen auf die TEER und auf den transepithalen Transport zu untersuchen. Ratten bieten weiterhin die Vorteile, dass an ihnen Krankheitsmodelle etabliert sind und die Größe ihrer Augen die Entfernung der Lederhaut (Sclera) erlaubt, ohne das RPE dabei zu verletzen.

Eine konstante TEER wurde erreicht, nachdem das RPE-Gewebe in Kombination mit Sclera und Retina (RRS Gewebe) untersucht wurde. Die TEER von RRS wurde über einen Zeitraum von 100 Minuten etabliert und lag bei $152 \pm 12 \Omega \cdot \text{cm}^2$ ($n=12$). In diesem Zeitraum fiel die TEER um 11% ab. Diese Werte machen die Verwendung des RRS empfehlenswert, insbesondere wenn ältere Tiere verwendet werden, weil deren RPE einer höheren Anfälligkeit für Verletzungen ausgesetzt ist. Es zeigte sich, dass die TEER der RPE nach der Entfernung von Retina und Sclera (RPE-Gewebe) nach 80 Minuten um 25% abfiel. Daraus wurde abgeleitet, dass dieses Gewebe nicht für die Evaluierung der physiologischen RPE geeignet ist. Der TEER-Wert des RPE-Gewebes wurde mit $133 \pm 7 \Omega \cdot \text{cm}^2$ ($n=32$) gemessen. Signifikant höhere Werte als bei RPE und RRS wurden von RPE-Retina (RR) erhalten ($209 \pm 13 \Omega \cdot \text{cm}^2$; $n=9$). TEER-Messergebnisse von Sclera ($7 \pm 2 \Omega \cdot \text{cm}^2$; $n=9$) und Retina ($19 \pm 2 \Omega \cdot \text{cm}^2$; $n=7$) deuten darauf hin, dass diese Gewebe nicht nur einen rein additiven Effekt zur TEER besitzen. Der transepithale Transport von apical nach basal von kleinen nicht-ionischen Molekülen über das RPE wurde mit Hilfe von Natrium-Fluoreszein (332 Da) analysiert. Von RPE, RRS und RR zeigte der RR-Komplex die höchste basale Fluoreszeinkonzentration.

Die Ergebnisse weisen darauf hin, dass das Ussing-Kammer-System eine neu etablierte Methode zur Evaluierung der äußeren BRS in Ratten ist. Es zeigte sich, dass die Trennung der RPE von der Retina die Barrierefunktion der RPE beeinflusst, und dass der RPE-Retina-Komplex essentiell für die Funktionalität und Vitalität der RPE zu sein scheint.

Keywords: Ussing chamber, transepithelial electrical resistance (TEER), outer blood-retinal barrier

Schlagworte: Ussing-Kammer, transepithaler elektrischer Widerstand, äußere Blut-Retina-Schranke

Table of Content

1	Introduction	1
1.1	The Blood-Brain Barrier (BBB) and Other Epithelial Barrier Systems	1
1.2	Anatomy of the Eye and the Retina	2
1.2.1	The Retinal Pigment Epithelium	5
1.3	Two Retinal Diseases Involving the RPE	7
1.3.1	Age-Related Macular Degeneration (AMD)	7
1.3.2	Diabetic Macular Edema (DME)	9
1.4	Interleukin-1 β	10
1.5	Evaluating the Outer Blood-Retinal Barrier	11
1.5.1	Transepithelial Electrical Resistance (TEER) Values of RPE Cell Cultures	12
1.5.2	Transepithelial Electrical Resistance (TEER) Values of non-RPE Cell Cultures	13
1.5.3	A Short Overview of the Ussing Chamber	13
1.5.4	Experimental Conditions of RPE Explants and Their Transepithelial Electrical Resistance (TEER)	14
2	Materials and Methods	17
2.1	List of Chemicals and Salts	17
2.2	List of Equipment	17
2.3	List of Consumable	19
2.4	List of Substances Applied to the Isolated Retinal Pigment Epithelium	19
2.5	List of Specialized Computer Software	20
2.6	Buffers and Solutions	20
2.7	Gas	22
2.8	The Ussing Chamber System	23
2.9	Preparation of Electrode Tips	25
2.10	Electrode Preparation	25
2.11	Use of Electrodes	25
2.12	Pre-Experimental Preparations of the Ussing Chamber	25
2.13	Compensation of the Voltage Clamp	26
2.14	Experimental Animals	27
2.14.1	Surgery and Tissue Preparation	27
2.14.2	Mounting of the RPE Tissue	28
2.15	Occurrence and Removal of Air Bubbles	29
2.16	Electrical Recordings	29
2.17	Administration of Substances to the Apical Side of the RPE Bathing Medium	30

2.18	Permeability Measurements Using Fluorescein	31
2.19	Data Analysis	31
2.20	Criteria for TEER Data Exclusion	32
2.21	Histochemistry	32
2.21.1	Staining of the Cytoskeleton-Component Actin	32
2.21.2	Nuclear Staining Using DAPI (4',6-diamidino-2-phenylindole, dihydrochloride)	33
2.21.3	Dead Cell Analysis Using <i>SYTOX Orange</i>	33
2.22	Microscopes and Cameras	33
2.23	Statistical Significance	34
3	Results	35
3.1	Establishing of an Ussing Chamber Assay for the Reliable Measurement of Transepithelial Electrical Resistance (TEER)	35
3.1.1	Experiments Using Hanks Buffered Salt Solution (HBSS)	35
3.1.2	Experiments Using Dulbecco's Modified Eagle Medium (DMEM)	35
3.1.2.1	Experiments Using RPE Tissue Without Removing Sclera in DMEM	38
3.1.3	Histological Analysis of the RPE Sheets Using HBSS and DMEM	38
3.1.4	Modifications of Physical Parameter	39
3.1.4.1	Establishment of a Dummy Membrane	39
3.1.4.2	Controlling the Chamber Temperature	40
3.1.4.3	Monitoring the Short Circuit Current (SCC)	41
3.1.4.4	Evaluation of Small Amounts of Medium Leakage through the Half-Chambers	42
3.1.4.5	Avoiding Immediate Changes in the TEER After Apical Substance Application	42
3.1.5	Application of IL-1 β to the Apical Bathing Solution Using DMEM	43
3.1.6	Changes in Gas Delivery to the Ussing Chamber	45
3.1.7	Establishing the RPE-Ringer Solution as Medium of Choice	45
3.1.8	Summarizing the Establishing Phase of the Ussing Chamber Assay	46
3.2	Experiments Using the Established Ussing Chamber Assay	47
3.2.1	Application of Control to the Apical Bathing Solution of the RPE Explant	47
3.2.2	Application of IL-1 β (50 ng/ml) to the Apical Bathing Solution of the RPE Explant	48
3.2.3	Application of LPS (500 ng/ml) to the Apical Bathing Solution	49
3.3	Retaining the Retina and Sclera on the RPE Sheets	50
3.3.1	Measuring the TEER of the Retina/RPE/Sclera (RRS) Explant	50
3.3.2	Measuring the TEER of the Retina/RPE (RR) Explant	51
3.3.3	Individual TEER Values of Retina and Sclera	52
3.3.4	Comparing the Individual Tissues	53
3.4	Evaluation of Fluorescein Transport Across the RPE Barrier	53

4	Discussion	58
4.1	Relevant Points of Discussion on the Establishment of a Suitable Ussing Chamber Assay	58
4.1.1	Definition of a Minimum TEER Value for Intact RPE	58
4.1.2	Choice of Medium and Gas	59
4.2	Discussion of the Results After the Ussing Chamber Establishment	60
4.2.1	Application of IL-1 β to the Apical Bathing Solution (RPE-Ringer) of RPE Explants	60
4.2.2	Exposure of the RPE Membrane to LPS	60
4.2.3	Comparison of the TEER of RPE Explants to Those Including Retina and Sclera	62
4.3	Permeability Evaluation Using Sodium-Fluorescein Transport Across the RPE	62
4.3.1	Fluorescein Transport From Apical to Basal for RPE Tissues Including Retina	63
4.3.2	Fluorescein Transport Across RPE Devoid of Retina and Sclera	64
4.3.3	Increased Apical Na ⁺ Concentration by Sodium-Fluorescein Application	64
4.3.4	Summarizing the Fluorescein Transport Experiments	65
4.4	Evaluation of RPE Samples Devoid of Retina or Sclera	66
4.5	The Continuous TEER Decrease in all Systems	66
4.6	Sensitivity of the Ussing Chamber Assay as Revealed by TEER Values	66
4.7	Other Methods for Evaluating an RPE Explant Devoid of Retina	67
5	References	68
6	Appendix	81
6.1	List of Figures	81
6.2	List of Tables	83
6.3	Publications	84
6.4	Curriculum Vitae	86
6.5	Acknowledgments	88

Abbreviations

AGE	Advanced glycation endproducts
AMD	Age-related macular degeneration
ATP	Adenosine triphosphate
BBB	Blood-brain barrier
BRB	Blood-retinal barrier
BSA	Bovine serum albumin
CC	Choroicapillaris
CFH	Complement factor H
CNV	Choroidal neovascularization
DME	Diabetic macular edema
DMEM	Dubelcco's modified Eagle's medium
DPBS	Dubelcco's phosphate buffered saline
DR	Diabetic retinopathy
EDTA	Ethylene diamine tetraacetic acid
EGTA	Ethylene glycol tatraacetic acid
EIU	Endotoxin-induces uveitis
EVOM	Epithelieal volt-ohm meter
HEPES	4-(2-hydroxyethyl)-1-piperazineethanesulfonic acid
HGF	Hepatocyte growth factor
HRP	Horseradish peroxidase
HUVEC	Human umbilical vein endothelial cell
IL	Interleukine
IPM	Interphotoreceptor matrix
LPS	Lipopolysaccharide
MDCK	Madin-Darby canine kidney
PBS	Phosphate buffered saline
PDT	Photodynamic therapy
POS	Photoreceptor outer segment
RBEC	Rat brain capillary endotheliel cell
ROS	Reactive oxygen species
RPE	Retinal pigment epithelium <i>or</i> Retinal pigment epithelium / choroid tissue

RR	Retina / RPE tissue
RRS	Retina / RPE / Sclera tissue
RT	Room temperature
TEER, TER	Transepithelial electrical resistance
TJ	Tight junction
TLR	Toll-like receptor
TNF- α	Tumor necrosis factor-alpha
VEGF	Vascular endothelial growth factor
ZOT	Zonula occludens toxin

1 Introduction

The eyes of primates have evolved into one of their order's defining organs. They are capable of the amazing translation of light into nerve signals. They allow seeing and differentiation between consistent light sources and short-lived light flashes and are capable of distinguishing different wavelengths which are then translated into colors by the brain. Their location in the primate skull enables great depth perception.

When eyesight is lost or reduced, alternative forms of orientation have to be acquired. Bio-medical research has made it possible to largely eliminate or reduce those forms of blindness and vision impairments that were related to the cornea or the lens.

As a result of these advances, age-related macular degeneration (AMD) and diabetic retinopathy (DR) are today the leading causes of blindness in the commonly called "western world" (1-4) while the two most dominant physiological imbalances that lead to AMD and DR are choroidal neovascularization (CNV) and diabetic macular edema (DME). Although for both diseases a limited number of approaches can help the afflicted persons, these treatments do not target the underlying pathogenesis.

In AMD as well as in DR, among others, the retinal pigment epithelium (RPE), which is also the integral part of the outer blood retinal barrier (BRB), plays a pivotal role. To gain access to more successful treatment methods for the devastating effects of vision loss, the biology of the involved RPE needs to be evaluated in greater detail. The desire to advance the current approaches of RPE cell culture, led to the idea of creating a new model for studying the physiological RPE characteristics. This was realized by harvesting tissue from the rat eye. Evaluation of the early experiments led to improvements in the design parameters, while the latest modifications resulted in a model that is stable for a time period of two hours. This model was established for RPE explants from rats on the basis of existing Ussing chamber assays.

1.1 The Blood-Brain Barrier (BBB) and Other Epithelial Barrier Systems

In 1885 Nobel Laureate Paul Ehrlich performed the first experiments that later led to the discovery of the blood-brain-barrier (BBB). By injecting into the blood stream of animals an organic dye used for microscopic staining, he observed that all organs except the brain were stained. In 1915, his student Edwin Goldmann injected a similar stain directly into the brain, which was then stained while the rest of the body remained unchanged.

The existence of the BBB was formally demonstrated by Reese and Karnovsky in 1967 (5) when they injected horse radish peroxidase intravascularly. The subsequent electron-microscopy clearly showed tight junctions as a barrier for their enzyme.

Tight junctions and their barrier function have now been studied for over 40 years. In 1964 Sedar and Forte (6) demonstrated that the tight junctions containing gastric mucosa of *Rana pipiens* showed a greater electrical conductance when the chelating agent EDTA (4 mM) was used. This effect was based on a widening of the intercellular space in the zonula adhaerens (intermediate junctions) and a marked separation of apposed leaflets in the desmosomes (macula adhaerens). The changes in the zonula occludens (tight junctions) were not as obvious, but appeared to be expressed in an increased frequency of the openings or separations in this epithelium. The effects of EDTA were reversible, after the tissue was placed in a bathing solution containing 2 mM Ca^{2+} . 14 years later Meldolesi et al. showed that the tight junctions of the pancreatic lobules in guinea pigs were disassembled after 1-2 h of incubation with 0.5 mM ethylene glycol tetraacetic acid (EGTA) (7). This effect was successfully restored by reintroducing Ca^{2+} . The observed changes in desmosomes and in some tight junctions, were well demonstrated using the freeze-fracture technique.

Other factors that have been shown to influence tight junction integrity in a variety of tissues are pronase (8), hypertonic solutions (9, 10), the cytokines IL-13 (11), interferon- γ (12) and tumor necrosis factor- α (TNF- α) (13), Vascular endothelial growth factor (VEGF) (14), hepatocyte growth factor (HGF) (15), pitavastatin (16), ethanol and hydrogen peroxide (17), zonula occludens toxin (ZOT) and its derivative zonulin (18, 19). Also some plant cytokines were shown to cause displacement and proliferation of some junctional proteins (20) and others.

To gain a better understanding of the outer BRB, which can be understood as a specific barrier of the BBB, it is helpful to take a look at the anatomy of the eye.

1.2 Anatomy of the Eye and the Retina

The vertebrate eye is part of the brain. It was dissociated from it in early development, and yet continued to keep nerve connections to it (21). It is spherical in shape and is for its most part encapsulated by a fibrous collagen tissue called the sclera. The thickness of the sclera is dependent on the animal and on its position on the eyeball. In humans it is of considerable thickness and reaches 1 mm at its posterior pole and 0.3 mm on the site where the rectus

muscle is inserted (22). Light enters the eye through the transparent cornea and travels through the aqueous humor of the anterior chamber, followed by the lens, before it enters the vitreous. The bending of light that occurs at the air-cornea surface accounts for two-thirds of the bending necessary to focus the light on the photoreceptor cells in the back of the eye (21). The active adjustment to focusing the light happens by the lens. The amount of light that

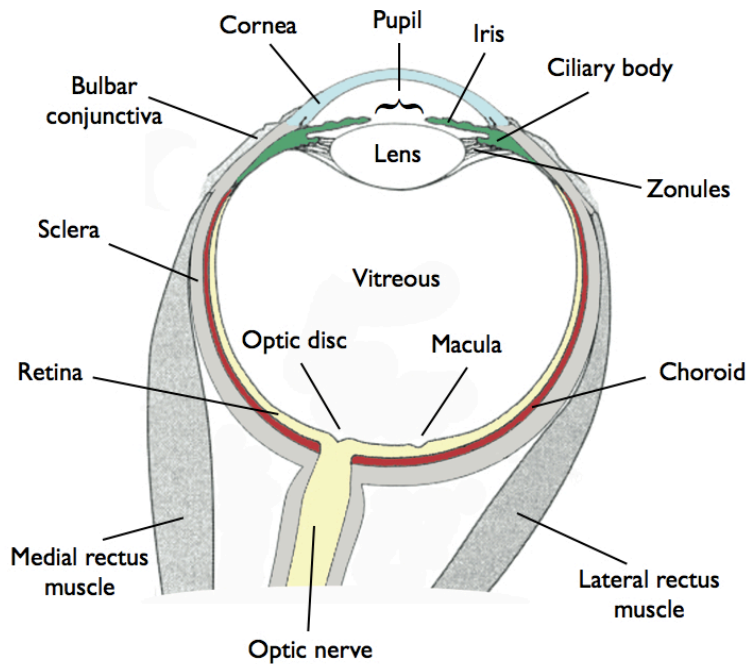


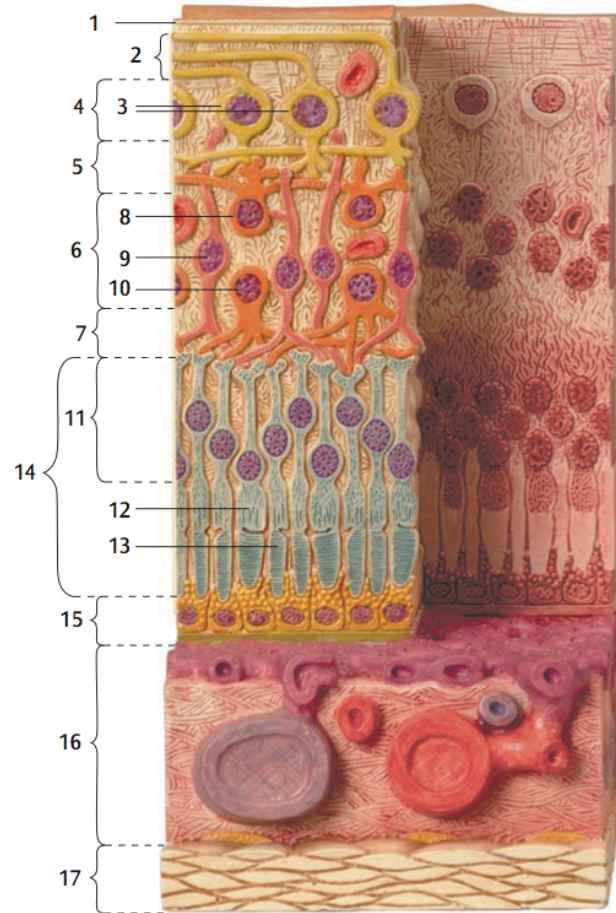
Figure 1-1: Anatomy of the eye. Top view.

enters the eye is controlled by the iris, which controls the central opening - the pupil. After the light has traveled through the transparent vitreous, it crosses the retina, which has been categorized into the following ten layers: [1] inner limiting membrane, [2] nerve fiber layer, [3] ganglion cell layer, [4] inner plexiform layer, [5] inner nuclear or bipolar layer, [6] outer plexiform layer [7] outer

nuclear layer, [8] external limiting membrane, [9] photoreceptor layer and [10] retinal pigment epithelium. Two distinct photoreceptor cell types are capable of recognizing and transmitting light signals: Rods and cones. Rods are responsible for the detailed recognition of light, while cones recognize color and are less light-sensitive. Their distribution varies greatly from species to species, with nocturnal animals having a greater amount of cones in their retina, especially in their area of central vision. Additional light energy is captured by the melanosomes of the RPE and to some extent by the melanosomes of the vascular choroid, which is not part of the retina.

The RPE is bordered by Bruch's membrane, an elastin- and collagen- rich extracellular matrix. Its inner layer is defined as the basal membrane of the RPE, followed by two collagenous zones separated by an elastic layer and concludes with the innermost layer of

Figure 1-2: Model of the retina and underlying tissue. 1 Inner glial limiting membrane, 2 Layer of nerve fibers, 3 Ganglion cell, 4 Ganglionic cell layer, 5 Inner plexiform layer, 6 Inner nuclear layer, 7 Outer plexiform layer, 8 Amacrine cell, 9 Bipolar cell, 10 Horizontal cell, 11 Outer nuclear layer, 12 Cone cell, 13 Rod cell, 14 Layer of rods and cones, 15 Retinal Pigment Epithelium (RPE), 16 Bruch's membrane, 17 Choriocapillaris, 18 Choroid, 19 Sclera. Image modified from Microanatomy eye model, Item F16, 3B Scientific GmbH, Hamburg, Germany



the choroid: the basement membrane of the choriocapillaris. The choroid and especially the choriocapillaris (CC) is a meshwork of fenestrated vessels, with a very high blood flow: The CC accounts for 70% of the total blood flow in the eye (23, 24).

The blood flow to the retina is ensured by two circulatory systems: the retinal arteries and the choroidal vessels. The retinal vessels originate from the central ophthalmic artery and branch out into the nerve fiber layer and the

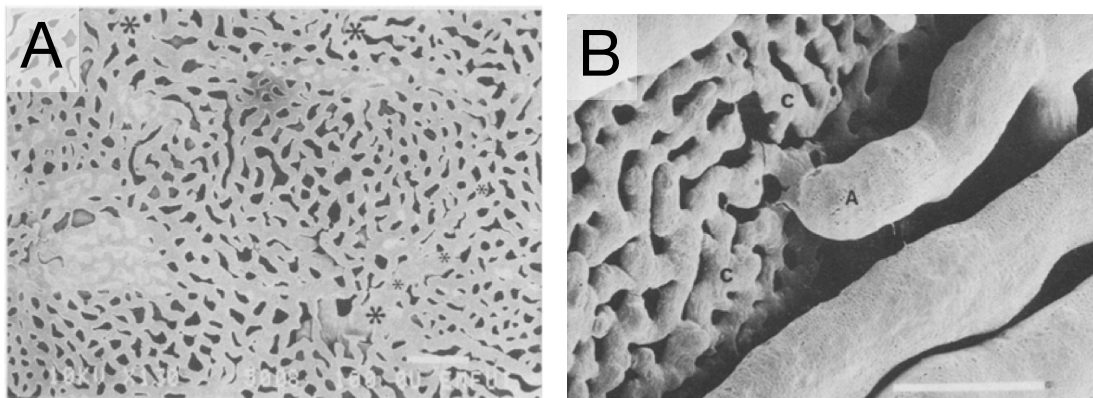


Figure 1-3: Macro-anatomy of the choriocapillaris. The images show the great density of vessels. **A.** Anterior (retinal) view of a choroidal cast in the posterior pole of a human eye (x130) **B.** Scleral view of a choroidal cast in the posterior fundus. An arteriole (A) joins the choriocapillaris (C) at a right angle (x300). Images taken from Yonega *et al.* 1983 (194).

ganglion layer. In the human eye the point of central vision, the fovea, is avascular and about 0.5 mm in diameter (25, 26). It is in the center of the macula, a region of about 5 mm diameter. This region is exclusively supplied with oxygen by the choroidal blood flow.

The photoreceptors comprise an “inner” and “outer” segment. The inner segment contains the nucleus and the majority of the cell body, while the outer segment is packed with about 1000 disks containing the visual pigment rhodopsin. Upon absorption of a sufficient amount of photons, the light signal is translated into an electric signal that gets carried to the brain via the neurons. The reconfiguration of the rhodopsin takes place in the RPE cells. The isomerization process from all-trans retinal to 11-cis retinal is separate from the process in which older optic discs are shed by the rods or cones and phagocytosed by the RPE. A large degree of the phagocytosed material also gets recycled and transferred back to the photoreceptors (27, 28).

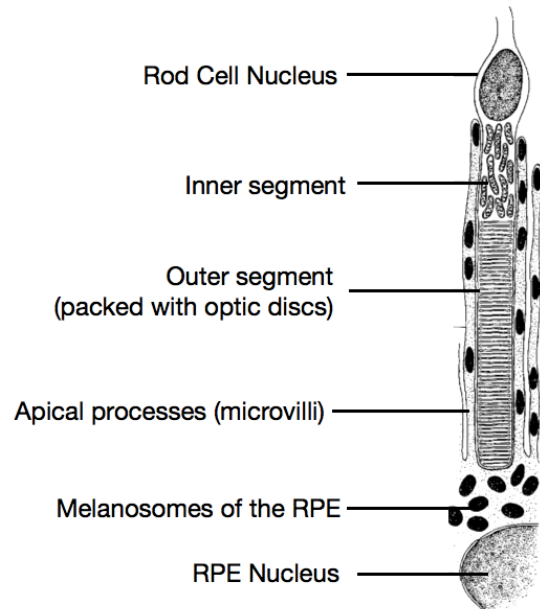


Figure 1-4: Association between RPE microvilli and rod cells. After Miller and Steinberg 1977 (150).

1.2.1 The Retinal Pigment Epithelium (RPE)

The RPE is the outermost layer of the retina and the essential component of the outer blood-retinal barrier (BRB).

It is a highly polarized epithelium consisting of a monolayer of cells that have a predominantly hexagonal shape, while the individual cells secure the barrier with their junctional complex consisting of tight junctions and adherens junctions. In most tissues, desmosomes are part of the junctional complex, however they are absent in avian, rat, mouse and human RPE (29).

Tight junctions are primarily comprise occludin and a group of tetraspan transmembrane proteins with 24 family members: the claudins (30, 31) of which nine have been identified in RPE (32). Claudins form either homo or hetero oligomers which determine the size and ion selectivity of the pore they form (33, 34). The regulatory process of this pathway is regulated

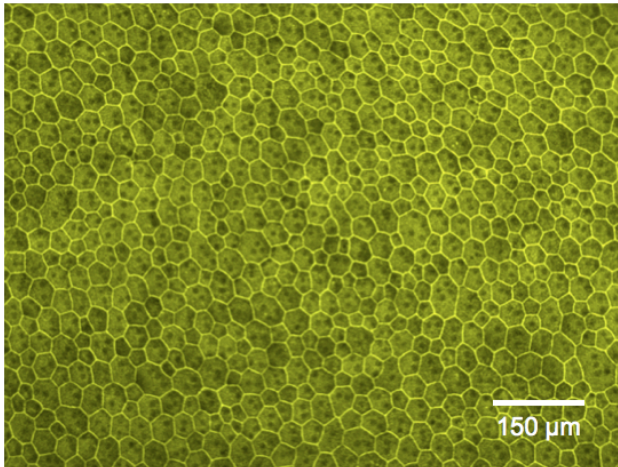


Figure 1-5: RPE cell layer from rat. Actin staining with rhodamine-phalloidine. Pseudo color.

One RPE cell is associated with 15 - 40 photoreceptors of differing rod/cone distribution, depending on the location in the eye (37, 38). On the basolateral side the RPE cells are in proximity to the fenestrated choriocapillaris, only separated by Bruch's membrane. The RPE is involved in a multitude of necessary processes assuring uninterrupted vision. It is responsible for delivering nutrients and oxygen to the photoreceptor outer layer, as well as removing their metabolites and plays a pivotal role in the visual cycle by restoring the visual chromophore 11-cis-retinal from the all-trans-retinal, which was generated after the absorption of a photon changed its conformation (39, 40). However the RPE is not the exclusive location of the isomerization from all-trans retinol to 11-cis retinal: another known process takes place in the Müller cells of the retina (41, 42). The pigments of the RPE absorb light energy that is not necessary for vision. With the capture of this excess light the RPE protects the photoreceptors from photo-oxidation damage (43). The need for a protection is apparent when the

by RhoA signaling and has been shown to involve actinomyosin driven processes (35, 36). In the process of opening and closing, the aqueous channels allow other substances to pass passively. In the RPE cells nine claudins have been identified to date: Claudin-1, -2, -3, -10, -12, -15, -16, -19 and -20 (32).

The apical side of the RPE faces the lumen of the eye. On this side the RPE is equipped with microvilli that engulf the cones and rods from the photoreceptors.

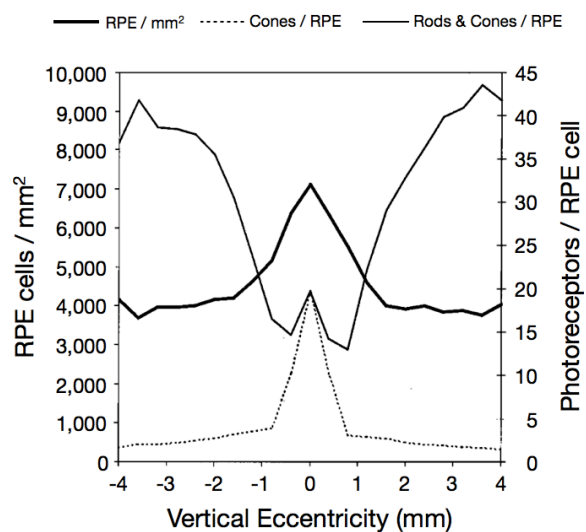


Figure 1-6: Association of photoreceptor cells and RPE cells according to their location in the eye. Graph was developed from examining rhesus monkey **Thick solid line:** mean RPE density. **Dashed line:** Mean cone number per RPE cell. **Thin solid line:** Mean number of rods and cones combined per RPE cell. Image taken from Snodderly et al. 2002 (37).

perfusion rate and the oxygen saturation of the blood of the choriocapillaris, are considered. 1.4 L of blood per minute per 100 g tissue circulate through this tissue with a venous (!) O₂ concentration of 90%, while blood from retinal veins show an O₂ concentration of 45% (44-46).

During the development of the eye, the RPE produces and secretes growth factors (e.g. vascular endothelial growth factor [VEGF]), angiogenic (e.g. interleukine (IL)-8, monocyte chemotactic protein [MCP]-1, IL-6) and angiostatic (e.g. MCP-3, interferon gamma-induced protein [IP]-10) cytokines and chemokines that are essential for the development of the choriocapillaris and the retina (46-48). It has been shown that the RPE produce immune-proteins such as complement factor H (CFH) and possess immune-receptors (48-50).

Another essential function of the intact RPE is the removal of water from the retina. The source of this retinal water is the high metabolic rate of the retinal cells, as well as the water contained in the vitreous (51, 52).

In their natural environment, the photoreceptor outer segments (POS) are exposed to high amounts of light and oxygen, which leads to the accumulation of radical oxygen species (ROS) (53). To maintain healthy and functioning POS, this waste material is shed and replaced by new material generated by the photoreceptors, while the shed POS are phagocytosed and broken down by the RPE.

1.3 Two Retinal Diseases Involving the RPE

A number of retinal diseases exist of which only a few are associated with the RPE. The dysfunctional RPE may only be the result of prolonged hyperactivity based on the problems originating, for example in the vasculature, however its eventual breakdown leads to the more severe complications in disease progress. Here only two diseases will be introduced in which the RPE does play an intrinsic role.

1.3.1 Age-Related Macular Degeneration (AMD)

AMD is the leading cause of blindness in the developed world and a complex disease in which genetics, environmental and demographic risk factors are involved (54-56). In the United States AMD affects 6.4% of the population aged 40 years and above or 13.3% of those aged 60 and above (57).

AMD's complexity has not yet allowed it to be understood entirely but more and more pieces that form the mosaic of AMD have been revealed.

The pathology of AMD starts to become evident with the definition of its two types: The dry and the wet form. Wet AMD is defined by the formation of new blood vessels derived from the choroid (choroidal neovascularization or CNV) that breach Bruch's membrane. In a first step fluid accumulates below the RPE, impairing vision by lifting the retina from its surface. As a result, affected individuals start seeing straight lines to be crooked. The new vessels can eventually grow through the RPE layer. In these more aggressive stages, the breach of the outer BRB leads to photoreceptor decay and eventually blind spots in the central vision (58, 59).

The formation of CNV is oftentimes explained by the lack of sufficient oxygen supply to the photoreceptors (60-63). The primary driving force of angiogenesis is VEGF (64-66), which is first targeted when treating the disease (67). It is essential to stop angiogenesis, because the new blood vessels are leaky.

Only 15% of all AMD cases are associated with the wet form, the majority of cases are classified as dry AMD (2). In dry AMD, the retina deteriorates in regions with dysfunctional RPE based on the separation of RPE and photoreceptors. This is commonly believed to be caused by basal deposits of lipids and cellular material that develop into drusen. The components of large drusen include apolipoprotein E, β -amyloid, vitronectin, immunoglobulins, activated complement components including C5b-9 and complement factor H as well as MHC-II antigens. All of these factors were synthesized locally by the retina, RPE, or the choroidal cells and improperly digested by the RPE (3, 68-71).

The formation of drusen is central in AMD pathogenesis because it has been associated with the thinning of the retina, destruction of the RPE and subsequently the loss of photoreceptors. Dry AMD can progress into wet AMD, but this is not a certain path. Currently no treatment for dry AMD exists while clinical studies are under way (72, 73).

Commonly found components in the cytoplasm of aged RPE that are associated with drusen are lipofuscin granules - autofluorescent material that accumulates over the lifetime of the largely non-mitotic RPE (74-76). Lipofuscin is generated in an environment that is high in oxygen and exposed to visible light, which contributes to the formation of reactive oxygen species (ROS). Eventually these granules can take up a substantial amount of the cells' cytoplasm (77). Some of the granules' components are photosensitive and are formed as a by-product of the vitamin A cycle. The best-characterized photodegradable component is N-

retinylidene-N-retinyl-ethanolamine (A2E). It has been shown that the photodegradation of A2E releases a product that has the ability to form advanced glycation endproducts (AGE), which are also commonly detected in drusen (78) hence it is suggested that drusen play a pivotal role in the early onset of AMD. Thus the early stages of pathogenesis that lead to RPE dysfunction have been attributed to aging (68, 69).

Some groups have suggested that the limited mitotic activity of the aged RPE cells leads to senescence and hence to a reduction in their metabolic capabilities and the accumulation of improperly digested waste products. Partial success to restore their function was shown when RPE cells were targeted and destroyed by laser pulses taking advantage of their self-renewal potential as a possible treatment plan (79, 80). Other groups have focused on the involvement of immunological factors, especially those deriving from the complement system (49, 81).

After AMD is diagnosed, it is treated by a combination of intravitreal anti-VEGF and/or steroid injections and verteporfin photodynamic therapy (PDT) (82). However, this approach is only successful in a limited portion of the patient population. Repeated intraocular injections of VEGF antagonists are dreaded by the patients and are not free of risks, as VEGF fulfills important physiological functions in the retina and choroidal microvasculature (47, 83).

The risk of AMD has been shown to be reduced when smoking is reduced or avoided, physical activity is increased and a diet of less fatty ingredients is chosen, while ingestion of vitamins and mineral supplements has also proven to be beneficial in certain patients (84-87).

1.3.2 Diabetic Macular Edema (DME)

Diabetic macular edema (DME) is one complication of patients with diabetic retinopathy (DR). The amount of people affected by DR or DME varies within the reports, but lies between 10% and 20% of diabetic patients (4, 88-91), with 10% to 16% of the US population being affected by diabetes (92, 93).

In DME, extracellular fluid leaks through the dysfunctional inner blood-retinal barrier, which is made up of the endothelial cells lining the retinal blood vessels, leading to its accumulation in the subretinal space and eventually retinal swelling (4, 88, 94-97). The excess fluid that the RPE fails to remove contributes to the severity of the edema (96). In most cases the accumulation of fluid leads to the disruption of the outer BRB. The changes in the hydrostatic conditions in the eye can furthermore lead to an influx of fluid to the retina.

Hyperglycemia is described to be the key factor that leads to DME. As diabetes is starting to be accepted as an inflammatory disease, it is not surprising that leukocytes have been involved in the process of vessel damage (95, 98, 99), where rolling leukocytes generate proteolytic enzymes that damage the endothelium and lead to the recruitment of more leukocytes. As this has become more clear, anti-inflammatory treatments have been used to positively affect DR in animal models (100).

1.4 Interleukin-1 β

The multipotent cytokine Interleukin (IL)-1 affects many processes in the inflammatory response including activation of antigen presenting cells, chemotaxis and angiogenesis (101). IL-1 exists as two agonistic proteins: IL-1 α and IL-1 β . Both forms bind to the same receptor and the differences between the responses they trigger are negligible, however one great difference exists in their location. The former is present primarily in the cytosol and active as a precursor or an associated molecule, while IL-1 β is largely secreted by inflammatory cells and present in the circulation or in local tissues (101). The characterized IL-1 receptor antagonist (IL-1 Ra) functions by actively blocking the IL-1 receptor site and is hence a physiological inhibitor (102). Involvement of IL-1 β in eye-related diseases such as in retinopathy (103-105) and age related degeneration (106, 107) has been reported. Abe *et al.* showed that the application of IL-1 β to RPE cultures leads to a reduction in the tight junctional protein occludin and hence a reduction in TEER over a period of several days (108). The angiogenic aspects of IL-1 β are based on its induction of VEGF-A, COX-2/prostanoids and CXC chemokines (109, 110) via the NF- κ B pathway (111).

On RPE cells the IL-1 β receptor has been shown to be predominantly expressed on the apical side (48), while a decrease in TEER after the application of an inflammatory cytokine mixture consisting of TNF- α , IL-1 β and interferon- γ (IFN- γ) was reported for cultured RPE cells. However no reports exist that evaluated the effect of IL-1 β on the barrier on its own.

1.5 Evaluating the Outer Blood-Retinal Barrier

The outer blood retinal barrier (BRB) can be understood as a specific barrier of the BBB because the vertebrate eye is part of the brain (21). The biology of this barrier has been

studied by evaluation of the transepithelial electrical resistance (TEER, also TER or R_t) and the transepithelial transport and the transepithelial potential (TEP), which are dependent upon the intactness of the tissue as well as the proper development and physiological function of the tight junctions in the RPE.

The TEER is a measure of the amount of ions crossing the epithelium and is composed of the trans- and paracellular resistances. In epithelia with relatively low resistances (below $400 \Omega \cdot \text{cm}^2$), the transcellular resistance is much greater than the paracellular one, hence the TEER reflects the paracellular resistance, to which the tight junctions (TJs) are the main contributors (112).

To obtain the TEER, a voltage pulse is placed over the epithelium, and the corresponding electric current is read. The resistance is calculated according to Ohm's law ($R=V/I$), while further multiplication with the exposed endothelial surface area results in the TEER. This multiplication is necessary to normalize the values because the resistance is inversely proportional to its area: When the voltage is kept constant, the corresponding current is lower in a tissue with smaller surface area, resulting in greater resistance.

Researchers understand the TEER as a measure for the amount of closed TJs at a given time-point, while the paracellular flux is an indicator for the epithelial permeability over a period of time. The switch between open and closed is attributed to aqueous channels in each diffusion barrier (113, 114). No other model has been proposed thus far.

The TEER is also used to determine confluence of cell cultures. While the TEER value is a measure for the intactness of the RPE sheet, a greater TEER value does not necessarily mean a more physiological RPE.

The transepithelial potential (TEP) is defined as the difference between the apical (V_a) and baso-lateral membrane potential (V_b) ($\text{TEP} = V_b - V_a$). To obtain these values a microelectrode is inserted into the cell and referenced to the apical or basal solution respectively (115).

In RPE research the continuing challenge is the creation of an appropriate cell culture that mimics the physiological interactions of the RPE in vivo, while the great heterogeneity of the RPE cells (116) has hampered the establishment of such a culture. The National Institute of Health (NIH) has set a goal to create and distribute a human based RPE culture to give the field a common reliable and well established cell line with a standardized protocol to increase the quality of the available cell cultures (117).

1.5.1 Transepithelial Electrical Resistance (TEER) Values of RPE Cell Cultures

The TEER in cell culture is measured with epithelial volt-ohm meter (EVOM) devices, which are ideally used on cells that have been grown on permanent transwell filter systems to minimize measuring errors.

The widely used **human** RPE cell line ARPE-19 arose spontaneously from a primary cell culture under laboratory conditions. It was reported to achieve mortality and senescence while its TEER was first described to be between 50 and 100 $\Omega\cdot\text{cm}^2$ (118). Another group reported the values of ARPE-19 cells to be as low as 40 $\Omega\cdot\text{cm}^2$ (119), and state that similar values were reached in the work of the original ARPE-19 publication (118).

Primary porcine RPE cell cultures have been reported to have a TEER of 80 $\Omega\cdot\text{cm}^2$ (120). Primary **rat** RPE cell cultures measured a TEER between 100 and 300 $\Omega\cdot\text{cm}^2$ (121). Another frequently used cell line is derived from **rat**: the RPE-J cell line was produced by transfection of the primary cells culture with a heat sensitive SV40 virus (122) and shows TEER values of 350 $\Omega\cdot\text{cm}^2$, while the Na/K ATPase and N-CAM were not located at their physiological position - in RPE, unlike almost all other epithelia with the exception of the choroid plexus, the Na/K pumps are located on the apical membrane (123-126).

The immortal **human** D407 RPE cell line fails to express pigments but retains differentiation at high passage numbers (127). While the original group did not report TEER, others described it to be less than 85 $\Omega\cdot\text{cm}^2$ (128), and one group reported a baseline as low as 25 $\Omega\cdot\text{cm}^2$ for their experiments (129).

In 2006 the above mentioned **human fetal** RPE cell line was described to resemble the physiology and morphology of native RPE, while expressing large numbers of RPE-specific markers that are found on native RPE cells (117, 130). Its original TEER values were measured at $501 \pm 138 \Omega\cdot\text{cm}^2$, while another group reported values between 800 - 1,200 $\Omega\cdot\text{cm}^2$ (131). A possible explanation for the variation in TEER values may be found in unintentional cloning effects, which occur when not all cells of the culture dish are scraped and transferred and reseeded to start a new culture, leading to a selection of certain subtypes.

1.5.2 Transepithelial Electrical Resistance (TEER) Values of Non-RPE Cell Cultures

TEER values of other cell-type cultures are frequently compared for their respective research. They include MDCK I (Madin-Darby canine kidney, strain I) cells, MDCK II (strain II) cells and

T84 (human colon adenocarcinoma) cells. MDCK I show morphological and biochemical characteristics of renal collecting duct epithelia, with high TEER values of 2,000 - 9,000 $\Omega\cdot\text{cm}^2$ (132-134). MDCK II show morphological and biochemical characteristics of renal proximal tubule epithelia with low TEER of 70-180 $\Omega\cdot\text{cm}^2$ (132-134), while T84 cells have characteristics of intestinal epithelia with moderately high TEER 900-1500 $\Omega\cdot\text{cm}^2$ (134, 135). The human intestinal cell line HT-29/B6 shows TEER values of 390 $\Omega\cdot\text{cm}^2$ (136) and the human umbilical vein endothelial (HUVEC) cells have reported TEER values between 25 $\Omega\cdot\text{cm}^2$ (137) and 74 $\Omega\cdot\text{cm}^2$ (138). In a model of rat brain capillary endothelial cells (RBEC) the TEER value was 114 $\Omega\cdot\text{cm}^2$ and increased to 130 $\Omega\cdot\text{cm}^2$ after statin treatment (16). Unfortunately it is also not uncommon for groups to report only relative changes in TEER values (139-145), which makes it very difficult to reproduce the data.

1.5.3 A Short Overview of the Ussing Chamber

When the TEER of an *ex-vivo* tissue is examined, the EVOM device cannot be used. A different type of device is used for its evaluation: Diffusion chambers, commonly called Ussing chambers to honor their inventor, Danish physiologist Hans Ussing (1911-2000), are defined by two half chambers filled with Ringer's solution (Ringer) that are separated by an epithelium. The medium in the half chambers is usually pH controlled via gassing. Ideally an

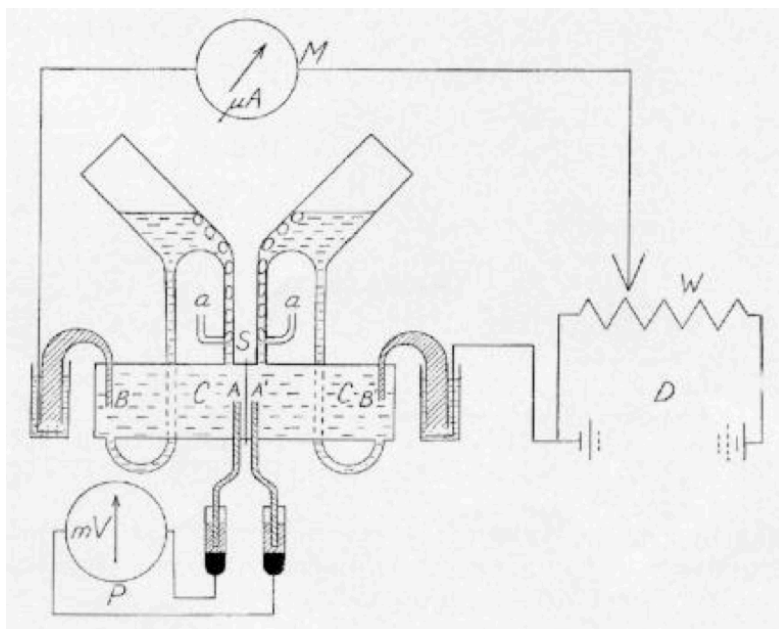


Figure 1-7: Diagram of the original Ussing chamber apparatus.

Abbreviations: **A** and **A'**: voltage-sensing electrodes; **a**: the air lines to aerate the frog skin; **B** and **B'**: current-passing electrodes; **C**: Ussing half-chambers; **S**: location where skin is inserted between the half-chambers; **D**: battery; **W**: potential divider used to adjust (by using current) the voltage across the skin to equal zero (i.e., short-circuited) as measured by **P**: potentiometer (voltmeter); **M**: the microammeter measures current passing the skin. Any recorded current while the chamber is short circuited is the short-circuited current (μA). Figure is taken from Ussing and Zerhahn (146).

Ussing chamber has an option that allows the slow exchange of medium to alter experimental conditions.

What led to the invention of the chamber was Ussing's desire in the 1950's to study the active ion transport across an epithelium. It was based on the need to eliminate any passive driving force responsible for transepithelial sodium transport: The electrochemical potential difference. In other words Ussing was interested in short-circuiting his epithelium of choice, the frog skin. Any measured current under these conditions (short-circuit current) would then essentially be determined by active transport. This led to the understanding that the short circuit current across the frog skin was essentially derived from active Na^+ transport. (146-148). With their work Ussing and Zerhahn laid the groundwork that led to the understanding of polarized cells.

Today Ussing chambers are still used for the same purposes, while the measurement of the TEER, the transepithelial potential and the movement of fluid are additional aspects being studied. The design, application and components vary by manufacturer.

1.5.4 Experimental Conditions of RPE Explants and Their TEER

Excised RPE explants have been used by a number of groups in the past and are still used at present. The animal RPE is usually derived from frog, chicken, rabbit and bovine. Below the experimental conditions as well as their TEER values are summarized:

From the family of Bufonidae (true toads), ***Bufo arenarum*** ($450 \Omega \cdot \text{cm}^2$) and in ***Bufo marinus*** ($600 \Omega \cdot \text{cm}^2$) tissues have been used with an area of 10 mm^2 being exposed to the bathing solution at pH 7.9 and room temperature (RT). Tissue was gassed with air. The medium was composed as follows (all in mM): 115.5 NaCl, 2.0 KCl, 1.0 CaCl, 2.4 NaHCO_3 , (149).

Miller and Steinberg used ***Rana catesbeiana***, the large bullfrog from the family of Ranidae (true frogs) from which they isolated 0.07 cm^2 RPE/choroid explants with $2800\text{-}5500 \Omega$ ($196\text{-}350 \Omega \cdot \text{cm}^2$) with a pH 7.4 using 95% O_2 and 5% CO_2 and the following medium: 82.5 NaCl, 2 KCl, 1.8 CaCl_2 , 1 MgCl_2 , 27.5 NaHCO_3 , 10 glucose, (all in mM); 227 mOsm (150).

Similar TEER values ($212 \Omega \cdot \text{cm}^2$) were reached by another group of the same species with 7 mm^2 , pH 7.4 at RT using 95% O_2 and 5% CO_2 with the following medium: 110 Na^+ , 2 K^+ , 1.8 Ca^{2+} , 1 Mg^{2+} , 90.1 Cl^- , 27.5 HCO_3^- , 10 glucose (all in mM) (151).

RPE of **embryonic chicken** (day 13-19), incubated at 37 °C showed a TEER of $144 \pm 22 \Omega \cdot \text{cm}^2$, while the size was 6.2 mm^2 . pH 7.4 using 95% O₂ and 5% CO₂, CO₂ tension 40 mmHg; O₂ tension 500 mmHg, the medium contained 143 Na⁺, 3.6 K⁺, 1.2 Ca²⁺, 2.5 Mg²⁺, 125 Cl⁻, 2.5 SO₄²⁻, 0.5 PO₄³⁻, 23 HCO₃⁻, 10 glucose (all in mM) (152).

TEER of RPE of **rabbit** (black dutch-belted, male and female 1.2-1.8 kg) has been reported at $350 \Omega \cdot \text{cm}^2$. The aperture had an area of 7 mm^2 and was measured at 37 - 39 °C, pH 7.4 using 95% O₂ and 5% CO₂ gas mixture with the medium containing 143 Na⁺, 3.6 K⁺, 1.2 Ca²⁺, 2.5 Mg²⁺, 125 Cl⁻, 2.5 SO₄²⁻, 0.5 PO₄³⁻, 23 HCO₃⁻, 10 glucose (all in mM) (153). The **rabbit** RPE (black dutch-belted, male and female 2-2.5 kg) TEER from another group was reported to be $90 \Omega \cdot \text{cm}^2$ using an area of 12 mm^2 and was measured at 37 °C, pH 7.4 using Dulbecco's phosphate buffered saline (DPBS) (154).

In **bovine** RPE explants (three to four hours post harvest) Zhang et al. reported TEER of $234 \pm 34 \Omega \cdot \text{cm}^2$ with an exposed tissue area of 1 cm^2 at 37 °C, pH 7.4 using 95% O₂ and 5% CO₂ gas and medium containing 119 NaCl, 3.6 KCl, 1.2 CaCl₂, 2.5 MgSO₄, 0.5 Na₂HPO₄, 23 NaHCO₃, 10 glucose (all in mM) (155). Their publication states that their TEER values were comparable to Joseph and Miller's results from **bovine** who described a mean TEER of $138 \pm 7 \Omega \cdot \text{cm}^2$ at 37 °C with a tissue size of 0.07 cm^2 , pH 7.4 using a gas containing 10% O₂, 5% CO₂, 85% N₂ and medium containing (all in mM): 120 NaCl, 5 KCl, 1.8 CaCl₂, 1 MgCl₂, 23 NaHCO₃, 10 glucose (115). In this report Joseph and Miller reported that the bovine RPE remained stable for 20-30 min, then decreasing with a rate of 30% per hour, which left a tissue with an initial TEER of $150 \Omega \cdot \text{cm}^2$ at $75 \Omega \cdot \text{cm}^2$. They reported having achieved a significant improvement in the longevity of the tissue, when 1 mM glutathione was added to the medium and they used a lower partial oxygen pressure of 10%. An O₂ tension of 80-100 mm Hg (10-13% P_{O2}), had been shown at the RPE of an intact cat eye (156), while glutathione is intrinsic to the bovine and rat retina and had been shown to have beneficial effects (157, 158). These changes led to a stable TEER for 4 - 5 hours and the TEER even increased by as much as $50 \Omega \cdot \text{cm}^2$. They also reported that the TEER decreased from 270 to $190 \Omega \cdot \text{cm}^2$ when the temperature was increased from 30 to 37 °C. They also reported having used only tissues with a TEER > $90 \Omega \cdot \text{cm}^2$ after they evaluated membrane depolarization results caused by ouabain (115, 159).

Native human adult RPE was evaluated with a mean TEER of $79 \pm 48 \Omega \cdot \text{cm}^2$ (values ranging from 36 to $148 \Omega \cdot \text{cm}^2$) and **native human fetal** RPE with $206 \pm 151 \Omega \cdot \text{cm}^2$ (values ranging from 18 to $486 \Omega \cdot \text{cm}^2$) (160). The use of almost all tissues even with low TEER has

been explained by the rare availability, while for bovine RPE this did not play a role. The medium for these experiments was kept at pH 7.4 using a gas mixture of 8% CO₂ or 10% CO₂ and contained 113.4 NaCl, 5 KCl, 1.8 CaCl₂, 0.8 MgCl₂, 1 NaH₂PO₄, 26.2 NaHCO₃, 15.6 glucose and 1 glutathione (all in mM). The osmolarity of the solution was 284 ± 3 mOsm. In a further publication of the same group it was reported that the exchange of MgCl₂ with MgSO₄ and the addition of 4 mM taurine had no effect on the maintenance of a healthy human fetal RPE (161), however the addition of a number of supplements such as vitamins and amino acids led to longer tissue survival, and this medium was also used during the dissection process.

These reports show that there is common ground for TEER values in RPE research, although the detailed experimental settings vary and are not always consistent. Standards for the TEER in the RPE have been established, however, they need to be constantly verified and modified in the appropriate systems, which makes it difficult to compare results.

This thesis aims to introduce a new model in which ex-vivo tissue from rats is used for the first time to gain a better understanding of the outer blood retinal barrier.

2 Materials and Methods

2.1 List of Chemicals and Salts

Name	Cat. No.	Company
CaCl ₂	C4901	Sigma-Aldrich, St. Louis, MO
DAPI (4',6-diamidino-2-phenylindole, dihydrochloride)	H-1200	Vector Laboratories, Burlingame, CA
Fluorescein-phalloidin	F432	Invitrogen; Carlsbad, CA
Formaldehyde (3.7-4%)	15714-S	Electron Microscopy Sciences; Hatfield, PA
Glucose	G7528	Sigma-Aldrich, St. Louis, MO
Glutathione	G4251	Sigma-Aldrich, St. Louis, MO
KCl	P9333	Sigma-Aldrich, St. Louis, MO
Methanol	M 3641	Sigma-Aldrich, St. Louis, MO
MgCl ₂	M8266	Sigma-Aldrich, St. Louis, MO
Mounting Medium	H-1000	Vector Laboratories Burlingame, CA
NaCl	S7653	Sigma-Aldrich, St. Louis, MO
NaHCO ₃	S6297	Sigma-Aldrich, St. Louis, MO
Rhodamine-phalloidin	R415	Invitrogen, Carlsbad, CA
Sodium fluorescein	F6377	Sigma-Aldrich, St. Louis, MO
<i>SYTOX Orange</i> (dimethylsulfoxide)	S11368	Molecular Probes, Eugene, OR

2.2 List of Equipment

Name	Cat. No/Model	Company
Ag and AgCl electrode pair	P2020-S	Physiologic Instruments, San Diego, CA
Analogue/digital converter	Powerlab/8SP	AD Instruments, Colorado Springs, CO
ATC (automatic temperature compensation) probe	598115	Beckman Coulter, Brea, CA
Bubble airstone	N/A	Petsmart, Everett, MA
Calomel electrode	511080	Beckman Coulter, Brea, CA

Ceiling dissecting microscope	MG 90	Leica, Solms, Germany
Colibri forceps	AE-4030	Asico, Weatmont, IL
Digital microscope camera	ORCA-ER C4742-95	Hamamatsu Photonics, Hamamatsu, Japan
Dissection forceps	RS-5136	Roboz Surgical Instruments, Gaithersburg, MD
Dissecting scissors	15017-10	Fine Science Tools, Heidelberg, Germany
Dissection forceps	5/15 INOX	Roboz Surgical Instruments Gaithersburg, MD
Dissecting microscope	MZ FLIII	Leica, Solms, Germany
Dissecting microscope	MZ 95	Leica, Solms, Germany
Fluorescent microscope	DM RXA	Leica, Solms, Germany
Gas valve	3051301-01-M1Q	Concoa, Virginia Beach, VA
Inverted microscope	CK2	Olympus, Tokyo, Japan
Microplate Reader (fluor.)	Spectramax Gemini	Molecular Devices, Sunnyvale, CA
Microprobe thermometer	BAT-12	Physitemp, Clifton, NJ
Microsurgery scissors	15017-10	Fine Science Tools, Heidelberg, Germany
Osmometer	5004	μOsmette, Precision Systems, Natick, MA
pH meter	Φ340	Beckman Coulter, Brea, CA
Ussing chamber system	EM-CSYS-2	Physiologic Instruments, San Diego, CA
Ussing half-chambers	P2400	Physiologic Instruments, San Diego, CA
Ussing slider (2 mm diameter)	P2407	Physiologic Instruments, San Diego, CA
Voltage Current Clamp	VCC 600	Physiologic Instruments, San Diego, CA
Water-bath	B-490	Büchi Labortechnik AG, Flawil, Switzerland
Water-pump (heated)	P/N 07999-000	Gaymar, Orchard Park, NY

2.3 List of Consumables

Name	Cat. No.	Company
0.2 ml reaction vial	05-408-120	Thermo Fisher Scientific, Waltham, MA
1.5 ml reaction vial	05-408-129	Thermo Fisher Scientific, Waltham, MA
15 ml reaction vial	352097	BD Falcon Franklin Lakes, NJ
18 gauge needle	305195	BD Falcon Franklin Lakes, NJ
30 gauge needle	305106	BD Falcon Franklin Lakes, NJ
50 ml reaction vial	352074	BD Falcon Franklin Lakes, NJ
Aluminum foil	N/A	Reynolds, Richmond, VA
Cover glass	12-548-5A	Thermo Fisher Scientific, Waltham, MA
Electrode tips	P2023	Physiologic Instruments, San Diego, CA
Gloves (vinyl)	V484313	Medline Industries, Mundelein, IL
Immersion oil	11 513 859	Leica, Wetzlar, Germany
Lint free task wipes	34155	Kimberly-Clark, Irving, TX
Parafilm M	PM996	Pechiney Plastic Packing, Chicago, IL
Sand paper (grit 600)	NC9499188	McMaster-Carr, Cleveland, OH
Syringe (1ml)	309602	BD, Franklin Lakes, NJ

2.4 List of Substances Applied to the Isolated Retinal Pigment Epithelium

Name	Cat. No.	Company
BSA (bovine serum albumin)	A9418-10G	Sigma-Aldrich, St. Louis, MO
DPBS (Dulbecco's phosphate buffered saline)	17-515Q	Lonza BioWhittaker, Walkersville, MD
IL-1 β (human)	201-LB	R&D Systems, Minneapolis, MN
LPS (lipopolysaccharide)	L2262	Sigma-Aldrich, St. Louis, MO

2.5 List of Specialized Computer Software

Name	Use	Company
LabChart	Data recording and analysis	AD Instruments, Colorado Springs, CO
SoftMax Pro	Microplate data software	Molecular Devices, Sunnyvale, CA
Keynote	Presentation and storage	Apple, Inc, Cupertino, CA

2.6 Buffer and Solutions

DPBS

Dulbecco's phosphate buffered saline (DPBS; Lonza BioWhittaker, Walkersville, MD) was diluted to a concentration of 1x.

HBSS

Hanks balanced salt solution (HBSS; H9394; Sigma, St. Louis, MO) without calcium, without magnesium.

KCl 5.4 mM (400 mg/l), KH_2PO_4 0.4 mM (60 mg/l), NaHCO_3 4.2 mM (350 mg/l), NaCl 136.9 mM (8000 mg/l), Na_2HPO_4 0.7 mM (48 mg/l), D-glucose 5.6 mM (1000 mg/l), phenol red 31 nM (11 mg/l).

DMEM

Dulbecco's modified Eagle's medium (DMEM/Ham's nutrient mixture F-12; D8437; Sigma, St. Louis, MO). A partial list of the components is listed here: NaCl 119.7 mM (6996 mg/L), NaHCO_3 14.3 mM (1200 mg/L), KCl 4.2 mM (311.8 mg/L), $\text{CaCl}_2 \cdot 2 \text{H}_2\text{O}$ 1.1 mM (155 mg/L), $\text{MgCl}_2 \cdot 6 \text{H}_2\text{O}$ 0.3 mM (61.2 mg/L), Na_2HPO_4 1 mM (71.02 mg/ml), NaH_2PO_4 0.45 mM (54.3 mg/L), and glucose 17.5 mM (3150 mg/L).

RPE-Ringer solution

This Ringer solution was used by one of the most accomplished RPE research groups led by Sheldon Miller. Its components are as follows:

NaCl 120 mM (7012.8 mg/L), NaHCO_3 23 mM (1932.2 mg/L), KCl 5 mM (372.8 mg/L), CaCl_2 1.8 mM (199.8 mg/L), MgCl_2 1 mM (95.2 mg/L), and glucose 10 mM (1801.6 mg/L). 1 mM of the antioxidant or reducing agent glutathione was added immediately before the experiment. The salts need to be solved individually before being added together. Otherwise a portion will

remained insoluble. Also it is important to note that anhydrous $MgCl_2$ and $CaCl_2$ should be stored in a desiccator if used for a prolonged period of time.

RPE-Ringer was used as the most successful medium during this study.

Table 2-1: Summary of the bathing media components. In addition DMEM contained vitamins and amino acids that are not listed here. * CO_2 requirements can be calculated using equations 2.1 - 2.4.

		<i>HBSS (9394)</i>	<i>DMEM (8437)</i>	<i>RPE-Ringer</i>	<i>RPE-Ringer + fluorescein</i>
<i>Substance</i>	<i>MW</i>	<i>Conc. [mM]</i>	<i>Conc. [mM]</i>	<i>Conc. [mM]</i>	<i>Conc. [mM]</i>
<i>NaCl</i>	58.44	136.9	119.7	120.0	120.0
<i>NaHCO₃</i>	84.01	4.2	14.3	23.0	23.0
<i>Na₂HPO₄</i>	141.96	0.7	1.0	N/A	N/A
<i>NaH₂PO₄</i>	119.98	N/A	0.5	N/A	N/A
<i>Pyruvic Acid•Na</i>	111.05	N/A	0.5	N/A	N/A
<i>Fluorescein•2Na</i>	376.27	N/A	N/A	N/A	26.6
<i>Na⁺ (from fluorescein sodium salt)</i>		N/A	N/A	N/A	53.2
<i>Sum Sodium</i>		142.5	137.0	143.0	196.2
<i>Sum Carbonate</i>		4.2	14.3	23.0	23.0
<i>KCl</i>	74.55	5.4	4.2	5.0	5.0
<i>KH₂PO₄</i>	136.09	0.4	N/A	N/A	N/A
<i>Sum Potassium</i>		5.8	4.2	5.0	5.0
<i>Sum Phosphate</i>		1.1	1.5	0.0	0.0
<i>CaCl₂</i>	110.98	N/A	1.1	1.8	1.8
<i>Sum Calcium</i>		0.0	1.1	1.8	1.8
<i>MgCl₂</i>	95.21	N/A	0.3	1.0	1.0
<i>MgSO₄</i>	120.37	N/A	0.4	N/A	N/A
<i>Sum Magnesium</i>		0.0	0.7	1.0	1.0
<i>Sum Chloride</i>		142.3	126.7	130.6	130.6
<i>Sum Sulfate</i>		0.0	0.4	0.0	0.0
<i>Glucose</i>	180.16	5.6	17.5	10.0	10.0
<i>HEPES</i>	238.30	N/A	15.0	N/A	N/A
<i>Phenol red • Na</i>	354.38	N/A	0.02	N/A	N/A
<i>Glutathione</i>	307.32	N/A	N/A	1.0	1.0
<i>Amount of CO₂ required to obtain pH 7.4*</i>		0.09%	3.1%	5%	5%

The medium was kept at 38 °C in a water bath (B-490; Büchi Labortechnik AG, Flawil, Switzerland). This temperature was chosen to compensate for an inevitable decline in temp. during the pipetting process, and resulted in negligible temperature adjustments.

To achieve pH 7.4, gas with a CO₂ content of 5% (see below) that had been moisturized was led through the medium for 2 minutes.

The osmolarity of the control solution was 286 ± 5 mOsm (model 5004; μOsmette, Precision Systems, Inc., Natick, MA) with no measurable changes when the cytokines or other substances were added.

When the permeability of the RPE cells was determined, sodium fluorescein (Sigma; F6377) was added to the medium destined for the apical bathing solution in a final concentration of 10 mg/ml. This resulted in an additional 53.2 mM Na⁺ and a change in the osmolarity to 343 ± 5 mOsm (for more details see below).

2.7 Gas

Gas containing 10% O₂, 5% CO₂, 85% N₂ (Z03 NI8522000112 Airgas East, Dorchester, MA) was used to maintain pH 7.4 in the RPE-Ringer. Others had shown that a reduction in the O₂ tension results in an increase in longevity of bovine RPE cells (115, 159). The gas was led through a fine bubble airstone (Petsmart, Everett, MA) in a 200 ml cylinder that was filled to one quarter of its capacity with dH₂O. The moisturized gas was led through the medium for 2 minutes until its pH was stabilized between 7.3 and 7.4.

The CO₂ amount necessary for achieving pH 7.4 is calculated by using, the Henderson-Hasselbalch equation. This equation relates the partial pressure of, in this case, carbon dioxide to the bicarbonate ion concentration and the pH.

$$pH = pK_a + \log \frac{[A^-]}{[HA]} \quad \text{Eq. 2.1}$$

with pK_a being the acid dissociation constant. For carbon dioxide the pK_a is 6.1

[A⁻] the concentration of the conjugated base and [HA] the concentration of the acid.

When using gas, the formula is adjusted accordingly:

$$pH = pK^1 + \log \frac{[HCO_3^-]}{\alpha P_{CO_2}} \quad \text{Eq. 2.2}$$

with K^1 being the first dissociation constant of carbonic acid, and α being the solubility constant of CO_2 , which is 0.03. α also converts the partial pressure from mmHg to mmols/L. PCO_2 is the partial pressure of CO_2 in the gas tank.

K^1 was determined in 1935 by Shedlovsky and MacInnes, while the second dissociation does not play a role in the Henderson-Hasselbalch equation and can be neglected for a $\text{pH} < 8$, after which the arising error rises.

The $[\text{HCO}_3^-]$ of the RPE-Ringer is 23 mM.

When using a gas with 8% CO_2 , the partial pressure is 0.08 atm (8.1 kPa or 60.8 mmHg).

$$\text{pH} = 6.1 + \log \frac{23 \text{ mmol/L}}{0.03(60.8 \text{ mmHg})} = 6.1 + \log 12.61 = 6.1 + 1.1 = 7.2 \quad \text{Eq. 2.3}$$

To be able to calculate the physiologic pH 7.4 based on a known concentration of bicarbonate, the following formula needs to be solved:

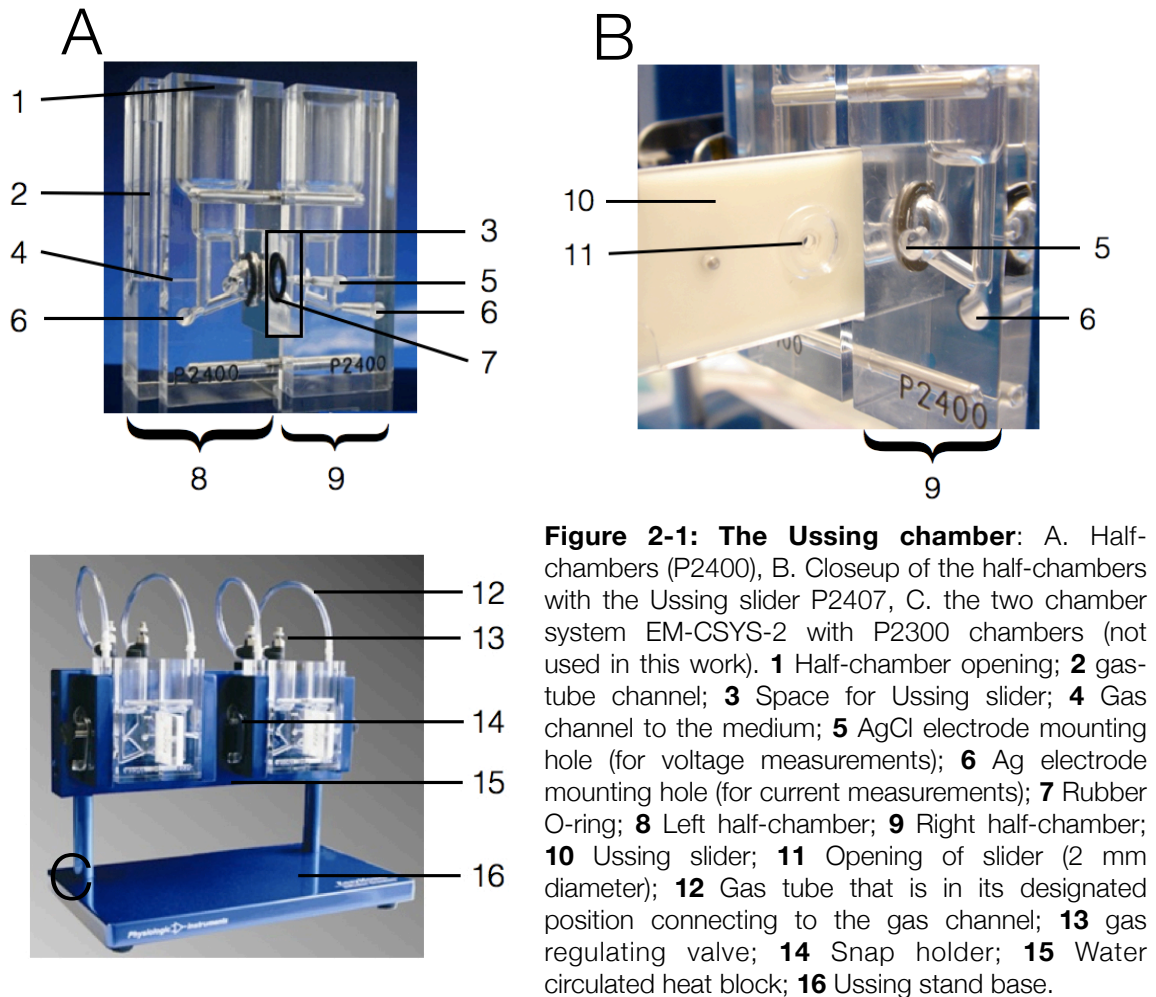
$$7.4 = 6.1 + \log \frac{23 \text{ mmol/L}}{0.03(x \text{ mmHg})} \Leftrightarrow 10^{1.3} = \frac{23}{0.03 \cdot x} \Leftrightarrow x = \frac{23}{0.03 \cdot 10^{1.3}} \approx \frac{23}{0.03 \cdot 19.95} \approx 38.42 \text{ mmHg} \quad \text{Eq. 2.4}$$

38.4 mmHg = 5.1 kPa or 0.05 atm, which require a CO_2 concentration of 5% in the gas of choice.

Note that in a medium that contains Mg^{2+} and/or Ca^{2+} , these two ions may form MgCO_3 and/or CaCO_3 , which can lead to an acidification of the solution.

2.8 The Ussing Chamber System

The Ussing chamber used for this study consists of three basic elements that were purchased from Physiologic Instruments (San Diego, CA): A 2 Chamber System (EM-CSYS-2), an Ussing chamber consisting of two half-chambers (P2400) and a specially sized Ussing slider (P2407), also referred to as insert, with an opening of 2 mm in diameter or an area of 0.0314 cm^2 ($A = \pi \cdot r^2 \Leftrightarrow A = 3.14 \text{ mm}^2$ or 0.0314 cm^2).



The electric pulses were generated using the Voltage Current Clamp 600 (VCC 600), which also allows compensating the system (Physiologic Instruments, San Diego, CA). A heated water-pump (Gaymar T/Pump: P/N 07999-000, Orchard Park, NY) was connected to the 2-chamber system. The temperature in the chamber was measured using a microprobe thermometer (Physitemp BAT-12, Clifton, NJ) that was connected to the Powerlab/8SP (AD Instruments, Colorado Springs, CO). The pH in the Ussing chamber was measured using a Beckman Φ 340 pH/Temp Meter with an automatic temperature compensation (ATC) probe (P/N 598115) and a refillable Calomel electrode (511080; all Beckman Coulter, Brea, CA).

2.9 Preparation of Electrode Tips

The electrode tips (Physiologic Instruments P2023) were filled using a 5 ml syringe by injecting hot bubble-free agar into the tips from their bottom, by holding the narrower end down and pressing the agar up into the tips. Only about 20-30 μ l of agar were injected, which filled the tips to the lower 6-10 mm. After the electrodes were filled, they were placed in 3 M KCl. and evaluated using a light microscope. When bubbles were noticed, the electrodes were recycled.

2.10 Electrode Preparation

The current-passing Ag electrode pair was chlorified by leaving them in common household bleach for 20 minutes or more. When chlorification needed to be repeated, 600 grid sandpaper was used to polish the electrodes. The AgCl electrodes were never chlorified. (P2020-S Ag and AgCl electrode pairs both Physiologic Instruments, San Diego, CA). Not chlorifying the electrodes led to quick deposition of potassium on one electrode and chloride on the other, as well as gas formation within the electrodes. Not chlorifying the electrodes influences the short-circuit current (see below).

2.11 Use of Electrodes

The electrodes were mounted into their designated tips. Any excessive KCl was washed off with H₂O and dried using a lint-free tissue. Electrodes were then placed in the designated holes of the Ussing chamber. After every experimental day, the Ag and AgCl electrodes were removed from the 3 M KCl, rinsed with H₂O, and dried. The next day the apical electrodes were used in the basolateral chamber and vice versa. This allowed reducing the amount of electrode care while maintaining stable conditions for the electrodes during a set of experiments.

2.12 Pre-Experimental Preparations of the Ussing Chamber

A piece of *Parafilm* (Pechiney Plastic Packing, Chicago, IL) no wider than 6.7 mm was placed in the Ussing chamber stand, creating an electrical insulation between the stand and the two half-chambers to prevent possible short-circuits. Initial experiments without this insulation

had resulted in a low, but recordable 60 Hz frequency which was likely caused by an undesirable transfer of electricity from the heat block to the chambers (Fig. 2-2).

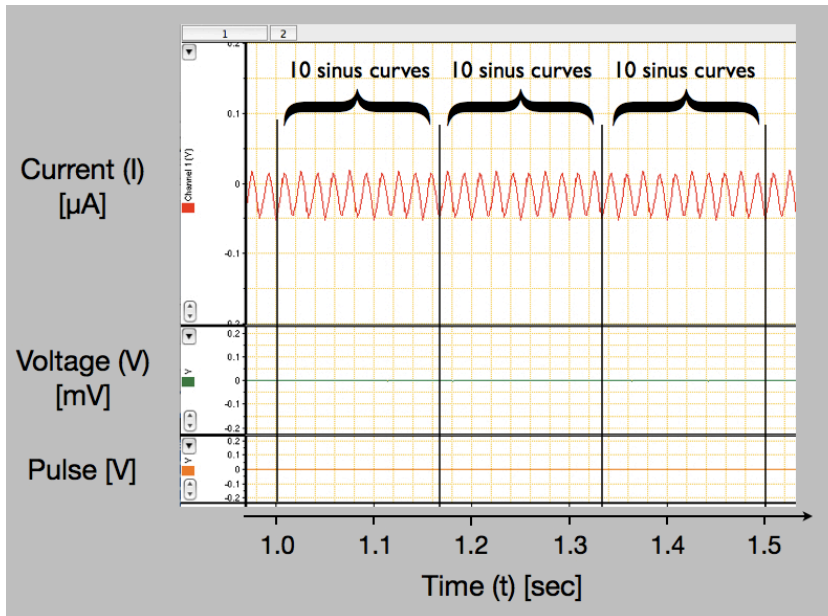


Figure 2-2: 60 Hz frequency during recordings when the heat block insulation is absent. Graph shows the recording using *LabChart* software. Independent from a given voltage, the current shows a 60 Hz frequency.

An empty mounting slider P2407 was placed between the two half-chambers, whose rubber o-rings were lubricated with immersion oil, and tightened.

The heated water pump was turned on and 4 ml RPE-Ringer were added to each half-chamber. Any air bubbles were removed by carefully flushing the system using a 1 ml pipette.

The gas hoses were placed on the top of each half-chamber and held in place with *Parafilm* that was loosely covering the chamber. This setup was preferred over the use of using the designated gas channels, whose use frequently led to the rupture of the RPE.

The intended side effect was the reduction in fluid evaporation and a slightly increased temperature.

2.13 Compensation of the Voltage Clamp

After the Ussing chamber was assembled, the VCC 600 was set up by taking an initial current reading in the “zero” function by pushing the “push to adjust” button. A value of ~64 μA indicated that the system was ready to be compensated. Values that were much greater or lower or not stable indicated that the electrode tips needed to be replaced.

The average fluid resistance was 76 Ω . When needed, the voltage offset of the system was then adjusted to zero in the “open” function, followed by compensation of the fluid resistance by switching the offset switch in either the positive or negative position and adjusting, so that the initial voltage in the system was zero. Prior to mounting the tissue, the offset and fluid resistance was rechecked and adjusted if needed.

2.14 Experimental Animals

All animal experiments adhered to the ARVO Statement for the Use of Animals in Ophthalmic and Vision Research. The animal protocol was approved and annually reviewed by the Animal Care Committee of the Massachusetts Eye and Ear Infirmary (protocol number 04-12-024). Brown Norway rats, of varying ages, usually 8 weeks and older, were used for the experiments. Animals were fed standard laboratory chow and allowed free access to water in a temperature controlled room with a 12-hour light/12-hour dark cycle. Animals were caged in pairs or individually.

2.14.1 Surgery and Tissue Preparation

Brown Norway rats were anesthetized during the light cycle adaptation using a 1:1 mixture of 100 mg/ml ketamine and 20 mg/ml xylazine. The dosage was applied intra muscular with a concentration of 100 mg/kg ketamine and 20 mg/kg xylazine. Rats of other strains required slightly different dosages of anesthetics.

Usually the left eye was enucleated first by gripping the distant part of the conjunctiva and starting to cut through it, while not applying any additional pressure to the eye. After the optic nerve was cut using FST 15017-10 microsurgery scissors (Fine Science Tools, Heidelberg, Germany), Roboz RS-5136 forceps (Roboz Surgical Instruments, Gaithersburg, MD) were carefully placed under the eye and the remaining tissue was cut to complete the enucleation. The anesthetized animals were then placed on a heating pad maintaining their body temperature at 37 °C or wrapped in aluminum foil until the second eye was harvested.

The eye was placed on a piece of *Kimwipe* (Kimberly-Clark, Irving, TX) that was moistened with RPE-Ringer to assure minimal sticking of the eye to the tissue while assuring optimal handling conditions.

The remaining conjunctiva and muscles on the eye were removed using the FST 15017-10 dissecting scissors, while the eyeball was held in place with colibri forceps (AE-4030; Asico, Weatmont, IL). Additional blood was removed from the large veins of the eye by applying slight pressure on them with the blunt side of Roboz 5/15 INOX forceps.

The cornea was pierced using a 30.5 gauge needle to remove the intra ocular pressure that would otherwise bulge out at a later step and break the RPE.

When desired, a circular piece of sclera (2.5 - 3 mm diameter) was carefully removed between the optic nerve and the limbus from the side opposite to the central retinal artery using microsurgery (iris-) scissors with a curved cutting edge to avoid piercing through the RPE, while the eye was continuously turned. Attention has to be paid if large veins are attached to the sclera.

After the sclera was removed, a greater circular piece was cut from the remaining eye, still not extending into more than one half of the eye. The connection between retina and vitreous was mechanically cut.

2.14.2 Mounting of the RPE Tissue

For rat eyes the P2407 mounting slider (also referred to as Ussing slider or insert) was used. A small amount of RPE-Ringer was applied over the opening of the slider filling the tissue collection area. The surface tension assures that the medium spreads over the hole. The explant was carefully placed over the slider opening and when desired the neurosensory retina was carefully peeled away from the RPE using two dissecting forceps. In the cases in which sclera and retina had been removed the tissue spanning over the hole consisted only of RPE and choroid (RPE explant), while the more distant areas retained some sclera. The sclera gave support during handling of the tissue.

The excess medium was then removed from the mounting slider using *Kimwipes* and the top slider-half carefully placed on top, while assuring that it did not touch until mounted into the Ussing chamber.

Before the mounting sliders were placed in the chamber, the chamber was once again compensated if needed.

The medium that had been used for the compensation and to adjust the chamber temperature was removed using a 1000 ml pipette. The empty mounting slider was taken out of its position and the tissue bearing slider placed in the center of the half chambers, with the

apical (retinal) side facing to the left. The chamber was carefully tightened, assuring that the sliders did not come apart.

This step is crucial. If the chambers are too tight, the amount of edge damage will increase, but if they are too loose, medium will leak out.

4 ml medium were added to each side of the chamber by alternating 1 ml to the apical and basolateral side of the tissue. The alternating application was done to prevent excess pressure buildup and possible tissue stress or tearing.

2.15 Occurrence and Removal of Air Bubbles

Despite careful and slow application of medium small air bubbles were trapped on the apical side of the mounting sliders, blocking the medium from directly touching the RPE. The best way to remove this bubble was to wait one minute and then carefully pipetting the medium toward the bubble using a 1000 ml pipette (Eppendorf, Hamburg, Germany). Attempts to do so earlier, had required more pressure and may have caused tissue rupture and a low TEER.

2.16 Electrical Recordings

A bipolar electric pulse of usually 6 mV was given every 30 seconds. If necessary, the voltage of the pulse was adjusted. The electric pulse and readouts were converted into digital signals and recorded to computer using a Powerlab analog/digital converter from AD Instruments (Powerlab/8SP; AD Instruments, Colorado Springs, CO). *LabChart* software (also AD Instruments) was used to record the signals. Four channels were recorded: The Voltage (mV), the corresponding current (μA), the electric pulse (V) and the temperature ($^{\circ}\text{C}$) (Fig. 2-3). At any given time signals could be analyzed and the TEER ($\Omega\cdot\text{cm}^2$) could be calculated using the following Ohm's law:

$$R = \frac{V}{I} \quad \text{Eq. 2.5}$$

With R being the resistance, V the voltage and I the current.

The resistance is inversely proportional to the surface area, so that the resistance needs to be multiplied by the area exposed to the voltage. The unit of the TEER is $\Omega\cdot\text{cm}^2$, not the intuitive

Ω/cm^2 . In the case of the measurements for rats using the mounting slider P2407, it is 0.0314 cm^2 as described above.

LabChart allowed note-taking during the ongoing recording. These notes were added at the time of recording, a helpful tool for documentation and archiving of the raw data.

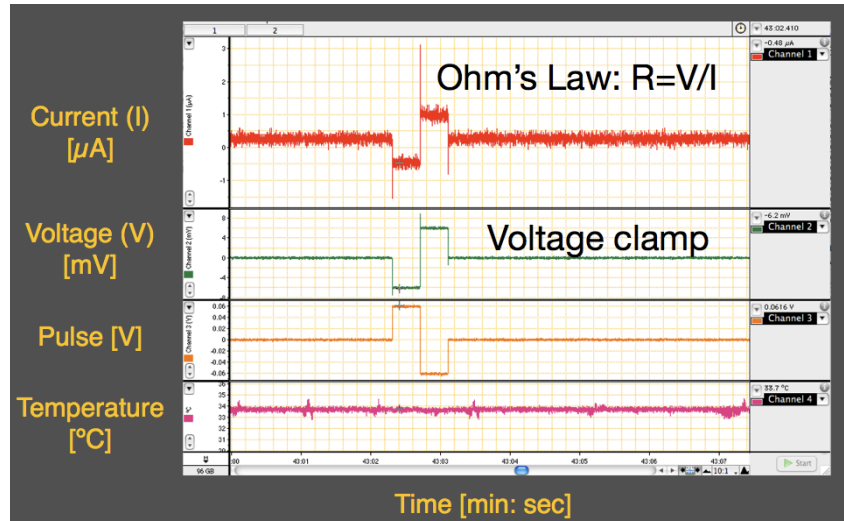


Figure 2-3: Recording the analogue Ussing chamber signals using the Powerlab and LabChart software. Four channels were recorded, while a bipolar voltage pulse (green) was given every 30 - 60 seconds. The corresponding current (red) is read and the TEER calculated as explained in the text.

2.17 Administration of Substances to the Apical Side of the RPE Bathing Medium

When desired, 20 minutes after the start of the recordings, 200 μl of the apical bathing solution were taken out and mixed with a small volume (2-10 μl) of the respective substance. Immediately after mixing, the solution was carefully pipetted back to the side of removal, and carefully dispersed using a 1 ml pipette. The applied substances were:

BSA (bovine serum albumin; A9418-10G, Sigma, St. Louis, MO) diluted in DPBS to obtain 0.1% (w/v).

Human IL-1 β (201-LB; R&D Systems, Minneapolis, MN) reconstituted in 0.1% BSA in PBS to obtain a stock concentration of 100 ng/ μ l or 20 ng/ μ l. The final concentration in the Ussing half-chamber was either 10 or 50 ng/ml.

Lipopolysaccharide (LPS; *Salmonella typhimurium*; Sigma, St. Louis, MO) reconstituted in saline to obtain a stock concentration of 2 μ g/1 μ l. The final concentration in the Ussing half-chamber was 500 ng/ml.

2.18 Permeability Measurements Using Fluorescein

Sodium fluorescein (F6377, Sigma, St. Louis, MO; MW 376.27) was used as a permeability tracer. The RPE-Ringer was treated as usual and sodium fluorescein was added to reach a final concentration of 10 mg/ml. The apical chamber was filled using this medium, while the basal chamber was filled using regular RPE-Ringer while maintaining all other experimental settings unchanged. After 30, 60, 90 and 120 minutes, 200 μ l of medium were taken from the basal bathing solution. While the original volume was restored by adding 200 μ l RPE-Ringer to this side, the fluorescein concentration was assessed using a 96-Microplate Fluorescence Reader (Spectramax Gemini) and SoftMax Pro, Microplate Data Software (both Molecular Devices, Sunnyvale, CA). The concentration for each sample was calculated by comparing it to a standard curve that was prepared using the original fluorescein containing RPE-Ringer.

2.19 Data Analysis

The average value of each recorded current response, stretching over 0.4 sec, was taken and subtracted from the average of the baseline value directly adjacent to the voltage pulse. These values were obtained by using the *data pad* function of the program *LabChart*. This was repeated in 1 min intervals until all values were analyzed. Following Ohm's law, the resistance was calculated ($R=U/I$) and multiplied with the area of the mounting slider hole (0.0314 cm²) to obtain the TEER in Ω ·cm². The individual graphs were prepared using *Microsoft Excel*.

Data point intervals 10 minutes apart from all experiments belonging to the same group were then copied into a separate *Excel* sheet. Based on the criteria of exclusion (see below),

experiments were eliminated from the total analysis. The success rates of the individual experimental series were calculated based on the amount of eliminated experiments. Bar diagrams were prepared using *Excel*. For the overview of all data the program *Keynote* (Apple, Cupertino, CA) was chosen.

2.20 Criteria for TEER Data Exclusion

TEER analysis revealed that it was necessary to discriminate values that did not fulfill the following two criteria:

1. The TEER was not decreasing more than $20 \Omega \cdot \text{cm}^2$ within the first 20 minutes
2. The TEER was $> 69 \Omega \cdot \text{cm}^2$ within this time period.

The value of $69 \Omega \cdot \text{cm}^2$ was chosen because a number of experiments were observed in which the resistance was stabilized at this value. To be more conservative, this value can be increased.

2.21 Histochemistry

2.21.1 Staining of the Cytoskeleton-Component Actin

The tissue integrity was evaluated by staining the f-actin with rhodamine-phalloidin (R415; Invitrogen, Carlsbad, CA) or fluorescein-phalloidin (F432; Invitrogen, Carlsbad, CA), while the manufacturer's instructions were followed. In brief the tissue explant was carefully removed from the Ussing slider, placed on a microscope slide and washed with PBS (pH 7.4, 37 °C). The tissue was then placed in 3.7-4% formaldehyde (15714-S; Electron Microscopy Sciences; Hatfield, PA) constituted in PBS for 10 minutes at room temperature and afterwards washed twice with PBS. The tissue was removed from its container, and placed in acetone at -20 °C for 3-5 minutes. Then the tissue was placed on a microscope slide and washed twice with PBS. 200 μl of a 1:40 dilution of methanolic rhodamine-phalloidin stock solution in 1% BSA in PBS were pipetted onto the tissue, placed in a glass Petri-dish and covered with aluminum foil and incubated for 20 minutes at room temperature. Alternatively the staining was performed at 4 °C overnight in a closed Eppendorf tube to avoid evaporation. The staining solution was removed by washing the tissues three times for 5 min

in PBS. Mounting medium (H-1000; Vector Laboratories, Burlingame, CA) was added on the tissue and a cover slide was placed on top.

2.21.2 Nuclear Staining Using DAPI (4',6-diamidino-2-phenylindole, dihydrochloride)

When desired, DAPI (H-1200; Vector Laboratories, Burlingame, CA) was used to stain the nuclei. DAPI was used in a final concentration of 0.5 μM in PBS and used solely or as the final step following all other staining. A volume of 200 μl was applied directly onto the cover slide with the RPE tissue and incubated for 15 minutes. Then DAPI was removed and tissue was washed twice with PBS .

When the mounting medium with DAPI was applied as intended by the manufacturer, it was not possible to detect DAPI in the micrographs.

2.21.3 Dead Cell Analysis Using SYTOX Orange

Where desired, the integrity of the cell membrane of the RPE tissue was evaluated using *SYTOX Orange* (dimethylsulfoxide) (S11368; Molecular Probes, Eugene, OR), a substance that stains the nucleic acid in cells with compromised cell membranes. The tissue was removed from the Ussing slider and washed twice with PBS. 200 μl of 0.25 μM *SYTOX Orange* diluted in PBS were pipetted onto the tissue and incubated for 15 minutes at room temperature. The tissue was then washed twice in PBS.

2.22 Microscopes and Cameras

Photomicrographs were taken using a digital high-sensitivity camera (ORCA-ER C4742-95; Hamamatsu Photonics, Hamamatsu, Japan) through an upright fluorescent microscope (DM RXA; Leica, Solms, Germany). Eyes were dissected using one of the following: MG 90 Ceiling, MZ FLIII or MZ 95 (all Leica, Solms, Germany). Electrode tips were evaluated using an inverted microscope (CK2; Olympus, Tokyo, Japan).

2.23 Statistical Significance

Values are expressed as mean \pm s.e.m. Significance was determined using Student's t-test. Differences between the experimental groups were considered statistically significant (*) or highly significant (**), when the probability value, P was < 0.05 or < 0.01 , respectively.

3 Results

3.1 Establishing an Ussing Chamber Assay for the Reliable Measurement of Transepithelial Electrical Resistance (TEER)

Setting up any new assay takes time and is accompanied by trials, errors and improvements. This first section of the results precisely describes the process of finding the most suitable medium for the RPE tissue and the improvement that led to a system that expressed stability for a time period of up to two hours.

3.1.1 Experiments Using Hank's Buffered Salt Solution (HBSS)

For the initial TEER measurements of retinal pigment epithelium tissue explants, Hank's balanced salt solution (HBSS), a medium commonly used for RPE extraction was used. The results show that the TEER at t_0 was $25 \pm 4 \Omega \cdot \text{cm}^2$ and declined to $8 \pm 2 \Omega \cdot \text{cm}^2$ within 15 minutes Figure 3-1.

While the literature shows a great variability in TEER values (117-119, 121, 149, 150, 153), the reduction in TEER in this case was caused by the lack of Ca^{2+} , a necessary component for the functionality of tight junctions (6).

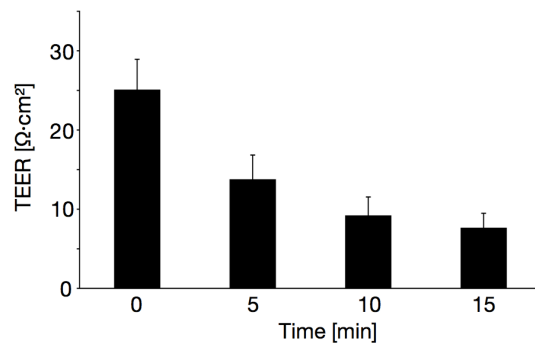


Figure 3-1: TEER of RPE in Hank's balanced salt solution (HBSS) lacking Ca^{2+} . The TEER decreases by 69% within 15 minutes; $n = 9$. Error bars are expressed as s.e.m.

3.1.2 Experiments Using Dulbecco's Modified Eagle Medium (DMEM)

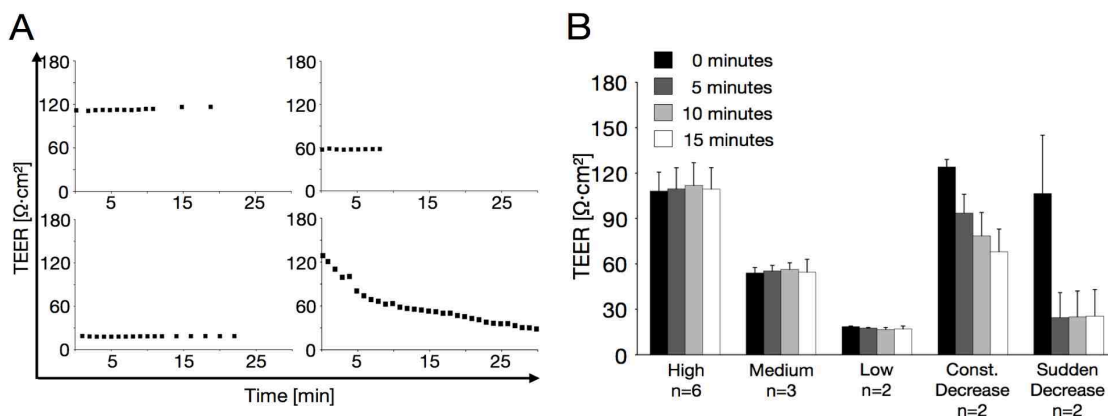


Figure 3-2: Variability in early TEER measurements using Dulbecco's modified Eagle medium (DMEM). **A:** Individual measurements. **B:** Bar diagrams of grouped results. Colors indicate different time points. Error bars are expressed as s.e.m.

In the following experiments, Dulbecco's modified Eagle medium (DMEM) mixture F-12 Ham, commonly used during RPE cell-culture procedures was used as the bathing medium.

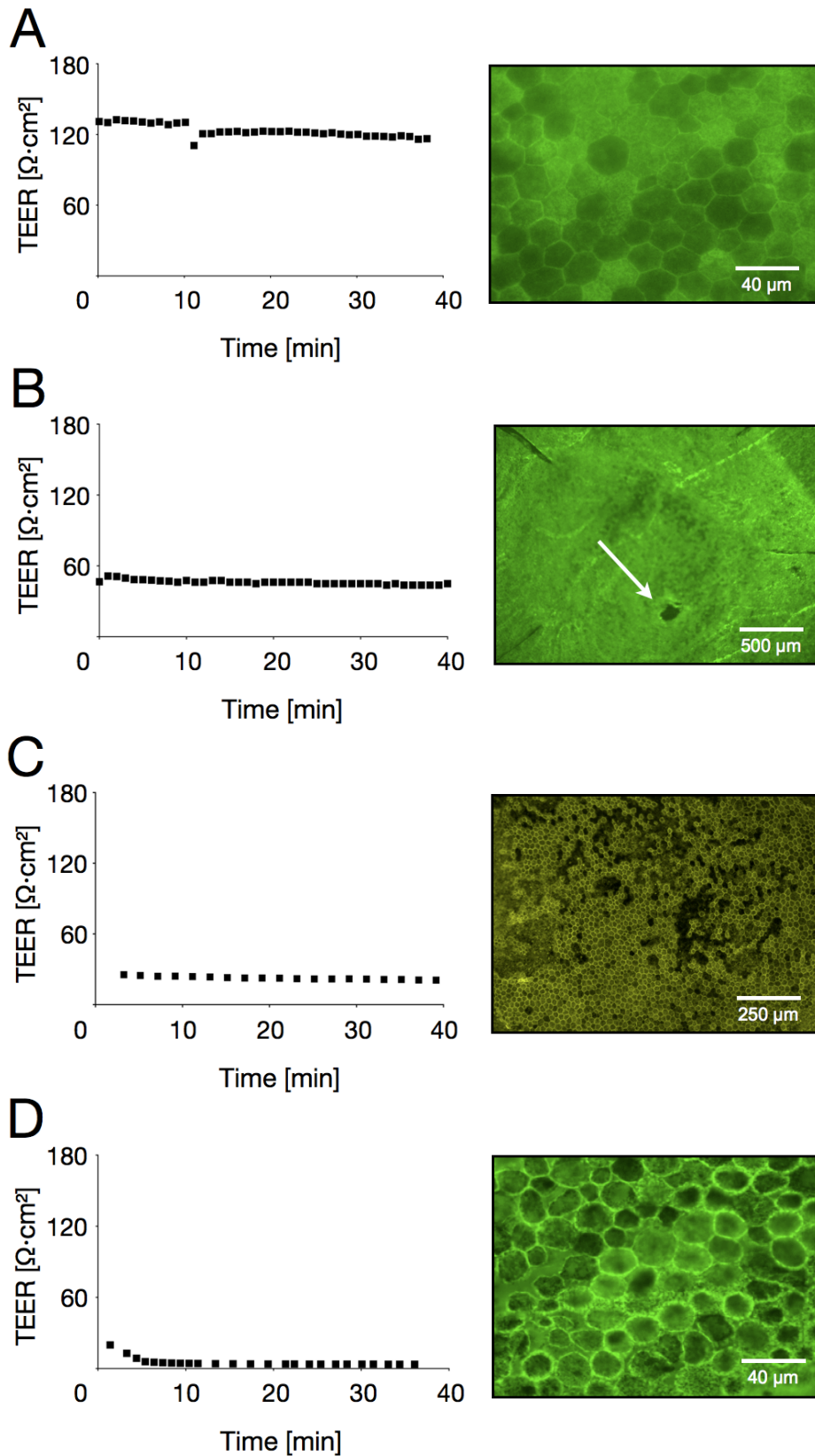


Figure 3-3: TEER is dependent on the integrity of the RPE. **A:** Intact RPE tissue results in a stable TEER of $120 \Omega \cdot \text{cm}^2$. **B:** A punctured RPE leads to a strong reduction of TEER. **C:** Apparent lack of RPE cells in dark areas leads to a greater reduction in TEER value. **D:** The lack of Ca^{2+} in HBSS medium leads to the rounded shape of RPE, loss of tight junctions and the complete breakdown of the TEER. A-D actin staining using fluorescein-phalloidin (A,B,D), or rhodamine-phalloidin (C), all pseudo color.

The results showed great variability (Fig 3-2) that could be organized in five subcategories: Constantly high TEER ($110 \pm 14 \Omega \cdot \text{cm}^2$), constantly medium ($55 \pm 5 \Omega \cdot \text{cm}^2$), constantly low ($17 \pm 1 \Omega \cdot \text{cm}^2$), constantly decreasing and suddenly decreasing. The suddenly and constantly decreasing values were eliminated from the analysis because they did not reflect stable experimental conditions. In the cases of high, medium and low TEER values, the cell's actin filaments were stained with fluorescein- or rhodamine-phalloidin (Fig. 3-3). These results showed that a TEER of $130 \Omega \cdot \text{cm}^2$ coincided with an intact RPE sheet, whereas the TEER of $50 \Omega \cdot \text{cm}^2$ showed tissue damage, and the low TEER of HBSS showed a clearly changed morphology of the cells, having rounded shapes and large interstitial spaces.

Further analysis showed that only TEER values greater than $68 \Omega \cdot \text{cm}^2$ would be considered for accumulative analysis, resulting in a TEER for RPE cells of $110 \pm 14 \Omega \cdot \text{cm}^2$ within the measured time period. These criteria eliminated 60% (9/15) of the samples, resulting in a 40% success rate of successful tissue analysis (Fig. 3-4).

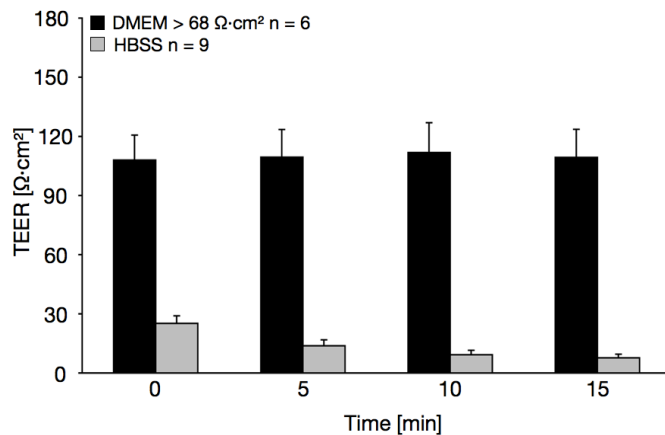


Figure 3-4: Comparison of the TEER values using DMEM and HBSS. The TEER remained stable over a time period of 15 minutes using DMEM. The success rate with the established minimum value of $69 \Omega \cdot \text{cm}^2$ was 40% (6/15). DMEM values are shown in black, HBSS in gray. Error bars are expressed as s.e.m.

Figure 3-4 also compares these results to those using HBSS as bathing medium. The low initial values of the HBSS experiments indicate that the lack of Ca^{2+} has an immediate effect on the TEER starting when the RPE is exposed to this medium and before the first

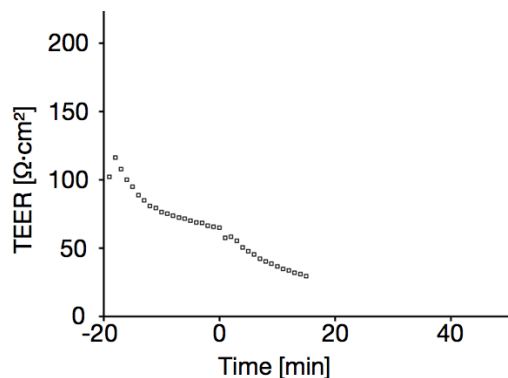


Figure 3-5: The effect of EDTA added to the apical RPE bathing solution. EDTA with a final concentration of 10 mM was applied at t_0 . An already decreasing TEER that indicates a compromised RPE, is immediately further reduced by EDTA's capture of free Ca^{2+} . This led to a decrease in TEER by 55% within 15 minutes.

measurement is taken. This was confirmed when the chelating agent EDTA (final concentration 10 mM EDTA) was applied to the apical bathing solution of RPE. It was demonstrated that the TEER decreased immediately after EDTA application, despite an already decreasing TEER (Fig. 3-5).

3.1.2.1 Experiments Using RPE Tissue Without Removing Sclera in DMEM

To further minimize the amount of possible injury that occurred to the RPE during the surgical process and as a result to increase the experimental success rate, the sclera was not removed from the RPE explants (RPE/sclera). However, the results did not show an advantage of using this tissue (Fig. 3-6). The success rate of these experiments was 25% (1 out of 4). Hence the sclera was continuously removed from the RPE in the following experiments.

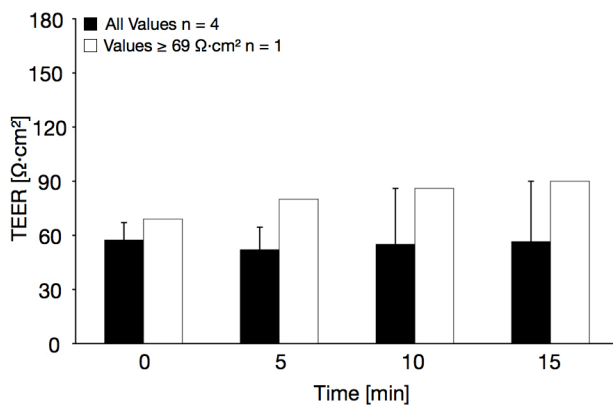


Figure 3-6: TEER of RPE without removing the sclera. Black bars represent all attempts, white bars represent those that met the exclusion criteria. The success rate was 25% (1/4). Error bars are expressed as s.e.m.

3.1.3 Histological Analysis of the RPE Sheets Using HBSS and DMEM

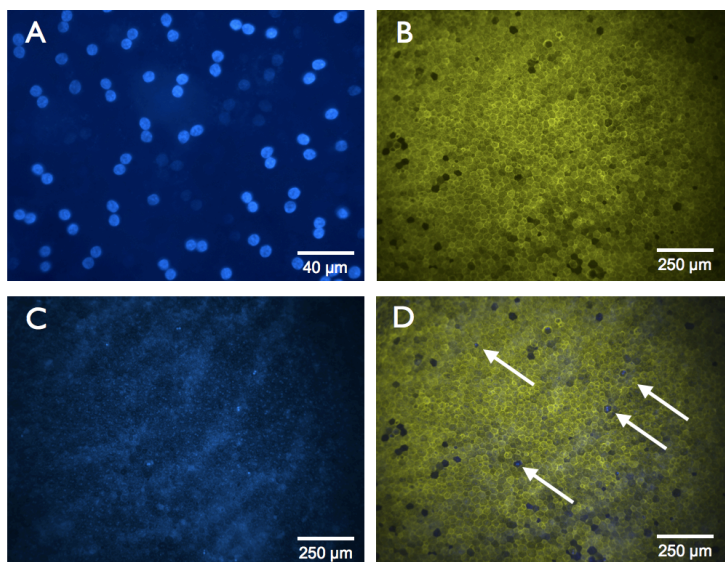


Figure 3-7: Localization of nuclei in RPE cells after Ussing chamber experiment using DMEM as bathing medium. **A:** Fluorescent micrograph of RPE cells, stained with DAPI (blue). **B:** Fluorescent micrograph of RPE, stained for actin using rhodamine-phalloidin (green). **C:** Counterstaining for the nuclei with DAPI (blue). **D:** Merged image of B and C. Arrows indicate the localization of bright DAPI staining. All pseudo color.

After the actin staining revealed a correlation of the intactness of the tissue and the TEER, further tissues were analyzed. When the nuclei were stained using 4', 6-diamidino-2-phenylindole (DAPI), it was noticed that the majority of the stained RPE sheets of animals older than 10 months had 2 nuclei, however the DAPI staining was not homogenous. The majority of the nuclei were stained faintly, while some took up more DAPI (Fig. 3-7). This led to the question, weather the brightly stained nuclei belonged to dead cells. To evaluate the number of dead cells, staining with *SYTOX Orange*, an assay was performed to reveal cells with compromised cell membranes. The results show that no dead cells were detectable within the area of TEER measurements. The cells outside the clamped area stained positive, indicating damage caused by the pressure of the half chambers (Fig. 3-8). These results indicated that these histological approaches could not differentiate between minor differences in the TEER of intact RPE sheets.

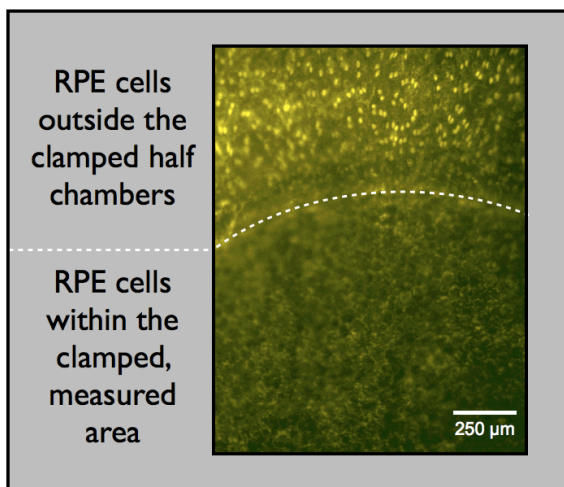


Figure 3-8: Staining dead RPE cells after Ussing chamber experiments using *SYTOX Orange*. Nuclear staining of *SYTOX Orange* reveals that cells with compromised plasma membrane lay outside the Ussing slider opening. The inner cells that are in contact with the bathing medium are *SYTOX Orange* negative. White perforated line represents the borders of the Ussing slider. RPE cells were bathed in RPE-Ringer solution.

3.1.4 Modifications of Physical Parameter

The results showed that the basic parameters of the system were set up; however the duration of stable TEER measurements was very limited. In the next steps, the physical details of the system were improved and stabilized to address this aspect.

3.1.4.1 Establishment of a Dummy Membrane

To spare animal lives during the phase of improving the physical parameters, a suitable dummy membrane was required.

First a layer of lint-free cleaning tissue (*Kimwipes*) was used and a TEER of $3 \Omega \cdot \text{cm}^2$ was observed, which continued to decrease (Fig. 3-9 A). The low value was not suitable for simulating an RPE. Then white copying paper (80 g/cm^2) was used to simulate a membrane. The initial results showed a TEER of $75 \Omega \cdot \text{cm}^2$, closer to that of RPE cells. These results were not reliably reproducible (Fig. 3-9 B-C).

The third choice was a plastic paraffin film (*Parafilm*) that was punctured to create a small hole. Its TEER was $27 \Omega \cdot \text{cm}^2$ (Fig. 3-9 D). While this value was still low and did not allow separation of the two chambers, it could be used to address basic questions, while maintaining a constant TEER.

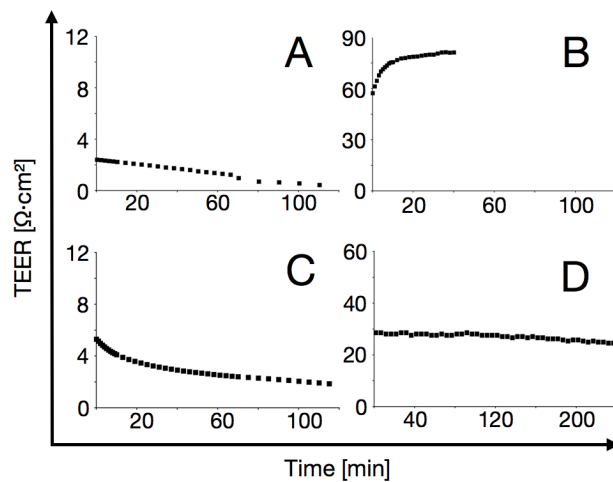


Figure 3-9: TEER values of different materials during the search for a suitable dummy membrane.

A: *Kimwipes*. **B:** Initial results using 80 g/mm^2 copying paper. **C:** Variability when using the same copying paper as in B. **D:** *Parafilm* with a punctured hole.

3.1.4.2 Controlling the Chamber Temperature

The first physical parameter addressed was the temperature of the bathing medium within the chamber. The system allowed a maximum temperature of $35 \pm 1 \text{ }^\circ\text{C}$ (Fig. 3-10). When the medium was kept at $37 \text{ }^\circ\text{C}$ and the chambers were filled using a 1 ml pipette, the medium's temperature was below optimum, as shown. To assure that the medium reached $35 \text{ }^\circ\text{C}$ when the RPE explants were mounted, it was kept in a heating bath at $38 \text{ }^\circ\text{C}$, allowing minimal temperature changes.

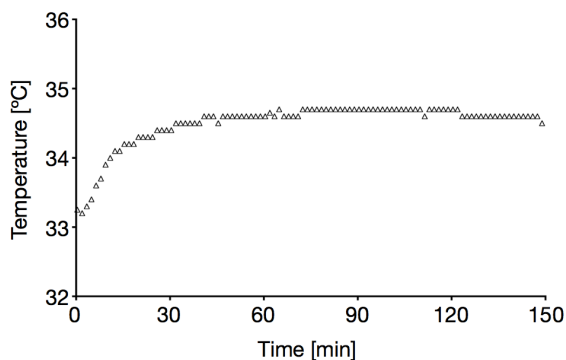


Figure 3-10: Temperature changes of the bathing solution in the Ussing chamber.

A microthermometer probe was placed in the basal bathing medium at all times and the temperature of the experiments was recorded. When the Ussing medium that was kept at $37 \text{ }^\circ\text{C}$ the temperature needed 30 minutes to reach its maximum value.

3.1.4.3 Monitoring the Short Circuit Current (SCC)

The short circuit current (SCC) is a measure for the total net amount of ions that a healthy epithelium transfers across the epithelial barrier. When a counter current of this exact amount is given, this natural current is “short-circuited” or eliminated. This means that any transported current must be actively transported, eliminating any passive transfer.

During the experiments, the SCC is recorded at any given time, as it represents the “baseline

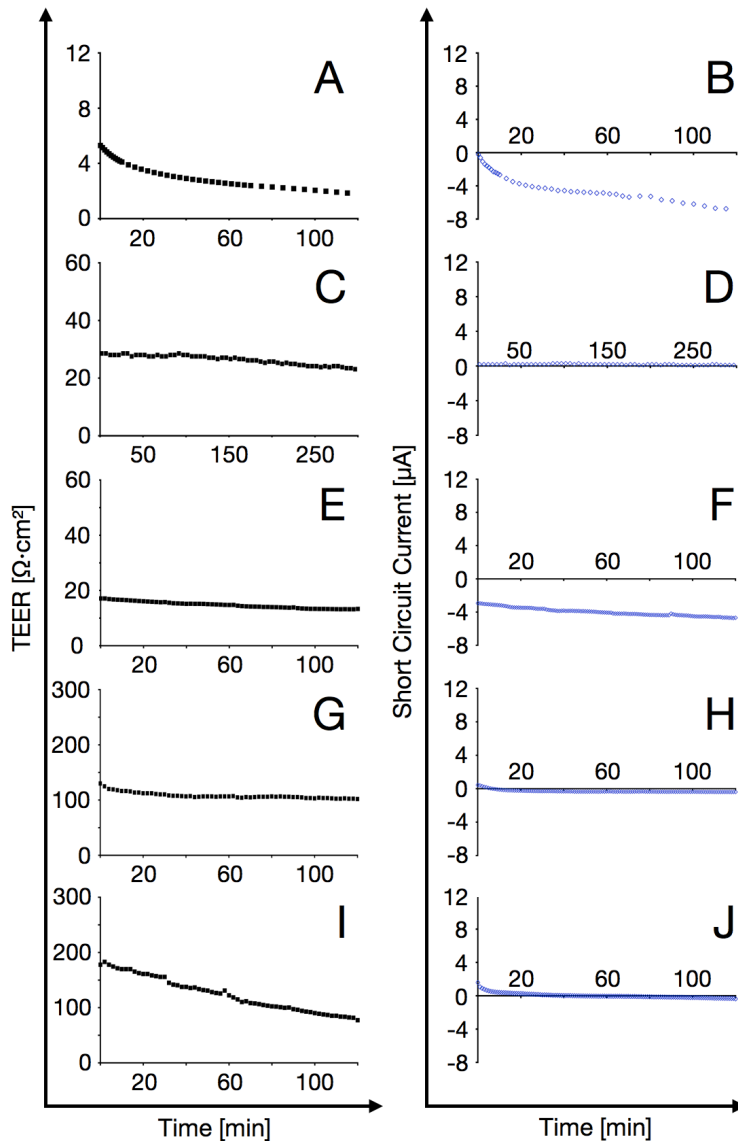


Figure 3-11: TEER and the corresponding short circuit current. A-B: Unchlorified electrodes were used with 80 g/cm² paper as a membrane. **C-D:** Chlorified Electrodes and punctured *Parafilm* as membrane. **E-F:** Sclera as membrane. **G-H:** Retina/RPE/Sclera tissue as membrane. **I-J:** RPE as membrane with declining TEER. Black color on left indicates TEER blue color on right indicates SCC.

current” that gets subtracted from the current pulses, as it can change over time. When unchlorified electrodes in combination with paper as membrane replacement were used, the SCC declined within the first 20 minutes by 4 μA and over a time period of 120 minutes by 7 μA (Fig. 3-11 A-B). In the following experiments only chlorified electrodes were used.

When the punctured *Parafilm* was used as a membrane, the SCC remained constant. This showed that the chlorification of the electrodes is essential. Here the term SSC is not accurate, because the change in current derives from the constant uptake of Cl^- on one electrode that is fast in the beginning and then slows down.

A similar but attenuated effect is seen if the electrodes are not sufficiently chlorified. This was the case when either sclera, Retina/

RPE/Sclera or RPE were used. The SSC was not greater than 1.5 μA over a time period of 2 hours, while changes in TEER did not have any effect on the SSC (Fig 3-11 C-J). Figure 3-11 F shows that the initial SSC of sclera was below zero, indicating that it was not adjusted to zero, because sclera has no ion transporting capability, hence it was not necessary.

To minimize the effect of electrode “autochlorification”, electrodes were placed in their opposite direction after every second experiment.

3.1.4.4 Evaluation of Small Amounts of Medium Leakage Through the Half-Chambers

On some occasions a leak of medium was observed between the two half-chambers. This leak would either fill the insert with medium or drip down. When this was noticed, the chambers were tightened. There were no apparent consequences on the TEER (Fig. 3-12), so that it was decided that the data could be used for analysis as long as no change in medium volume was seen.

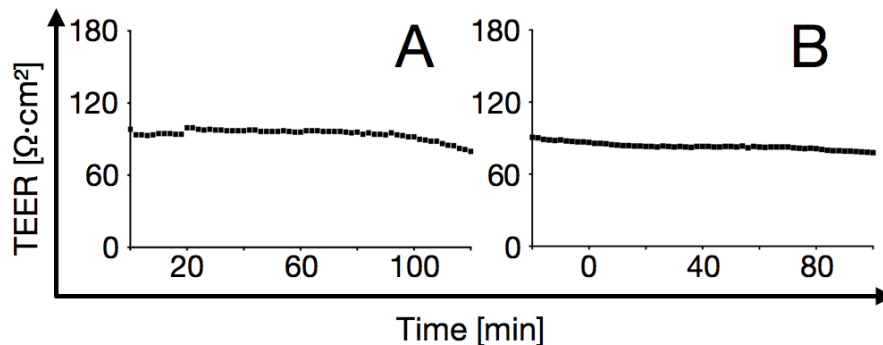


Figure 3-12: Influence of medium leaking from the Ussing chamber on the TEER. In both shown cases small amounts of liquid were detected below the Ussing half-chambers. After the system was tightened, this could cause a minor shift in TEER (A), or no change in TEER (B).

3.1.4.5 Avoiding Immediate Changes in the TEER After Apical Substance Application

In the early phase of substance application to the apical side of the RPE bathing solution, 500 μl of medium were apically removed, mixed with the respective substance and replaced. In a number of these experiments, an immediate change in TEER was noticed. Detailed analysis showed that the removal and replenishing of 500 μl medium not only resulted in a

shift of the TEER over time, but that it also transiently changed the TEER at the time-point of application (Fig. 3-13). This phenomenon was avoided by removing only 200 μl , which were then mixed with the respective substance before they were carefully placed back into the half-chamber.

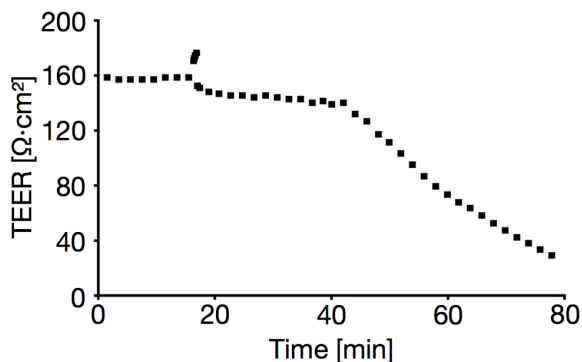


Figure 3-13: Effect of the removal of 500 μl medium from the apical bathing medium. A transient increase of TEER is noted followed by a reduction in TEER upon replenishing the same amount of medium. At t_{40} the TEER decreases abruptly. The cause for this is not entirely clear, but may be linked to changes in the gas distribution (refer to section 3.1.6).

3.1.5 Application of IL-1 β to the Apical Bathing Solution Using DMEM

After the physical parameters were improved, IL-1 β in a final concentration of 10 and 50 ng/ml or their respective control (0.1% BSA in PBS) were added to the apical bathing solutions of the RPE. The substances were added 20 minutes after measurements had started and were continued for a total of 80 minutes. The last time point before application was defined as t_0 , while this value represents 20 minutes after the first data point was collected.

The TEER started to decline about 20 minutes after application of the control. A significant difference was seen between t_0 and t_{60} (Fig. 3-14 A). The mean TEER at t_0 was $118 \pm 8 \Omega\cdot\text{cm}^2$ and the decline toward t_{60} was 40%.

When IL-1 β was added with a final concentration of 10 ng/ml, 20 minutes after the first measurement, the mean TEER at t_0 was $109 \pm 4 \Omega\cdot\text{cm}^2$, a statistical significance between the time of application (t_0) and t_{20} was observed which continued until t_{60} . The overall variability of the measured values was very small (Fig. 3-14 B). The overall drop in TEER was 44%. The data resulting from the final concentration of 50 ng/ml IL-1 β in the apical solution showed a statistical significance between t_0 and t_{30} that continued until t_{60} (Fig. 3-14 C). The mean TEER at t_0 was $143 \pm 11 \Omega\cdot\text{cm}^2$ and the overall drop of TEER was 68% at t_{60} .

When comparing the values of the 10 and 50 ng/ml IL-1 β applications to their controls, no significant difference was observed between equal time points (Fig. 3-14 D, E), while the time points -10, 0 and 10 showed a significant difference when comparing the 10 with the 50 ng/ml values (Fig. 3-14 F).

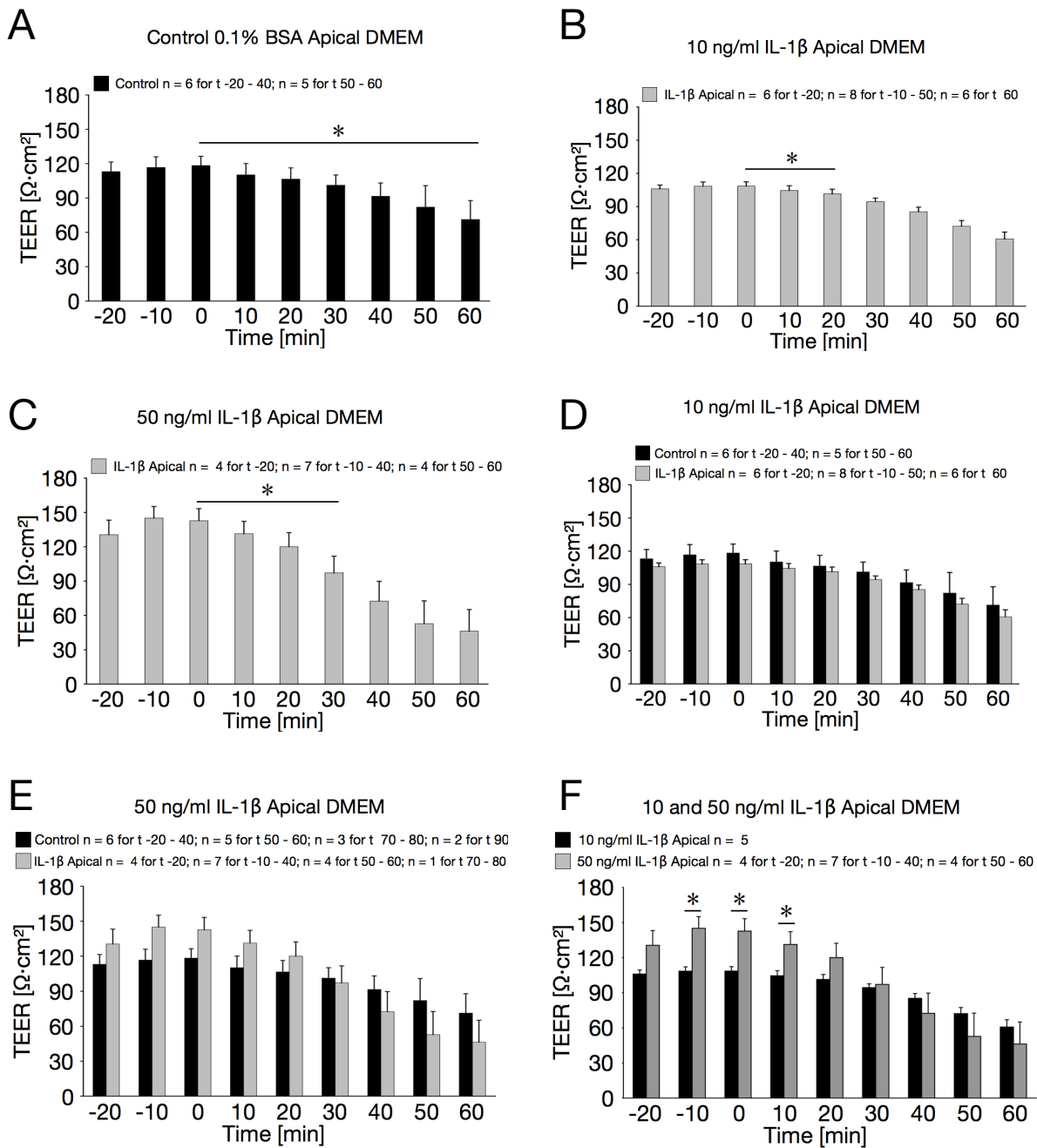


Figure 3-14: Apical application of IL-1 β using DMEM to the RPE/choroid explant. A: Application of the carrier control 0.1% BSA in PBS. **B:** Apical application of 10 ng/ml IL-1 β . **C:** Apical application of 50 ng/ml IL-1 β . **D:** Comparison between the control and 10 ng/ml IL-1 β shows no significant differences. **E:** Comparison between the control and 50 ng/ml IL-1 β shows no significant differences. **F:** Comparison between 10 ng/ml IL-1 β and 50 ng/ml IL-1 β shows differences at three time points. All applications were done 20 minutes after the initial TEER value was recorded. Asterisks indicate statistical significance $p < 0.05$. In **B** and **C** only the first stat. significant value is noted; all following time points are also stat. significant. Error bars are expressed as s.e.m.

3.1.6 Changes in Gas Delivery to the Ussing Chamber

The results of the experiments using DMEM showed a decrease in TEER of 40% in the control conditions. One explanation involved the application of gas to keep the medium oxygenated and the pH stable. The experimental setup made it very difficult to keep the gas flow constant, which had caused problems. The gas flow had either stopped or slowed down, while attempts to restart or adjust the gassing sometimes caused the RPE to rupture and the TEER to drop immediately (Fig. 3-15). Therefore the route of gas application was changed from the designated channels of the Ussing chamber to a diffusion exchange through the surface of the bathing medium, while a *Parafilm* seal was used to hold the gas tubes in place and to minimize evaporation.

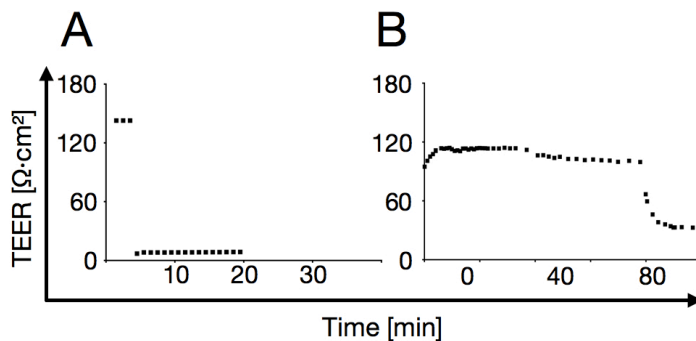


Figure 3-15: Use of designated gas channels in the Ussing chamber leads to immediate TEER reduction when gas flow adjustments are required. A: The gas was connected at the beginning of the experiment. Its onset at t_4 led to the complete breakdown of TEER. **B:** The gas flow had stopped during the measurement and was restarted after 78 minutes.

3.1.7 Establishing the RPE-Ringer Solution as Medium of Choice

To further improve the method, the medium was changed to a modified Ringer solution, henceforth called RPE-Ringer. The measured osmolarity of the medium was 286 ± 5 mOsm

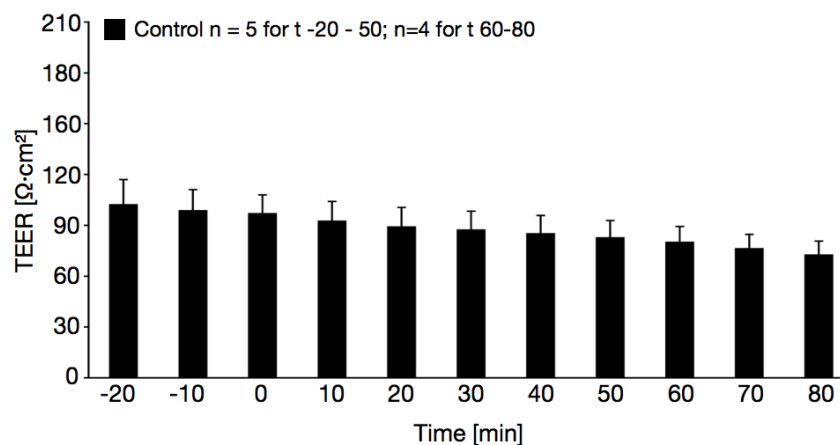


Figure 3-16: TEER values using RPE/choroid explant in RPE-Ringer solution over a period of 100 minutes. No significant differences were observed during this time period, while the TEER decreased by 25% between t_0 and t_{80} . Error bars are expressed as s.e.m.

for all of the experiments. During the first experiments using RPE-Ringer as medium, the TEER of the RPE explant showed a decrease of 17% after 60 minutes (Δt_{60}) and 25% after 80 minutes (Δt_{80}) (Fig. 3-16 and table 3-1), which was an indication that the RPE-Ringer was better suited than DMEM. The mean TEER value at t_0 was $97 \pm 11 \Omega \cdot \text{cm}^2$. The low success rate of 29% (5/18 samples) was not seen as problematic. This value did not display the specific success rate objectively, but instead gave a general summary of all experiments that were started.

3.1.8 Summarizing the Establishing Phase of the Ussing Chamber Assay

The results obtained during the establishing phase providing valuable insight into the details of the experimental conditions.

It was established that the lack of Ca^{2+} led to an immediate reduction of TEER using medium lacking Ca^{2+} or adding EDTA.

Criteria for data exclusion were established stating that **a)** TEER values had to be $\geq 69 \Omega \cdot \text{cm}^2$ within the initial 20 minutes of the experiment and **b)** TEER must not decrease more than $20 \Omega \cdot \text{cm}^2$ within the first 20 minutes.

It was shown that staining of actin could not discriminate between the variability of TEER values if the sheets were intact, while staining using *SYTOX Orange* showed that no dead RPE cells could be detected after an experiment lasting 100 minutes.

The temperature within the chamber was found to be stabilized at $35 \pm 1 \text{ }^\circ\text{C}$ and the conditions to obtain this temperature with the smallest timely delay were found. Artifacts such as immediate changes of TEER after application were identified and eliminated by reducing the mixing volume. Finally, control substance and IL-1 β were applied to the apical bathing solution and the results showed that the system was not sensitive enough to detect differences between control and experimental group, while there was a significant decrease of TEER within the time span of the experiments (minimum 40%). The way the medium was gassed to assure a physiological pH 7.4 was changed. This assured continued gas flow and stable pH. Simultaneously the medium was changed to a modified RPE-Ringer solution. The results showed a decrease in TEER within the same time period, but an improvement by 2.4 fold or a total decrease of 17%. These conditions were seen as a significant improvement. A schematic overview of the final Ussing chamber set-up is shown in figure 3-17.

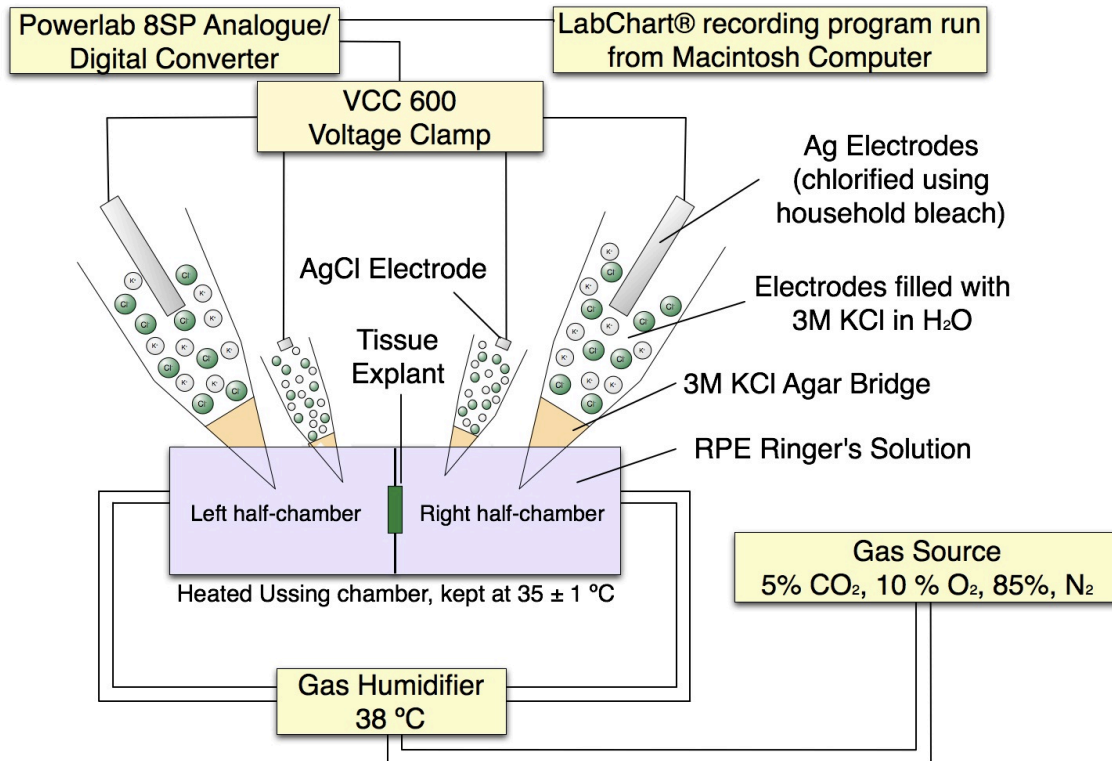


Figure 3-17: Schematic overview of the Ussing chamber set-up and associated equipment after the establishing phase.

3.2 Experiments Using the Established Ussing Chamber Assay

After the modified condition showed promising results, it was decided to repeat the experiments in which IL-1 β was applied apically. First the application of the control substance was established.

3.2.1 Application of Control to the Apical Bathing Solution of the RPE Explant

When the carrier control experiments were performed using the RPE-Ringer, the mean TEER value at t_0 was $103 \pm 20 \Omega \cdot \text{cm}^2$, wherein t_0 refers to the last time-point before substance application. The first measured recording was taken 20 minutes prior to substance application (t_{-20}). No significant difference was observed between t_0 and any other time point (Fig. 3-18 A). The overall decline in TEER between t_0 and t_{60} was 16%, and between t_0 and t_{80} it was 34%. Compared to the experiments using DMEM, this was an improvement of system stability, where a statistical difference was observed between t_0 and t_{60} (Fig. 3-14 A) and the TEER decline was at 40% after 60 minutes.

3.2.2 Application of IL-1 β (50 ng/ml) to the Apical Bathing Solution of the RPE Explant

A baseline TEER at t_0 of $117 \pm 3 \Omega \cdot \text{cm}^2$ was observed for the experiments in which IL-1 β in a final concentration of 50 ng/ml was added to the apical bathing solution. Between time-points t_0 and t_{80} , as well as between t_{-10} and t_{70} a significant difference was found (Fig. 3-18 B) while the DMEM measurements showed a significance between t_0 and t_{30} . The overall decline in TEER at t_{60} was 22% and at t_{80} was 27%, compared to 68% with DMEM at t_{60} . When comparing the control and the 50 ng/ml IL-1 β application, no significant difference between the paired time points was observed (Fig. 3-18 C).

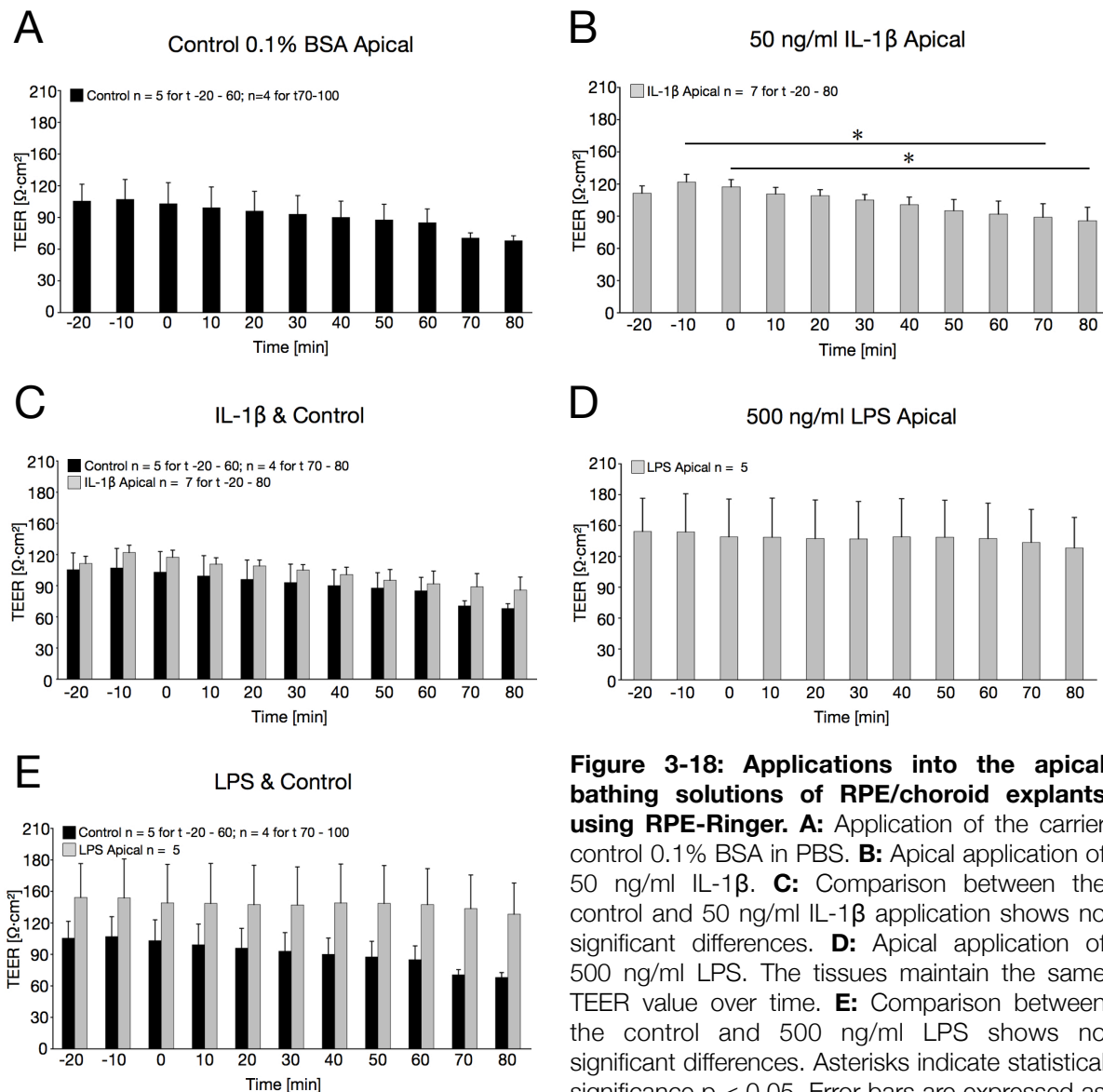


Figure 3-18: Applications into the apical bathing solutions of RPE/choroid explants using RPE-Ringer. **A:** Application of the carrier control 0.1% BSA in PBS. **B:** Apical application of 50 ng/ml IL-1 β . **C:** Comparison between the control and 50 ng/ml IL-1 β application shows no significant differences. **D:** Apical application of 500 ng/ml LPS. The tissues maintain the same TEER value over time. **E:** Comparison between the control and 500 ng/ml LPS shows no significant differences. Asterisks indicate statistical significance $p < 0.05$. Error bars are expressed as s.e.m.

3.2.3 Application of LPS (500 ng/ml) to the Apical Bathing Solution

In an additional test of the RPE system, it was decided to check for an effect of lipopolysaccharide (LPS) on RPE cells. LPS dissolved from *E. coli* in a final concentration of 500 ng/ml was added to the apical bathing solution 20 minutes after the recordings were started. Mean TEER at t_0 was $139 \pm 37 \Omega \cdot \text{cm}^2$. The decline in TEER between t_0 and t_{60} was 1% and between t_0 and t_{80} 8% (Fig. 3-18 D). These were the most stable TEER values observed of any given experimental settings. No significant difference was observed between the LPS application and its control (Fig. 3-18 E).

Table 3-1: Overview of the TEER values of RPE/choroid explants at different time points using DMEM and RPE-Ringer media. The last time point before application was defined as t_0 ; this value represents 20 minutes after the first data point was collected. Δt_{60} and Δt_{80} represent the differences between t_{60} and t_0 or t_{80} and t_0 respectively. Differences are given as percentage and absolute TEER value. Success rate describes the amount of experiments whose results were considered for analysis, vs. those that were eliminated based on the exclusion criteria. 46% (6/13) means that 6 experiments were considered, whereas 13 had been begun. In all cases the first 20 minutes were counted as -20 and -10. Therefore the t_0 reflects the last measured value before application, while in case of Ringer no application, no substance was added at this time point.
* The success rate of these experiments is not objective because the 18 samples were not foreseen for this experiment, but when a low initial TEER was seen, no substance or control was added.

	t_0	t_{60}	t_{80}	Δt_{60}	Δt_{80}	Success rate
DMEM control	$118 \pm 8 \Omega \cdot \text{cm}^2$	$71 \pm 17 \Omega \cdot \text{cm}^2$	NA	40 % 47 $\Omega \cdot \text{cm}^2$	NA	46% (6/13)
DMEM 10 ng/ml IL-1β	$109 \pm 4 \Omega \cdot \text{cm}^2$	$61 \pm 6 \Omega \cdot \text{cm}^2$	NA	44 % 48 $\Omega \cdot \text{cm}^2$	NA	50% (8/16)
DMEM 50 ng/ml IL-1β	$143 \pm 11 \Omega \cdot \text{cm}^2$	$46 \pm 19 \Omega \cdot \text{cm}^2$	NA	68 % 97 $\Omega \cdot \text{cm}^2$	NA	64% (7/11)
Ringer no application	$102 \pm 15 \Omega \cdot \text{cm}^2$ n = 5	$85 \pm 11 \Omega \cdot \text{cm}^2$ n = 5	$86 \pm 9 \Omega \cdot \text{cm}^2$ n = 5	17% 17 $\Omega \cdot \text{cm}^2$	25% 24 $\Omega \cdot \text{cm}^2$	* 29% (5/18)
Ringer control	$103 \pm 20 \Omega \cdot \text{cm}^2$ n = 5	$85 \pm 13 \Omega \cdot \text{cm}^2$	$68 \pm 5 \Omega \cdot \text{cm}^2$	18 % 18 $\Omega \cdot \text{cm}^2$	34 % 35 $\Omega \cdot \text{cm}^2$	45 % (5/11)
Ringer 50 ng/ml IL-1β	$117 \pm 7 \Omega \cdot \text{cm}^2$ n = 7	$92 \pm 12 \Omega \cdot \text{cm}^2$	$86 \pm 13 \Omega \cdot \text{cm}^2$	22 % 25 $\Omega \cdot \text{cm}^2$	27 % 32 $\Omega \cdot \text{cm}^2$	78 % (7/9)
Ringer 500 ng/ml LPS	$139 \pm 37 \Omega \cdot \text{cm}^2$ n = 5	$137 \pm 34 \Omega \cdot \text{cm}^2$	$128 \pm 30 \Omega \cdot \text{cm}^2$	1 % 2 $\Omega \cdot \text{cm}^2$	8 % 11 $\Omega \cdot \text{cm}^2$	71 % (5/7)

Table 3-1 gives a summary of the described values and highlights that the change in medium from DMEM to RPE-Ringer lowered the TEER decline over a time period of 60 minutes in all cases and allowed the measurements to continue until t_{80} without dramatic TEER decline.

The success rates depict those experiments that were considered for analysis from the total of all started experiments in the specific group. The change of Ringer and gassing methods improved the overall rate except in Ringer control, which can be linked to technical difficulties.

3.3 Retaining the Retina and Sclera on the RPE Sheets

The results using RPE sheets with RPE-Ringer solution had been an improvement compared to the DMEM experiments. To further minimize the TEER decline, a change was introduced that stabilized the TEER values. The RPE explant had been obtained by removing the sclera and retina, however after retina removal, a number of pigments were seen on the retina that may have caused possible damage (Fig. 3-19). To avoid this additional stress factor on the RPE, the retina was retained on the RPE.

3.3.1 Measuring the TEER of the Retina/RPE/Sclera (RRS) Explant

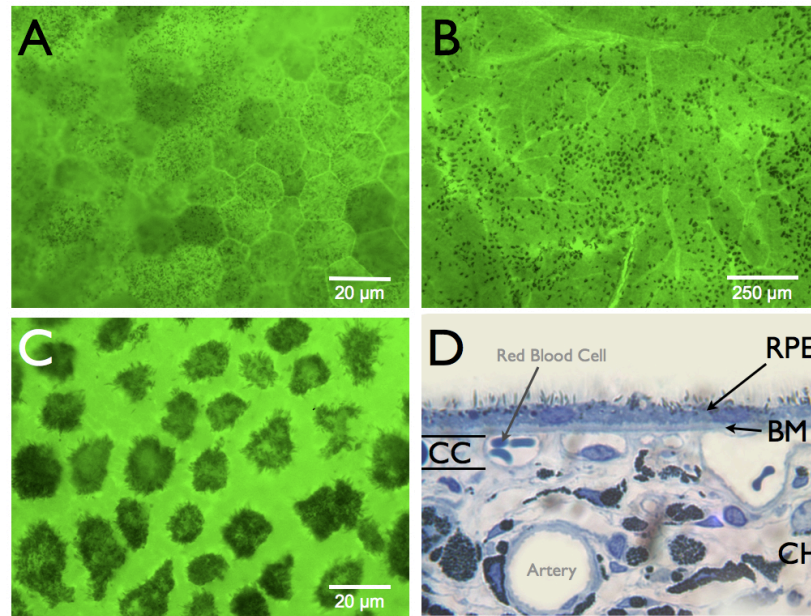


Figure 3-19: Micrograph of RPE and retina individually after retina removal. A: Actin staining reveals an intact RPE sheet, while little black dots are melanosomes within the RPE, especially in the microvilli. **B:** Actin staining of the retina highlights retinal vessels and melanosomes. **C:** Magnification of B reveals that the pattern has the same size as the RPE cells. **D:** Toluidin-blue cross section of RPE and choroid after retinal removal shows that a large fraction of the microvilli are still present on the RPE. BM: Bruch's membrane, CC: choroid capillaries, CH: choroid. Magnification: 20 x (**D**). A, B, C pseudo-color.

A Retina/RPE/Sclera (RRS) tissue complex was extracted and the TEER was recorded. Its mean TEER at t_0 was $147 \pm 11 \Omega \cdot \text{cm}^2$. For these and the following experiments (retina/RPE, RPE, retina, sclera) t_0 represents the first value at the initiation of the measurements, because no substance was added. The decline of TEER after 80 minutes was 2% and after 120 minutes 15% (Fig. 3-20 A and table 3-2). The overall TEER values showed little variability and the success rate was at 80%. In order to compare these values to the previous results, the t_{20} value needs to be considered. Table 3-3 lists the data that can be compared to the values of the previous application experiments. The t_{20} value of this series is equivalent to the t_0 of the experiments with application. The t_{80} compares to t_{60} and t_{100} to t_{80} , respectively.

3.3.2 Measuring the TEER of the Retina/RPE (RR) Explant

The results of the Retina/RPE (RR) complex are shown in figure 3-20 B. The mean TEER value at t_0 was $192 \pm 12 \Omega \cdot \text{cm}^2$, with a decline in TEER of 9% after 120 minutes. Interestingly the t_{10} value was 10% greater than the t_0 value. The increase of TEER in this set of

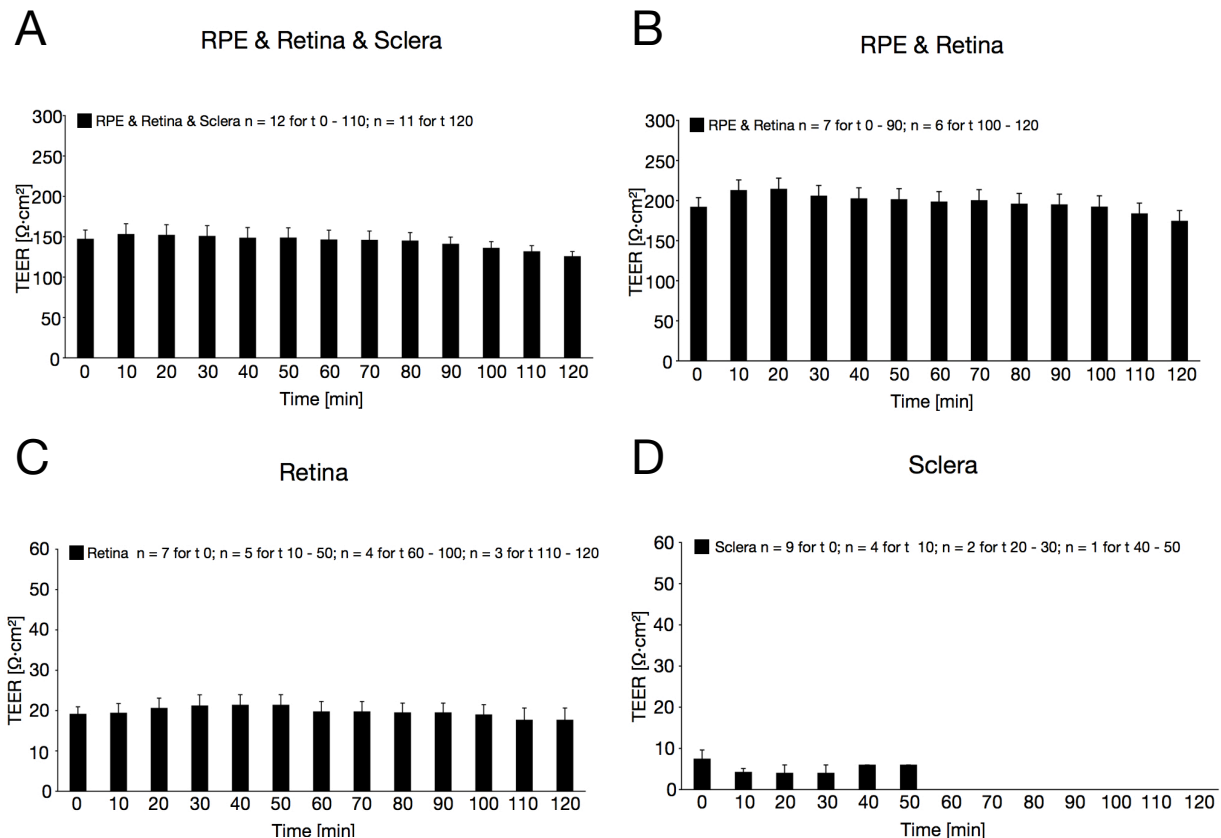


Figure 3-20: TEER values of RPE tissues including retina with or without sclera and individual retina and sclera values. A: RPE/Retina/Sclera explant. **B:** RPE/Retina explant. **C:** Retina. **D:** Sclera. Numbers varied over the time course of the recorded values as noted in the charts. The recordings of sclera were not continued for the full time period. Error bars are s.e.m.

experiments stressed the importance of giving the cells an equilibration time of 10-20 minutes before applying any substance.

Table 3-2: Overview of the TEER values at different time points using RRS (Retina/RPE/Sclera) and RR (Retina/RPE). t_0 is defined as initial measured value. Δt_{80} and Δt_{120} represent the differences between t_{80} and t_0 or t_{120} and t_0 respectively. Differences are given as percentage and absolute TEER value. Success rate describes the amount of experiments whose results were considered for analysis, vs. those that were eliminated based on the exclusion criteria. 80% (12/15): 12 experiments qualified for analysis, 15 had been started in total.

	t_0	t_{80}	t_{120}	Δt_{80}	Δt_{120}	Success rate
RRS	$147 \pm 11 \Omega \cdot \text{cm}^2$ n = 12	$145 \pm 10 \Omega \cdot \text{cm}^2$ n = 12	$126 \pm 6 \Omega \cdot \text{cm}^2$ n = 11	2 % $2 \Omega \cdot \text{cm}^2$	15 % $22 \Omega \cdot \text{cm}^2$	80 % (12/15)
RR	$192 \pm 12 \Omega \cdot \text{cm}^2$ n = 7	$196 \pm 13 \Omega \cdot \text{cm}^2$ n = 7	$175 \pm 13 \Omega \cdot \text{cm}^2$ n = 6	-2 % $-4 \Omega \cdot \text{cm}^2$	9 % $18 \Omega \cdot \text{cm}^2$	64 % (7/11)
Retina	$19 \pm 2 \Omega \cdot \text{cm}^2$ n = 7	$20 \pm 2 \Omega \cdot \text{cm}^2$ n = 4	$18 \pm 3 \Omega \cdot \text{cm}^2$ n = 3	-2 % $-1 \Omega \cdot \text{cm}^2$	7 % $-1 \Omega \cdot \text{cm}^2$	N/A
Sclera	$7 \pm 2 \Omega \cdot \text{cm}^2$ n = 9	N/A	N/A	N/A	N/A	N/A

Table 3-3: Data of TEER values from Retina/RPE/Sclera (RRS) and Retina/RPE (RR) to facilitate data comparison with the values of the application experiments. Δt_{80-20} and Δt_{100-20} represent the differences between t_{80} and t_{20} or t_{100} and t_{20} respectively. Differences are given as percentage and absolute TEER value.

	t_{20}	t_{80}	t_{100}	Δt_{80-20}	Δt_{100-20}	Δt_{120-20}
RRS	$152 \pm 13 \Omega \cdot \text{cm}^2$ n = 12	$145 \pm 10 \Omega \cdot \text{cm}^2$	$136 \pm 8 \Omega \cdot \text{cm}^2$	5 % $7 \Omega \cdot \text{cm}^2$	11 % $16 \Omega \cdot \text{cm}^2$	18 % $27 \Omega \cdot \text{cm}^2$
RR	$214 \pm 14 \Omega \cdot \text{cm}^2$ n = 7	$196 \pm 13 \Omega \cdot \text{cm}^2$	$192 \pm 14 \Omega \cdot \text{cm}^2$	9 % $18 \Omega \cdot \text{cm}^2$	10 % $22 \Omega \cdot \text{cm}^2$	19 % $40 \Omega \cdot \text{cm}^2$

3.3.3 Individual TEER Values of Retina and Sclera

The individual measurements of retina showed an initial TEER of $19 \pm 2 \Omega \cdot \text{cm}^2$, which remained very stable over the recorded time period (Fig. 3-20 C). The TEER of sclera was not measured over a prolonged time. The initial value was at $7 \pm 2 \Omega \cdot \text{cm}^2$, while one data point was more than 3 times the value of the average values with an average TEER of $5 \Omega \cdot \text{cm}^2$ between t_{10} and t_{50} as shown in figure 3-20 D.

3.3.4 Comparing the Individual Tissues

Figure 3-21 shows an overview of the different tissue resistances. The first 15 minutes of each measurement were considered and the values are displayed as mean. The first 15 minutes were chosen for this overview to be able to obtain sufficient values to reach a stable value for RPE/choroid explants. The RPE values were derived from experiments without application, or from the time period prior to application of any substance. A highly significant difference was found between the Retina/RPE/Sclera ($152 \pm 12 \Omega \cdot \text{cm}^2$) and the Retina/RPE tissues ($209 \pm 13 \Omega \cdot \text{cm}^2$) as well as between the Retina/RPE and RPE ($133 \pm 7 \Omega \cdot \text{cm}^2$) (for both $p < 0.01$), while the difference between retina ($19 \pm 2 \Omega \cdot \text{cm}^2$) and sclera ($7 \pm 2 \Omega \cdot \text{cm}^2$) is also significant ($p < 0.01$). Highly significant is also the difference between RPE, RRS and RR compared to these two tissues. The high TEER of the Retina/RPE sample was unexpected.

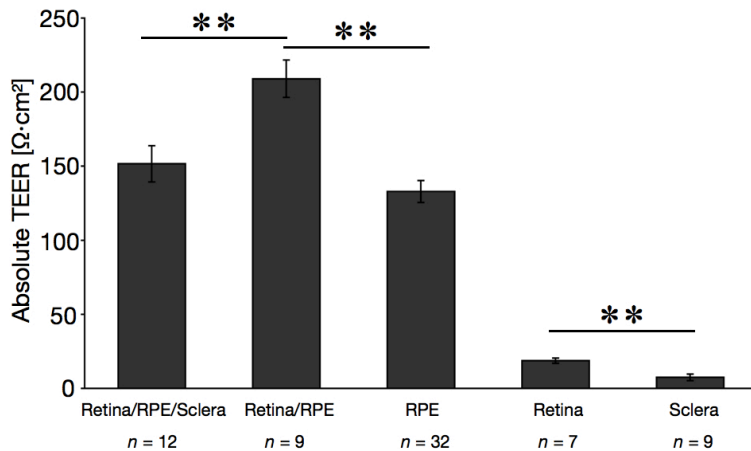


Figure 3-21: Comparison of the TEER values of the examined tissues of the eye. The values of the first 15 minutes of the respective tissues were analyzed and the average calculated to obtain the TEER values. No significance was found between Retina/RPE/Sclera and RPE tissues. All tissues including RPE were highly significant to either retina or sclera (not indicated by asterisks) ** Represents $p < 0.01$. Error bars represent s.e.m.

3.4 Evaluation of Fluorescein Transport Across the RPE Barrier

To examine the permeability of the barrier of the tissues with their differing TEER values, the transport of fluorescein (10 mg/ml) from the apical to the basolateral side was evaluated.

The TEER values of these experiments are displayed in figure 3-22 and table 3-4. They were in line with those of the previous ones with the Retina/RPE reaching the greatest measured values of $230 \pm 10 \Omega \cdot \text{cm}^2$, and the RRS showing very consistent TEER. Interestingly the initial TEER of RPE was greater than the one from RRS ($193 \pm 41 \Omega \cdot \text{cm}^2$ and $116 \pm 14 \Omega \cdot \text{cm}^2$ respectively), while the TEER of RPE alone decreased rapidly. 60% of the RPE/choroid experiments had to be discarded because the chamber was leaky.

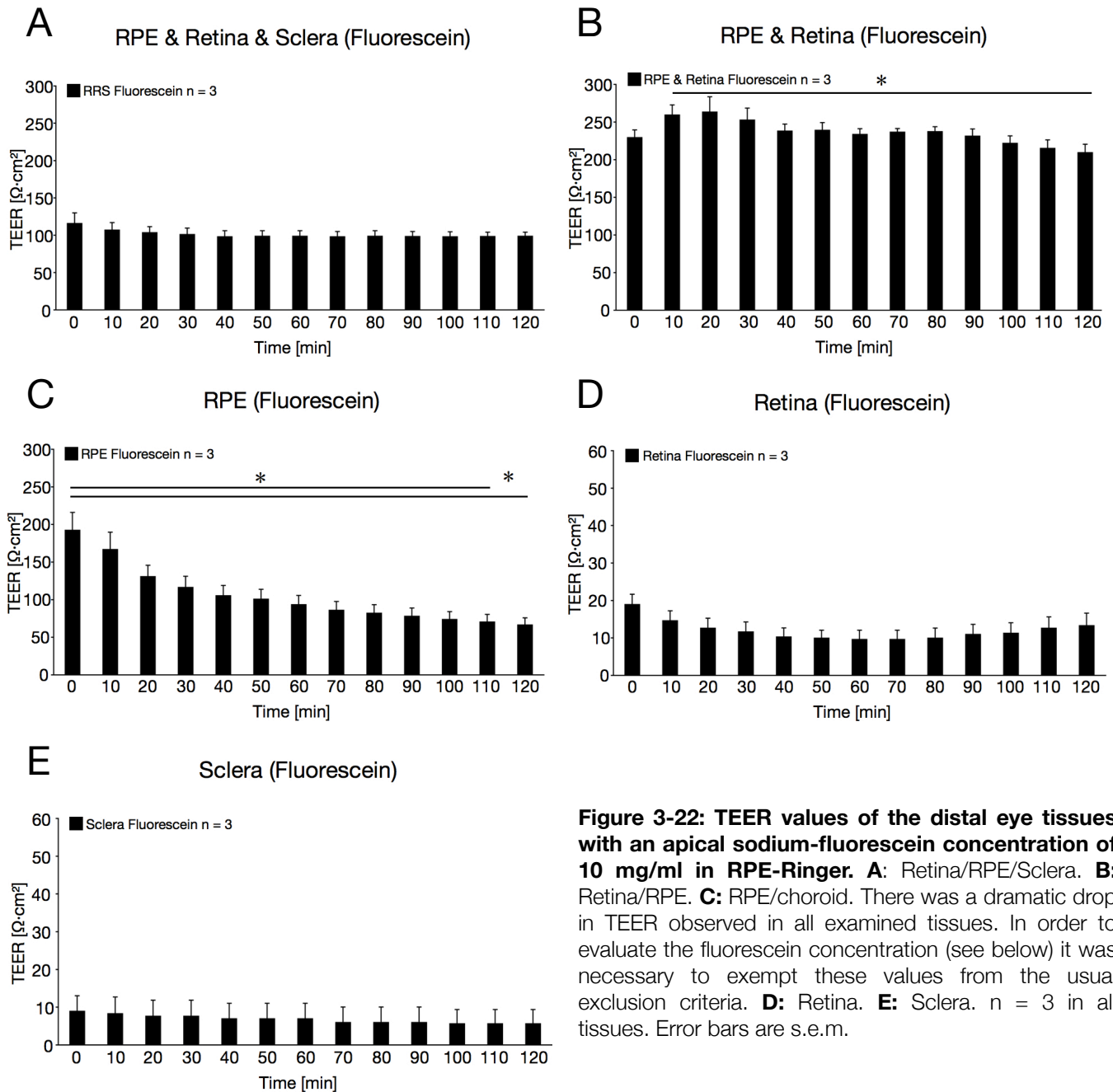


Figure 3-22: TEER values of the distal eye tissues with an apical sodium-fluorescein concentration of 10 mg/ml in RPE-Ringer. A: Retina/RPE/Sclera. **B:** Retina/RPE. **C:** RPE/choroid. There was a dramatic drop in TEER observed in all examined tissues. In order to evaluate the fluorescein concentration (see below) it was necessary to exempt these values from the usual exclusion criteria. **D:** Retina. **E:** Sclera. $n = 3$ in all tissues. Error bars are s.e.m.

The high TEER values of the RR tissue did not correlate with a low fluorescein concentration in the basolateral medium as expected. Instead the medium obtained from the basal RPE/Retina chamber held significantly greater concentrations of fluorescein than the RRS chamber at t_{60} , t_{90} and t_{120} (Fig. 3-23 and table 3-5). The fluorescein concentration of the RR samples was also significantly greater than that of the RPE medium at t_{60} . In contrast, the medium of the RPE samples at t_{30} and t_{60} showed the lowest fluorescein concentrations of

any measured tissue. While the increases in basolateral fluorescein concentration in RRS and RR were highly linear ($r^2 = 0.9997$ and $r^2 = 0.9999$), the increase for RPE was less linear ($r^2 = 0.95$).

Table 3-4: Overview of TEER values during the evaluation of the RPE barrier using 10 mg/ml sodium fluorescein in the apical bathing solution. t_0 represents the first measurement of the series, while Δt_{80-20} and Δt_{120-20} show the changes of the t_{80} and t_{120} value compared to t_{20} . The t_{20} value was chosen to make comparisons to previous results more consistent. Differences are given as percentage and absolute TEER value.

	t_0	t_{20}	t_{80}	t_{120}	Δt_{80-20}	Δt_{120-20}
RRS	116 ± 14 $\Omega \cdot \text{cm}^2$ $n = 3$	104 ± 8 $\Omega \cdot \text{cm}^2$ $n = 3$	99 ± 7 $\Omega \cdot \text{cm}^2$	99 ± 5 $\Omega \cdot \text{cm}^2$	15 % $17 \Omega \cdot \text{cm}^2$	15 % $17 \Omega \cdot \text{cm}^2$
RR	230 ± 10 $\Omega \cdot \text{cm}^2$ $n = 3$	264 ± 20 $\Omega \cdot \text{cm}^2$ $n = 3$	238 ± 6 $\Omega \cdot \text{cm}^2$	210 ± 11 $\Omega \cdot \text{cm}^2$	10 % $26 \Omega \cdot \text{cm}^2$	20 % $54 \Omega \cdot \text{cm}^2$
RPE	193 ± 41 $\Omega \cdot \text{cm}^2$ $n = 3$	131 ± 25 $\Omega \cdot \text{cm}^2$ $n = 3$	82 ± 19 $\Omega \cdot \text{cm}^2$	67 ± 14 $\Omega \cdot \text{cm}^2$	37 % $49 \Omega \cdot \text{cm}^2$	49 % $64 \Omega \cdot \text{cm}^2$
Retina	19 ± 3 $\Omega \cdot \text{cm}^2$ $n = 3$	13 ± 3 $\Omega \cdot \text{cm}^2$ $n = 3$	10 ± 3 $\Omega \cdot \text{cm}^2$	13 ± 3 $\Omega \cdot \text{cm}^2$	20 % $3 \Omega \cdot \text{cm}^2$	0 % $0 \Omega \cdot \text{cm}^2$
Sclera	9 ± 4 $\Omega \cdot \text{cm}^2$ $n = 3$	8 ± 4 $\Omega \cdot \text{cm}^2$ $n = 3$	6 ± 4 $\Omega \cdot \text{cm}^2$	6 ± 4 $\Omega \cdot \text{cm}^2$	22 % $2 \Omega \cdot \text{cm}^2$	26 % $3 \Omega \cdot \text{cm}^2$

Table 3-5: Basal fluorescein concentration of all measured tissues in $\mu\text{g/ml}$. 200 μl were taken after the indicated time points and photometrically analyzed and compared to the standard to obtain the reported concentrations.

	RRS	RR	RPE	Retina	Sclera
30 min	0.096 ± 0.03	0.175 ± 0.05	0.092 ± 0.04	2.10 ± 0.42	5.02 ± 1.15
60 min	0.474 ± 0.05	0.769 ± 0.06	0.368 ± 0.12	4.87 ± 0.61	11.30 ± 2.26
90 min	0.847 ± 0.08	1.377 ± 0.11	0.881 ± 0.15	7.83 ± 1.52	16.51 ± 3.23
120 min	1.250 ± 0.14	2.003 ± 0.15	1.683 ± 0.22	10.95 ± 1.83	21.23 ± 3.69

As expected the sclera showed the greatest amount of fluorescein in its basal medium, while no significant difference was found between the fluorescein concentrations of retina and sclera (Fig. 3-24). However all retina and sclera values showed significant differences to the tissues including RPE (RRS, RR, RPE). Sclera and retina fluorescein concentration increases were both highly linear as expected ($r^2 = 0.9993$ for retina and $r^2 = 0.9957$ for sclera).

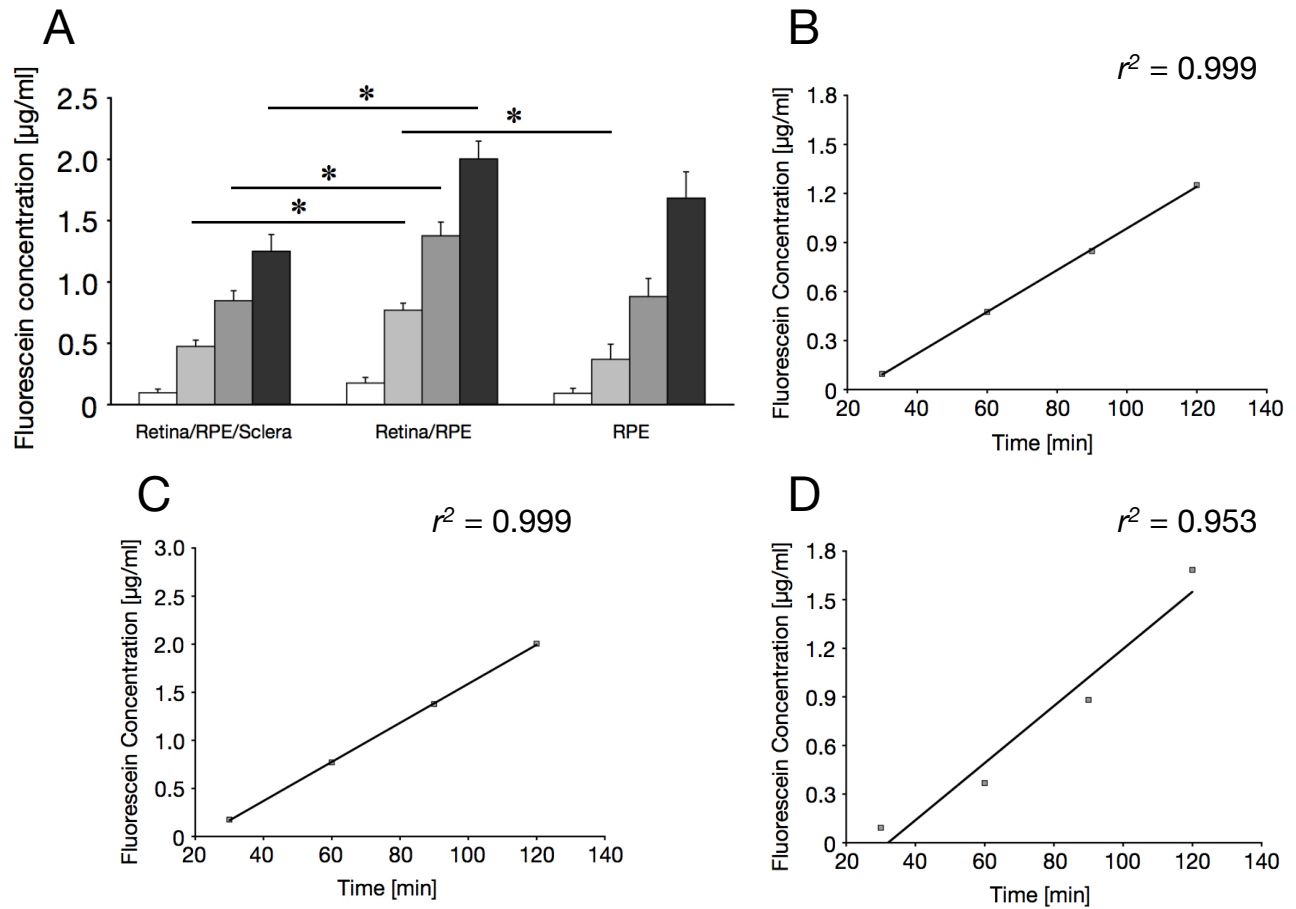


Figure 3-23: Fluorescein concentration of the basal bathing medium of RPE-containing tissues. **A:** Overview of the concentration using RRS, RR and RPE tissues with increasing time points from left to right: white: 30 minutes, light gray: 60 min, intermediate gray: 90 min, dark gray 120 min. Asterisks indicates significance $p < 0.05$. **B.** Linearity of the increase of basal fluorescein concentration in RRS (**B**), RR (**C**) and RPE (**D**). $n = 3$ (**A-D**). Asterisks indicate significance $p < 0.05$.

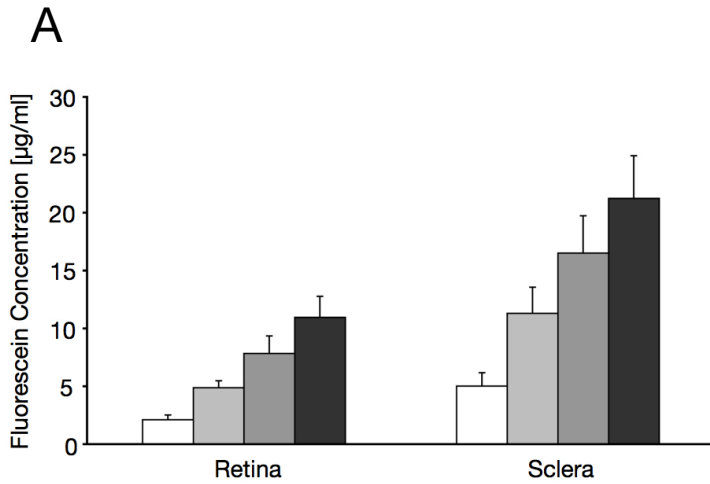
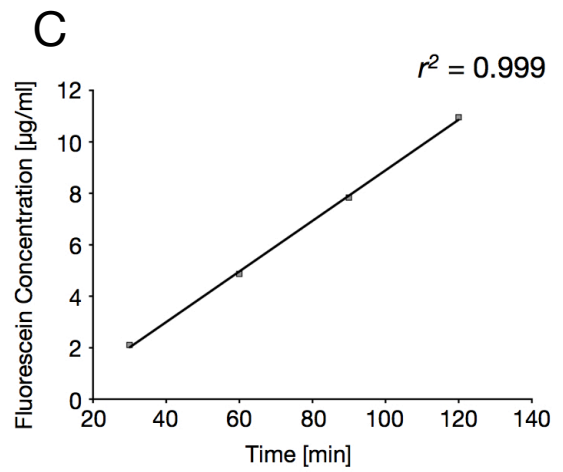
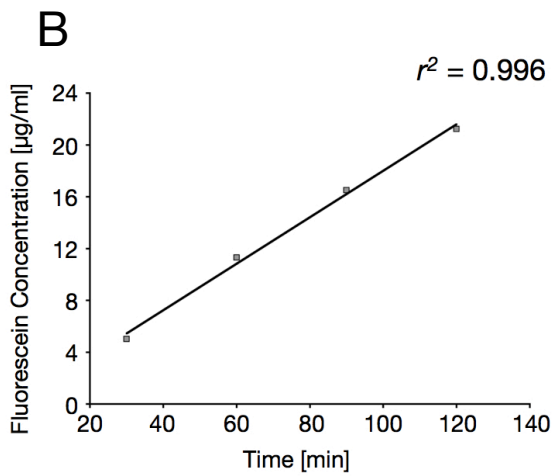


Figure 3-24: Fluorescein concentration of the basal bathing medium of retina and sclera. A: Overview of the concentration using Retina and Sclera with increasing time points from left to right: white: 30 minutes, light gray: 60 min, intermediate gray: 90 min, dark gray 120 min. Student's T-test showed no differences between the values. **B.** Linearity of the increase of basal fluorescein concentration in Retina (**B**) and Sclera (**C**). n = 3 for **A-C**.



4 Discussion

RPE research plays a pivotal role in understanding the underlying mechanism has led to eye diseases such as AMD and DR. Over the years there have been several groups that have used RPE cultures or tissue explants to gain a better understanding of the physiology of RPE. However, there is a great need in the field to obtain a widely accepted and accessible method for attaining that goal.

4.1 Relevant Points of Discussion on the Establishment of a Suitable Ussing Chamber Assay

Data that have led to the assessment on how to improve the system (e.g. IL-1 β application using DMEM and the preceding gas delivery) are not discussed in this section. All relevant conclusions that had been drawn from those experiments are described in the Results section, and the appropriate changes were made and described there. This first part of this discussion is focuses on two crucial aspects of successful implementation in order to evaluate the TEER of rat RPE explants.

4.1.1 Defining a Minimum TEER Value Describing Intact RPE

To evaluate the gathered data, a minimum value expressed in TEER had to be established. for an intact barrier. Data suggested that this value was found in a TEER > 68 Ω ·cm². Tissues with values at this mark remained stable for at least 20 minutes, while TEER values below it rapidly decreased further. Values that remained consistently below this value represented compromised tissues as shown in figure 3-3. The definition of this value was crucial and allowed making clear cuts along recorded values, especially during the early phase when limitations in the dissection method yielded a variety of stable low TEER values. These definitions were established using DMEM medium.

4.1.2 Choice of Medium and Gas

The initial experiments using RPE were done using DMEM as the RPE bathing medium. DMEM is a medium widely used for RPE culture, independent of the species of origin (32, 120, 128, 162). Results showed that during this phase, the system was not suited for comparison studies. The TEER frequently dropped at similar time points in a number of control experiments. The reasons were searched in the medium of choice and one initial explanation was the presence of HEPES (15 mM) in DMEM in combination with the exposure to laboratory light. HEPES was reported to be toxic in thymocyte cultures at a concentration of 25 mM after light exposure for more than 30 minutes (163). In the experimental settings of the Ussing chamber, the HEPES concentration is lower, but the time of exposure is greater. As another possible limiting factor in DMEM, the presence of phenol red in a concentration of 24 μ M was considered. Phenol red has protective properties against ROS production in the RPE and acts as a weak estrogen (164-166). The affinity of phenol red is 0.001% that of estradiol (166), the major estrogen in humans, which is effective at 1 μ M (164). The great differences in concentration led to the conclusion that this component is a less likely to be a possible risk factors for RPE stability.

However, the reasons may not have been the medium itself, but rather in complications in the delivery of the gas intended to maintain a stable pH. The DMEM that was used requires a CO₂ concentration of 3.1% (table 2-1). It was noticed that the use of the gas channels of the Ussing chamber did not allow for a constantly equal gas flow, which made it impossible to assure the pH 7.4 at all times.

When it was decided to change the medium, it was decided to use only basic components and the choice fell on a Ringer solution that was first reported in 1991 and used for bovine tissue explants and later for cell culture of human fetal RPE cells (115, 117). Shortly after the medium was changed, the gassing conditions were addressed, so that the use of the new medium was accompanied by improved stability of gassing delivery. The results showed a general improvement in the stability of the TEER, and were continuously used.

Making adjustments to the medium currently used may be a possibility for further improvements in the stability of the system. However this has not been tested.

4.2 Discussion of the Results After the Ussing Chamber Implementation

Below the experiments are discussed that were conducted after the establishing phase was concluded; reference is made to the data following section 3.2.

4.2.1 Application of IL-1 β to the Apical Bathing Solution (RPE-Ringer) of RPE Explants

In 2008 an article was published describing the presence of IL-1 β receptor 1 on the apical side of human fetal RPE cells in culture (48), which was an exciting indication that IL-1 β may have a direct effect on RPE cells. A possible source of IL-1 β on the retinal side are immune cells resident in the retina, cells of or within the vitreous, RPE itself or infiltrated leukocytes that entered the eye through the retinal vessels. To examine if IL-1 β had an effect on the barrier function of the RPE, it was applied to the apical bathing solution of RPE explants devoid of retina and sclera. No differences between IL-1 β (50 ng/ml) and the control application were observed, and no visible damage to the RPE cells was detectable using actin staining. However the TEER of control and IL-1 β application decreased over the time period of the experiments.

This decrease indicated that the Ussing chamber system was not yet sufficiently stable to detect possible effects of the applied substance on the RPE.

When the retina was more closely examined, it became evident that a great number of microvilli had been compromised during that process of mechanical removal. It is likely that the microvilli are the bearer of the IL-1 β receptors, which would explain the tolerance against IL-1 β . Yet the answer could be much simpler: IL-1 β at the given concentration has no effect on the barrier function of the RPE.

4.2.2 Exposure of the Apical RPE Membrane to LPS

LPS is a major component of the outer membrane of Gram-negative bacteria and is in vision science most commonly used to generate a model of uveitis, an inflammatory disease in which leukocytes infiltrate the eye. In this endotoxin induced uveitis (EIU) LPS is injected into the footpad of a rodent generating a severe inflammatory response especially in the eyes (167). As one of many effects of EIU, infiltrated neutrophils compromise the outer BRB (168).

In contrast to the EIU approach, this study wanted to analyze the direct effect of LPS on the RPE.

Compared to any other application, including the control, the application of LPS seemed to stabilize the TEER. This was not significant, but it showed for the first time that differences in TEER behavior could be detected with this system.

The high values of this series can be traced back to one very high value, while the overall TEER was very stable across the individual measurements. These data suggest that the RPE can detect and react to LPS exposure, which is in line with the reported presence of TLR4, the universal receptor for LPS, on RPE cells (168-170). Yet these publications did not reveal whether TLR4 is located on the retinal or choroidal side of the RPE.

A study by Ishibashi's group (171) showed that IL-6 and VEGF expression increase after LPS stimulation on mouse RPE cell cultures, while this increase is absent in the RPE of TLR4^{-/-} mice. VEGF has been associated with the onset of AMD, and its blockage or capture is the leading therapeutic agent aimed to soothe the effects of AMD, because its inhibition stops the growth of blood vessels (82, 172, 173). While one group suggest that VEGF lowers the TEER of the RPE, another group did not find any changes (120, 131). IL-6, a potent inflammatory cytokine is an attractant of leukocytes and had also been shown to be produced by RPEs in the presence of subtoxic levels of H₂O₂ (174). These reports would lead to the hypothesis that LPS would rather reduce the TEER.

A consolidation of these results is outstanding. However, the presented results indicate that an increase or at least a stabilization of TEER may be an initial reaction of the RPE to exposure to LPS. Prolonged exposure may have different effects.

In an immediate response RPE, which has been shown to bear TLR2, TLR4 and several TLR1s, may actively secure the barrier toward the choroid through which bacteria could gain access to the circulatory system. Keeping bacteria localized in this fashion, they can, for example, become targets for resident macrophages and other leukocytes that respond to the IL-6 stimulus. Possibly RPE could be involved in such a phagocytosis - their ability to take up microorganisms has been reported (175).

The above-mentioned reports and the results presented in this thesis make a closer investigation into the effect of LPS on RPE a promising target for further investigation. As suggested by results that followed this set of experiments (discussed below), the use of RPE explants that include retina and sclera may have great benefits instead of using the RPE explants.

4.2.3 Comparison of the TEER of RPE Explants to Those Including Retina and Sclera

The results of the IL-1 β experiments showed that application of the control substance (0.1% BSA in PBS) to the apical bathing solution of the RPE explant, led to a decrease of the TEER by 18% after an examination time of 60 minutes (Δt_{60} - table 3-1). During the same time period the TEER of RRS decreased by 5% and that of RR by 9% (Δt_{80-20} - table 3-3). After an additional 20 minutes the TEER of the RPE explants had decreased by a total of 34%, compared to 11% of the RRS and 10% of the RR tissues.

Interestingly, the absolute TEER values of RR were significantly greater than those from RRS, which was unexpected and will be discussed in the following section.

The data demonstrated that the stability of the TEER of RRS and RR improved three-fold compared to that of RPE alone. They were also sustainable for longer time periods with a lower decreasing rate.

Based on these results as well as on retinal micrographs showing pigments on the retina, the RPE tissue alone was not considered to represent the physiological nature of the RPE; on the contrary, the RPE tissue can be understood as a condition of trauma.

4.3 Permeability Evaluation Using Sodium-Fluorescein Transport Across the RPE

To assess the permeability of the RPE barrier in a first step, specifically the permeability to small non-ionic molecules, sodium-fluorescein was added to the apical bathing solution, and the basal fluorescein concentration at different time points was measured. The general understanding was that in physiological conditions the TEER is inversely proportional to its permeability (131, 162, 176). In physiological conditions the RPE constantly removes water from the retinal side (39, 51). While this process is complex, it is known that it can be altered. Lowering the pH via an increase of the apical CO₂ concentration induces an increase in fluid transport across the RPE (177, 178).

With no fluorescein-specific receptors that would allow for an active transport of fluorescein, passive or co-transport via the para- or transcellular pathways remains as a possible option.

4.3.1 Fluorescein Transport From Apical to Basal for RPE Tissues Including Retina

The RR tissue, which had the greatest TEER values ($192 \pm 12 \Omega \cdot \text{cm}^2$ at t_0) continuously showed the greatest basal fluorescein concentration of the examined RPE associated tissues. In an apparent discrepancy, however, these experiments did not distinguish between the trans- or paracellular pathway.

To get a better understanding of these results, work by the groups of Matter and Cerejido was consolidated. They reported a similar discrepancy for the permeability of mannitol (182 Da), which is in the same size category as fluorescein (332 Da). When the TJ protein occludin was overexpressed in MDCK II cells, they reported a greater amount of mannitol in the basal bathing solution compared to control, while the TEER was also greatly increased (113). This was explained by a change in the TJ protein conformation, which can fluctuate between open and closed status (113, 114). According to this model, the TEER is a measure for the closed barriers at a given time point, while the paracellular flux is an indicator for permeability over a period of time. The open/closed status was attributed to aqueous channels in each diffusion barrier of the TJ strands.

To determine whether the fluorescein permeability of the experiments of this thesis was regulated by the trans- or paracellular pathway further experiments need to be conducted, which were not done. The Methods article by Balda and Matter gives an excellent overview of discriminating between the two (179). To determine the amount of transcellular pathway, they suggest incubating the RPE with 3-10 mg/ml with horse radish peroxidase (HRP, 44 kDa) for 10 minutes. Other than described in the article, for the rat RPE system, this needs to be done prior to placing the RPE in the Ussing chamber because a successful change of medium without tissue damage has not yet been achieved. For this reason the exclusiveness of the apical transcytosis is not guaranteed and an accurate numerical assessment of the transepithelial transport is not possible. However, the amount of basal release of HRP can be determined after 90-120 minutes by enzymatic reaction and subsequent photometric analysis. What has to be overcome will be the low concentration in the system with 4 ml bathing solution, which will require some adjustments.

To determine the paracellular pathway, which is regulated by the TJ complex, the use of tracers with sizes of 40-400 kDa, such as FITC- or rhodamine-labeled dextran, is suggested in addition to fluorescein: The greater size selectivity of the TJs, will give a clearer understanding of the paracellular pathway and thus an understanding whether the TJs have

a functional response to the removal of the retina. Without these or similar experiments it will not be possible to answer the question of para- or transcellular transport.

A condition that should also be avoided in future experiments is the difference in osmolarity between the basal and the apical bathing solutions, which can be achieved by lowering the fluorescein concentration.

4.3.2 Fluorescein Transport Across RPE Devoid of Retina and Sclera

To evaluate the barrier integrity of the RPE samples lacking retina and sclera, it was necessary to divert from the established criteria for data exclusion because all seven samples had shown a decreasing TEER starting at minute one. Those samples that were eliminated were leaking fluorescein-containing medium through the Ussing sliders.

Initially the RPE showed the lowest basal fluorescein concentration, although it had increased non-linearly by t_{90} and t_{120} . The high concentrations at t_{90} and t_{120} are thought to be directly linked to the breakdown of TEER and therefore the breakdown of the RPE's integrity.

A possible explanation of the low values at t_{30} and t_{60} is a reduction of fluid transport across the epithelium. During the removal of the retina also a number of microvilli are removed as suggested in figure 3-19. The removal of the microvilli may not alter the viability of the cells as indicated by cell viability assays, but could be sufficient to reduce the fluid transport.

The underlying hypothesis is that the majority of water transport across the RPE happens through the transcellular pathway, which is driven by the K^+ and Cl^- transport. The catalysts of this transport are the Kir 7.1 K^+ channels as well as their colocalized $Na^+-K^+-ATPase$, which are located on the roots of the microvilli surrounding the photoreceptors, proximate to the apical membrane of the RPE (180, 181).

4.3.3 Increased Apical Na^+ Concentration by Sodium-Fluorescein Application

The difference in osmolarity between the apical and basal side of the bathing solutions (343 ± 5 vs 286 ± 5 mOsm), as well as the increased Na^+ concentration on the apical side (from 143 mM to 196 mM) altered the experimental conditions by more than one component. It is expected that these changes primarily target the ion transport of the RPE. However, no significant differences in the TEER values were seen. In physiological conditions, the sodium gradient between the subretinal space and the lumen of the RPE is maintained by the Na^+/K^+

ATPase located on the apical membrane and leads to a co-transport of $\text{Na}^+/\text{K}^+/\text{2Cl}^-$ (182-184). While sodium ions are transported out of the cell to the apical side via the Na^+/K^+ ATPase, this leads to an apical influx of Cl^- . When this process is interrupted by ouabain, the adhesion force between the RPE and the retina is interrupted. The increase in the extracellular Na^+ concentration can, however, also affect the retinal cells and in this regard trigger a secondary effect on the RPE. The functionality of the photoreceptor outer segments of rods, which are in direct contact with the RPE, has been shown to be dependent on the extracellular Na^+ and Ca^{2+} concentrations as well as the membrane potentials. When sodium is removed, the Ca^{2+} exchange of the POS and hence the response to light is abolished, but this is also dependent on the extracellular Ca^{2+} concentration (185-188). The exchange of internal Ca^{2+} remains, however, unaffected when the membrane potential changes or if the external Na^+ concentration changes between the ranges of 55 - 220 mM (188, 189), suggesting that a sodium concentration of 193 mM will not affect the functionality of the light response in a dramatic way.

However, without further experimental evidence or available publications, on how exactly an increase of $[\text{Na}^+]$ to 193 mM influences the RPE/retina interaction, reducing the sodium-fluorescein concentration by 20-fold or more is suggested, to avoid this as a possible source of intervention. The small surface area of the explant may require a switch to other tracers, such as HRP, or inulin, that are either enzymatically activated, or radioactively labelled.

4.3.4 Summarizing the Fluorescein Transport Experiments

A final conclusion on the trans- and paracellular transport in response to retina or choroid removal cannot be provided without the suggested experiments. However, it is anticipated that the increase of basolateral fluorescein in the RR sample is the reaction to a signal for apical fluid removal. This signal must result from the damages occurring to the choroid. Physiologically this is plausible, because one of the RPEs functions is to remove water from the subretinal space and to maintain the retina/RPE interaction (51, 184). If the choroid is compromised, there may be a threat of excessive fluid influx, which can jeopardize this interaction. The significantly greater TEER in the RR tissues may be a protective reaction from RPE towards the retina shielding it from possible damage, or it could be an indicator to achieve greater surveillance along the paracellular pathway.

4.4 Evaluation of RPE Samples Devoid of Retina or Sclera

The removal of sclera and retina (RPE samples) yielded TEER values between $133 \pm 7 \Omega \cdot \text{cm}^2$ (n=32) and $103 \pm 15 \Omega \cdot \text{cm}^2$ (n=5), while the results from the fluorescein transport showed the initial TEER at $193 \pm 41 \Omega \cdot \text{cm}^2$ (n=3). The difference in the absolute TEER values of these tissues is not understood in its entire scope.

The greater TEER decrease of RPE compared to RR or RRS shows that an RPE explant from rat eyes devoid of sclera and retina is not a suitable model for understanding the ordinary physiology of the RPE. The accelerated reduction in TEER is a result of the mechanical retina removal, because the results of the retina/RPE complex did not show signs of accelerated TEER decrease, while preliminary results of RPE/sclera tissues showed a severe impact on the TEER.

To study the ordinary physiology of the RPE, the RRS explants should be used. The greatest advantage lies in the continuous presence of the retina, which ensures the continuous interaction between photoreceptors and the RPE.

4.5 The Continuous TEER Decrease in All Systems

The TEER decrease varies in its amplitude but is consistent in all examined tissues. A possible cause for this are the cells on the edge of the insert, whose cell membranes are severely compromised by the half chambers, as was demonstrated by the cell viability assay. In this process, intracellular components such as growth factors are released without surveillance that can act paracrine, possibly leading to reparation processes in which the microfilaments, and therefore the barrier, need to be rearranged (190, 191). If reparation processes are initiated, a reorganization of the RPE grid and therefore the unraveling of TJs would be necessary. Considering the interwoven net of TJs, adherens junctions and desmosomes in the RPE, the compromised cells may elicit a reaction in their adjacent healthy cells, such that this signal could be carried forward.

4.6 Sensitivity of the Ussing Chamber Assay as Revealed by TEER Values

When tissue damage in the RPE samples had occurred, this fact was immediately revealed by a low initial TEER. In other cases, TEER values were decreasing, while actin or *SYTOX Orange* staining did not show any apparent abnormalities. The TEER analysis was therefore

able to distinguish these from intact RPE sheets. This was a major finding because it revealed the sensitivity of the Ussing chamber assay for TEER measurements. No additional ultrastructural analyses were made to correlate the measured TEER, although highly desirable to further strengthen this point.

4.7 Other Methods for Evaluating an RPE Explant Devoid of Retina

If the removal of the retina from the RPE is desired, different approaches need to be chosen. RRS or RR can be incubated with enzymes such as chondroitinase or neuraminidase prior to their placement in the Ussing chamber. Both enzymes haven been shown to remove interphotoreceptor matrix (IPM) from the retina, which is the molecular contributor to the retina/RPE adhesion (192).

Another approach can be the use of an established method in which the retina is removed from the RPE: Experimental retinal detachment (193). In this case a 1% sodium hyaluronate is injected subretinally to gently separate the retina from the RPE. While this method induces apoptosis in the retinal cells, it may also alter the physiology of the RPE, which has not been investigated to date.

References

1. Penfold, P. L., Madigan, M. C., Gillies, M. C., and Provis, J. M. (2001) Immunological and aetiological aspects of macular degeneration. *Prog Retin Eye Res* **20**, 385-414
2. Klein, R., Peto, T., Bird, A., and Vannewkirk, M. R. (2004) The epidemiology of age-related macular degeneration. *Am J Ophthalmol* **137**, 486-495
3. Abdelsalam, A., Del Priore, L., and Zarbin, M. A. (1999) Drusen in age-related macular degeneration: pathogenesis, natural course, and laser photocoagulation-induced regression. *Surv Ophthalmol* **44**, 1-29
4. Ferris, F. L., 3rd, and Patz, A. (1984) Macular edema. A complication of diabetic retinopathy. *Surv Ophthalmol* **28 Suppl**, 452-461
5. Reese, T. S., and Karnovsky, M. J. (1967) Fine structural localization of a blood-brain barrier to exogenous peroxidase. *J Cell Biol* **34**, 207-217
6. Sedar, A. W., and Forte, J. G. (1964) Effects of Calcium Depletion on the Junctional Complex between Oxyntic Cells of Gastric Glands. *J Cell Biol* **22**, 173-188
7. Meldolesi, J., Castiglioni, G., Parma, R., Nassivera, N., and De Camilli, P. (1978) Ca⁺⁺⁺-dependent disassembly and reassembly of occluding junctions in guinea pig pancreatic acinar cells. Effect of drugs. *J Cell Biol* **79**, 156-172
8. Orci, L., Amherdt, M., Henquin, J. C., Lambert, A. E., Unger, R. H., and Renold, A. E. (1973) Pronase effect on pancreatic beta cell secretion and morphology. *Science* **180**, 647-649
9. Erij, D., and Martinez-Palomo, A. (1972) Opening of tight junctions in frog skin by hypertonic urea solutions. *J Membr Biol* **9**, 229-240
10. Brightman, M. W., Hori, M., Rapoport, S. I., Reese, T. S., and Westergaard, E. (1973) Osmotic opening of tight junctions in cerebral endothelium. *J Comp Neurol* **152**, 317-325
11. Heller, F., Florian, P., Bojarski, C., Richter, J., Christ, M., Hillenbrand, B., Mankertz, J., Gitter, A. H., Burgel, N., Fromm, M., Zeitz, M., Fuss, I., Strober, W., and Schulzke, J. D. (2005) Interleukin-13 is the key effector Th2 cytokine in ulcerative colitis that affects epithelial tight junctions, apoptosis, and cell restitution. *Gastroenterology* **129**, 550-564
12. Madara, J. L., and Stafford, J. (1989) Interferon-gamma directly affects barrier function of cultured intestinal epithelial monolayers. *J Clin Invest* **83**, 724-727
13. Mullin, J. M., and Snock, K. V. (1990) Effect of tumor necrosis factor on epithelial tight junctions and transepithelial permeability. *Cancer Res* **50**, 2172-2176
14. Schmitt, M., Horbach, A., Kubitz, R., Frilling, A., and Haussinger, D. (2004) Disruption of hepatocellular tight junctions by vascular endothelial growth factor (VEGF): a novel mechanism for tumor invasion. *J Hepatol* **41**, 274-283
15. Nusrat, A., Parkos, C. A., Bacarra, A. E., Godowski, P. J., Delp-Archer, C., Rosen, E. M., and Madara, J. L. (1994) Hepatocyte growth factor/scatter factor effects on epithelia. Regulation of intercellular junctions in transformed and nontransformed cell lines, basolateral polarization of c-met receptor in transformed and natural intestinal epithelia, and induction of rapid wound repair in a transformed model epithelium. *J Clin Invest* **93**, 2056-2065

16. Morofuji, Y., Nakagawa, S., So, G., Hiu, T., Horai, S., Hayashi, K., Tanaka, K., Suyama, K., Deli, M. A., Nagata, I., and Niwa, M. (2010) Pitavastatin Strengthens the Barrier Integrity in Primary Cultures of Rat Brain Endothelial Cells. *Cell Mol Neurobiol*
17. Catalioto, R. M., Triolo, A., Giuliani, S., Altamura, M., Evangelista, S., and Maggi, C. A. (2008) Increased paracellular absorption by bile salts and P-glycoprotein stimulated efflux of otilonium bromide in Caco-2 cells monolayers as a model of intestinal barrier. *J Pharm Sci* **97**, 4087-4100
18. Fasano, A., Baudry, B., Pumplun, D. W., Wasserman, S. S., Tall, B. D., Ketley, J. M., and Kaper, J. B. (1991) *Vibrio cholerae* produces a second enterotoxin, which affects intestinal tight junctions. *Proc Natl Acad Sci U S A* **88**, 5242-5246
19. Fasano, A., Not, T., Wang, W., Uzzau, S., Berti, I., Tommasini, A., and Goldblum, S. E. (2000) Zonulin, a newly discovered modulator of intestinal permeability, and its expression in coeliac disease. *Lancet* **355**, 1518-1519
20. Bentzel, C. J., Hainau, B., Edelman, A., Anagnostopoulos, T., and Benedetti, E. L. (1976) Effect of plant cytokinins on microfilaments and tight junction permeability. *Nature* **264**, 666-668
21. Hubel, H. (1995) *Eye, Brain, and Vision*, W.H. Freeman
22. Stevenson, T. C. (1963) Intrasccleral nerve loops. A clinical study of frequency and treatment. *Am J Ophthalmol* **55**, 935-939
23. Roh, S., and Weiter, J. J. (2004) Retinal and choroidal circulation. In *Ophthalmology* (Yanoff, M., and Duker, J. S., eds) pp. 518-521, Mosby Elsevier
24. Braun, R. D., Dewhirst, M. W., and Hatchell, D. L. (1997) Quantification of erythrocyte flow in the choroid of the albino rat. *Am J Physiol* **272**, H1444-1453
25. Wise, G. N., Dollerby, C. T., and Henkind, P. (1971) *The retinal circulation*, Harper & Row, New York
26. Roh, S., and Weiter, J. J. (2004) *Retinal and choroidal circulation.*, Mosby Elsevier
27. Bok, D. (1993) The retinal pigment epithelium: a versatile partner in vision. *J Cell Sci Suppl* **17**, 189-195
28. Bosch, E., Horwitz, J., and Bok, D. (1993) Phagocytosis of outer segments by retinal pigment epithelium: phagosome-lysosome interaction. *J Histochem Cytochem* **41**, 253-263
29. Owaribe, K., Kartenbeck, J., Rungger-Brandle, E., and Franke, W. W. (1988) Cytoskeletons of retinal pigment epithelial cells: interspecies differences of expression patterns indicate independence of cell function from the specific complement of cytoskeletal proteins. *Cell Tissue Res* **254**, 301-315
30. Colegio, O. R., Van Itallie, C. M., McCrea, H. J., Rahner, C., and Anderson, J. M. (2002) Claudins create charge-selective channels in the paracellular pathway between epithelial cells. *Am J Physiol Cell Physiol* **283**, C142-147
31. Kiuchi-Saishin, Y., Gotoh, S., Furuse, M., Takasuga, A., Tano, Y., and Tsukita, S. (2002) Differential expression patterns of claudins, tight junction membrane proteins, in mouse nephron segments. *J Am Soc Nephrol* **13**, 875-886

32. Peng, S., Rao, V. S., Adelman, R. A., and Rizzolo, L. J. (2011) Claudin-19 and the barrier properties of the human retinal pigment epithelium. *Invest Ophthalmol Vis Sci* **52**, 1392-1403
33. Krause, G., Winkler, L., Mueller, S. L., Haseloff, R. F., Piontek, J., and Blasig, I. E. (2008) Structure and function of claudins. *Biochim Biophys Acta* **1778**, 631-645
34. Van Itallie, C. M., and Anderson, J. M. (2006) Claudins and epithelial paracellular transport. *Annu Rev Physiol* **68**, 403-429
35. McKenzie, J. A., and Ridley, A. J. (2007) Roles of Rho/ROCK and MLCK in TNF-alpha-induced changes in endothelial morphology and permeability. *J Cell Physiol* **213**, 221-228
36. Nusrat, A., Turner, J. R., and Madara, J. L. (2000) Molecular physiology and pathophysiology of tight junctions. IV. Regulation of tight junctions by extracellular stimuli: nutrients, cytokines, and immune cells. *Am J Physiol Gastrointest Liver Physiol* **279**, G851-857
37. Snodderly, D. M., Sandstrom, M. M., Leung, I. Y., Zucker, C. L., and Neuringer, M. (2002) Retinal pigment epithelial cell distribution in central retina of rhesus monkeys. *Invest Ophthalmol Vis Sci* **43**, 2815-2818
38. Wikler, K. C., Williams, R. W., and Rakic, P. (1990) Photoreceptor mosaic: number and distribution of rods and cones in the rhesus monkey retina. *J Comp Neurol* **297**, 499-508
39. Strauss, O. (2005) The retinal pigment epithelium in visual function. *Physiol Rev* **85**, 845-881
40. Besharse, J. C., and DeFoe, D. M. (1998) Role of the retinal pigment epithelium in photoreceptor membrane turnover. In *The retinal pigment epithelium: Function and disease* (Marmor, M. F., and Wolfenberger, T. J., eds), Oxford University Press, New York
41. Arshavsky, V. (2002) Like night and day: rods and cones have different pigment regeneration pathways. *Neuron* **36**, 1-3
42. Mata, N. L., Radu, R. A., Clemmons, R. C., and Travis, G. H. (2002) Isomerization and oxidation of vitamin a in cone-dominant retinas: a novel pathway for visual-pigment regeneration in daylight. *Neuron* **36**, 69-80
43. Boulton, M. (1998) The role of melanin in the RPE. In *The Retinal Pigment Epithelium* (Marmor, M. F., and Wolfenberger, T. J., eds), Oxford University Press, Oxford, UK
44. Alm, A. (1972) Effects of norepinephrine, angiotensin, dihydroergotamine, papaverine, isoproterenol, histamine, nicotinic acid, and xanthinol nicotinate on retinal oxygen tension in cats. *Acta Ophthalmol (Copenh)* **50**, 707-719
45. Alm, A., and Bill, A. (1972) The oxygen supply to the retina. II. Effects of high intraocular pressure and of increased arterial carbon dioxide tension on uveal and retinal blood flow in cats. A study with radioactively labelled microspheres including flow determinations in brain and some other tissues. *Acta Physiol Scand* **84**, 306-319
46. Hollyfield, J. G., and Witkovsky, P. (1974) Pigmented retinal epithelium involvement in photoreceptor development and function. *J Exp Zool* **189**, 357-378
47. Marneros, A. G., Fan, J., Yokoyama, Y., Gerber, H. P., Ferrara, N., Crouch, R. K., and Olsen, B. R. (2005) Vascular endothelial growth factor expression in the retinal pigment epithelium is essential for choriocapillaris development and visual function. *Am J Pathol* **167**, 1451-1459

48. Shi, G., Maminishkis, A., Banzon, T., Jalickee, S., Li, R., Hammer, J., and Miller, S. S. (2008) Control of chemokine gradients by the retinal pigment epithelium. *Invest Ophthalmol Vis Sci* **49**, 4620-4630
49. Mandal, M. N., and Ayyagari, R. (2006) Complement factor H: spatial and temporal expression and localization in the eye. *Invest Ophthalmol Vis Sci* **47**, 4091-4097
50. Clark, S. J., Bishop, P. N., and Day, A. J. (2010) Complement factor H and age-related macular degeneration: the role of glycosaminoglycan recognition in disease pathology. *Biochem Soc Trans* **38**, 1342-1348
51. Marmor, M. F. (1990) Control of subretinal fluid: experimental and clinical studies. *Eye (Lond)* **4 (Pt 2)**, 340-344
52. Hamann, S. (2002) Molecular mechanisms of water transport in the eye. *Int Rev Cytol* **215**, 395-431
53. Ohia, S. E., Bagchi, M., and Stohs, S. J. (1994) Age-related oxidative damage in Long-Evans rat retina. *Res Commun Mol Pathol Pharmacol* **85**, 21-31
54. Coleman, H. R., Chan, C. C., Ferris, F. L., 3rd, and Chew, E. Y. (2008) Age-related macular degeneration. *Lancet* **372**, 1835-1845
55. Ding, X., Patel, M., and Chan, C. C. (2009) Molecular pathology of age-related macular degeneration. *Prog Retin Eye Res* **28**, 1-18
56. Jager, R. D., Mieler, W. F., and Miller, J. W. (2008) Age-related macular degeneration. *N Engl J Med* **358**, 2606-2617
57. Klein, R., Chou, C. F., Klein, B. E., Zhang, X., Meuer, S. M., and Saaddine, J. B. (2011) Prevalence of age-related macular degeneration in the US population. *Arch Ophthalmol* **129**, 75-80
58. Campochiaro, P. A. (1999) The pathogenesis of age-related macular degeneration. *Mol Vis* **5**, 24
59. Campochiaro, P. A., Soloway, P., Ryan, S. J., and Miller, J. W. (1999) The pathogenesis of choroidal neovascularization in patients with age-related macular degeneration. *Mol Vis* **5**, 34
60. Stellmach, V., Crawford, S. E., Zhou, W., and Bouck, N. (2001) Prevention of ischemia-induced retinopathy by the natural ocular antiangiogenic agent pigment epithelium-derived factor. *Proc Natl Acad Sci U S A* **98**, 2593-2597
61. Bhutto, I. A., McLeod, D. S., Hasegawa, T., Kim, S. Y., Merges, C., Tong, P., and Lutty, G. A. (2006) Pigment epithelium-derived factor (PEDF) and vascular endothelial growth factor (VEGF) in aged human choroid and eyes with age-related macular degeneration. *Exp Eye Res* **82**, 99-110
62. Tombran-Tink, J., and Barnstable, C. J. (2003) PEDF: a multifaceted neurotrophic factor. *Nat Rev Neurosci* **4**, 628-636
63. Tombran-Tink, J., Shivaram, S. M., Chader, G. J., Johnson, L. V., and Bok, D. (1995) Expression, secretion, and age-related downregulation of pigment epithelium-derived factor, a serpin with neurotrophic activity. *J Neurosci* **15**, 4992-5003

64. Ferrara, N., and Henzel, W. J. (1989) Pituitary follicular cells secrete a novel heparin-binding growth factor specific for vascular endothelial cells. *Biochem Biophys Res Commun* **161**, 851-858
65. Folkman, J. (2007) Angiogenesis: an organizing principle for drug discovery? *Nat Rev Drug Discov* **6**, 273-286
66. Italiano, J. E., Jr., Richardson, J. L., Patel-Hett, S., Battinelli, E., Zaslavsky, A., Short, S., Ryeom, S., Folkman, J., and Klement, G. L. (2008) Angiogenesis is regulated by a novel mechanism: pro- and antiangiogenic proteins are organized into separate platelet alpha granules and differentially released. *Blood* **111**, 1227-1233
67. Miller, J. W., Adamis, A. P., Shima, D. T., D'Amore, P. A., Moulton, R. S., O'Reilly, M. S., Folkman, J., Dvorak, H. F., Brown, L. F., Berse, B., and et al. (1994) Vascular endothelial growth factor/vascular permeability factor is temporally and spatially correlated with ocular angiogenesis in a primate model. *Am J Pathol* **145**, 574-584
68. Hageman, G. S., Luthert, P. J., Victor Chong, N. H., Johnson, L. V., Anderson, D. H., and Mullins, R. F. (2001) An integrated hypothesis that considers drusen as biomarkers of immune-mediated processes at the RPE-Bruch's membrane interface in aging and age-related macular degeneration. *Prog Retin Eye Res* **20**, 705-732
69. Sarks, S., Cherepanoff, S., Killingsworth, M., and Sarks, J. (2007) Relationship of Basal laminar deposit and membranous debris to the clinical presentation of early age-related macular degeneration. *Invest Ophthalmol Vis Sci* **48**, 968-977
70. Johnson, L. V., Ozaki, S., Staples, M. K., Erickson, P. A., and Anderson, D. H. (2000) A potential role for immune complex pathogenesis in drusen formation. *Exp Eye Res* **70**, 441-449
71. Mullins, R. F., Aptsiauri, N., and Hageman, G. S. (2001) Structure and composition of drusen associated with glomerulonephritis: implications for the role of complement activation in drusen biogenesis. *Eye (Lond)* **15**, 390-395
72. Yehoshua, Z., Rosenfeld, P. J., and Albini, T. A. (2011) Current Clinical Trials in Dry AMD and the Definition of Appropriate Clinical Outcome Measures. *Semin Ophthalmol* **26**, 167-180
73. Kuno, N., and Fujii, S. (2011) Dry Age-related Macular Degeneration: Recent Progress of Therapeutic Approaches. *Curr Mol Pharmacol*
74. Feeney-Burns, L., Hilderbrand, E. S., and Eldridge, S. (1984) Aging human RPE: morphometric analysis of macular, equatorial, and peripheral cells. *Invest Ophthalmol Vis Sci* **25**, 195-200
75. Lamb, L. E., and Simon, J. D. (2004) A2E: a component of ocular lipofuscin. *Photochem Photobiol* **79**, 127-136
76. Sparrow, J. R., Fishkin, N., Zhou, J., Cai, B., Jang, Y. P., Krane, S., Itagaki, Y., and Nakanishi, K. (2003) A2E, a byproduct of the visual cycle. *Vision Res* **43**, 2983-2990
77. Burke, J. M., and Skumatz, C. M. (1998) Autofluorescent inclusions in long-term postconfluent cultures of retinal pigment epithelium. *Invest Ophthalmol Vis Sci* **39**, 1478-1486

78. Wu, Y., Yanase, E., Feng, X., Siegel, M. M., and Sparrow, J. R. (2010) Structural characterization of bisretinoid A2E photocleavage products and implications for age-related macular degeneration. *Proc Natl Acad Sci U S A* **107**, 7275-7280
79. Roider, J., Hillenkamp, F., Flotte, T., and Birngruber, R. (1993) Microphotocoagulation: selective effects of repetitive short laser pulses. *Proc Natl Acad Sci U S A* **90**, 8643-8647
80. Birngruber, R., Gabel, V. P., and Hillenkamp, F. (1983) Experimental studies of laser thermal retinal injury. *Health Phys* **44**, 519-531
81. Ambati, J., Anand, A., Fernandez, S., Sakurai, E., Lynn, B. C., Kuziel, W. A., Rollins, B. J., and Ambati, B. K. (2003) An animal model of age-related macular degeneration in senescent Ccl-2- or Ccr-2-deficient mice. *Nat Med* **9**, 1390-1397
82. Miller, J. W. (2010) Treatment of age-related macular degeneration: beyond VEGF. *Jpn J Ophthalmol* **54**, 523-528
83. Saint-Geniez, M., Kurihara, T., Sekiyama, E., Maldonado, A. E., and D'Amore, P. A. (2009) An essential role for RPE-derived soluble VEGF in the maintenance of the choriocapillaris. *Proc Natl Acad Sci U S A* **106**, 18751-18756
84. Thornton, J., Edwards, R., Mitchell, P., Harrison, R. A., Buchan, I., and Kelly, S. P. (2005) Smoking and age-related macular degeneration: a review of association. *Eye (Lond)* **19**, 935-944
85. Knudtson, M. D., Klein, R., and Klein, B. E. (2006) Physical activity and the 15-year cumulative incidence of age-related macular degeneration: the Beaver Dam Eye Study. *Br J Ophthalmol* **90**, 1461-1463
86. Prasad, P. S., Schwartz, S. D., and Hubschman, J. P. (2010) Age-related macular degeneration: current and novel therapies. *Maturitas* **66**, 46-50
87. (2001) A randomized, placebo-controlled, clinical trial of high-dose supplementation with vitamins C and E, beta carotene, and zinc for age-related macular degeneration and vision loss: AREDS report no. 8. *Arch Ophthalmol*, 1417-1436
88. Klein, R., Klein, B. E., Moss, S. E., and Cruickshanks, K. J. (1998) The Wisconsin Epidemiologic Study of Diabetic Retinopathy: XVII. The 14-year incidence and progression of diabetic retinopathy and associated risk factors in type 1 diabetes. *Ophthalmology* **105**, 1801-1815
89. Saaddine, J. B., Honeycutt, A. A., Narayan, K. M., Zhang, X., Klein, R., and Boyle, J. P. (2008) Projection of diabetic retinopathy and other major eye diseases among people with diabetes mellitus: United States, 2005-2050. *Arch Ophthalmol* **126**, 1740-1747
90. Fong, D. S., Aiello, L. P., Ferris, F. L., 3rd, and Klein, R. (2004) Diabetic retinopathy. *Diabetes Care* **27**, 2540-2553
91. Cheung, N., Mitchell, P., and Wong, T. Y. (2010) Diabetic retinopathy. *Lancet* **376**, 124-136
92. Wild, S., Roglic, G., Green, A., Sicree, R., and King, H. (2004) Global prevalence of diabetes: estimates for the year 2000 and projections for 2030. *Diabetes Care* **27**, 1047-1053
93. Klein, R., Klein, B. E., Moss, S. E., Davis, M. D., and DeMets, D. L. (1984) The Wisconsin epidemiologic study of diabetic retinopathy. IV. Diabetic macular edema. *Ophthalmology* **91**, 1464-1474

94. Antcliff, R. J., and Marshall, J. (1999) The pathogenesis of edema in diabetic maculopathy. *Semin Ophthalmol* **14**, 223-232
95. Miyamoto, K., Khosrof, S., Bursell, S. E., Rohan, R., Murata, T., Clermont, A. C., Aiello, L. P., Ogura, Y., and Adamis, A. P. (1999) Prevention of leukostasis and vascular leakage in streptozotocin-induced diabetic retinopathy via intercellular adhesion molecule-1 inhibition. *Proc Natl Acad Sci U S A* **96**, 10836-10841
96. Vinores, S. A., Derevjani, N. L., Ozaki, H., Okamoto, N., and Campochiaro, P. A. (1999) Cellular mechanisms of blood-retinal barrier dysfunction in macular edema. *Doc Ophthalmol* **97**, 217-228
97. Miyamoto, N., de Kozak, Y., Jeanny, J. C., Glotin, A., Mascarelli, F., Massin, P., BenEzra, D., and Behar-Cohen, F. (2007) Placental growth factor-1 and epithelial haemato-retinal barrier breakdown: potential implication in the pathogenesis of diabetic retinopathy. *Diabetologia* **50**, 461-470
98. Chibber, R., Ben-Mahmud, B. M., Chibber, S., and Kohner, E. M. (2007) Leukocytes in diabetic retinopathy. *Curr Diabetes Rev* **3**, 3-14
99. Gregor, M. F., and Hotamisligil, G. S. (2011) Inflammatory mechanisms in obesity. *Annu Rev Immunol* **29**, 415-445
100. Tang, J., and Kern, T. S. (2011) Inflammation in diabetic retinopathy. *Prog Retin Eye Res*
101. Dinarello, C. A. (1996) Biologic basis for interleukin-1 in disease. *Blood* **87**, 2095-2147
102. Arend, W. P. (1991) Interleukin 1 receptor antagonist. A new member of the interleukin 1 family. *J Clin Invest* **88**, 1445-1451
103. Kern, T. S. (2007) Contributions of inflammatory processes to the development of the early stages of diabetic retinopathy. *Exp Diabetes Res* **2007**, 95103
104. Kowluru, R. A., and Odenbach, S. (2004) Role of interleukin-1beta in the development of retinopathy in rats: effect of antioxidants. *Invest Ophthalmol Vis Sci* **45**, 4161-4166
105. Demircan, N., Safran, B. G., Soylu, M., Ozcan, A. A., and Sizmaz, S. (2006) Determination of vitreous interleukin-1 (IL-1) and tumour necrosis factor (TNF) levels in proliferative diabetic retinopathy. *Eye (Lond)* **20**, 1366-1369
106. Patel, M., and Chan, C. C. (2008) Immunopathological aspects of age-related macular degeneration. *Semin Immunopathol* **30**, 97-110
107. Tatar, O., Adam, A., Shinoda, K., Yoeruek, E., Szurman, P., Bopp, S., Eckardt, C., Bartz-Schmidt, K. U., and Grisanti, S. (2007) Influence of verteporfin photodynamic therapy on inflammation in human choroidal neovascular membranes secondary to age-related macular degeneration. *Retina* **27**, 713-723
108. Abe, T., Sugano, E., Saigo, Y., and Tamai, M. (2003) Interleukin-1beta and barrier function of retinal pigment epithelial cells (ARPE-19): aberrant expression of junctional complex molecules. *Invest Ophthalmol Vis Sci* **44**, 4097-4104
109. Nakao, S., Kuwano, T., Tsutsumi-Miyahara, C., Ueda, S., Kimura, Y. N., Hamano, S., Sonoda, K. H., Saijo, Y., Nukiwa, T., Strieter, R. M., Ishibashi, T., Kuwano, M., and Ono, M. (2005) Infiltration of COX-2-expressing macrophages is a prerequisite for IL-1 beta-induced neovascularization and tumor growth. *J Clin Invest* **115**, 2979-2991

110. Kuwano, T., Nakao, S., Yamamoto, H., Tsuneyoshi, M., Yamamoto, T., Kuwano, M., and Ono, M. (2004) Cyclooxygenase 2 is a key enzyme for inflammatory cytokine-induced angiogenesis. *FASEB J* **18**, 300-310
111. Nakao, S., Hata, Y., Miura, M., Noda, K., Kimura, Y. N., Kawahara, S., Kita, T., Hisatomi, T., Nakazawa, T., Jin, Y., Dana, M. R., Kuwano, M., Ono, M., Ishibashi, T., and Hafezi-Moghadam, A. (2007) Dexamethasone inhibits interleukin-1 β -induced corneal neovascularization: role of nuclear factor- κ B-activated stromal cells in inflammatory angiogenesis. *Am J Pathol* **171**, 1058-1065
112. Gonzalez-Mariscal, L., Islas, S., Contreras, R. G., Garcia-Villegas, M. R., Betanzos, A., Vega, J., Diaz-Quinonez, A., Martin-Orozco, N., Ortiz-Navarrete, V., Cerejido, M., and Valdes, J. (1999) Molecular characterization of the tight junction protein ZO-1 in MDCK cells. *Exp Cell Res* **248**, 97-109
113. Balda, M. S., Whitney, J. A., Flores, C., Gonzalez, S., Cerejido, M., and Matter, K. (1996) Functional dissociation of paracellular permeability and transepithelial electrical resistance and disruption of the apical-basolateral intramembrane diffusion barrier by expression of a mutant tight junction membrane protein. *J Cell Biol* **134**, 1031-1049
114. Claude, P. (1978) Morphological factors influencing transepithelial permeability: a model for the resistance of the zonula occludens. *J Membr Biol* **39**, 219-232
115. Joseph, D. P., and Miller, S. S. (1991) Apical and basal membrane ion transport mechanisms in bovine retinal pigment epithelium. *J Physiol* **435**, 439-463
116. Burke, J. M., and Hjelmeland, L. M. (2005) Mosaicism of the retinal pigment epithelium: seeing the small picture. *Mol Interv* **5**, 241-249
117. Maminishkis, A., Chen, S., Jalickee, S., Banzon, T., Shi, G., Wang, F. E., Ehalt, T., Hammer, J. A., and Miller, S. S. (2006) Confluent monolayers of cultured human fetal retinal pigment epithelium exhibit morphology and physiology of native tissue. *Invest Ophthalmol Vis Sci* **47**, 3612-3624
118. Dunn, K. C., Aotaki-Keen, A. E., Putkey, F. R., and Hjelmeland, L. M. (1996) ARPE-19, a human retinal pigment epithelial cell line with differentiated properties. *Exp Eye Res* **62**, 155-169
119. Geiger, R. C., Waters, C. M., Kamp, D. W., and Glucksberg, M. R. (2005) KGF prevents oxygen-mediated damage in ARPE-19 cells. *Invest Ophthalmol Vis Sci* **46**, 3435-3442
120. Ablonczy, Z., and Crosson, C. E. (2007) VEGF modulation of retinal pigment epithelium resistance. *Exp Eye Res* **85**, 762-771
121. Chang, C. W., Defoe, D. M., and Caldwell, R. B. (1997) Retinal pigment epithelial cells from dystrophic rats form normal tight junctions in vitro. *Invest Ophthalmol Vis Sci* **38**, 188-195
122. Nabi, I. R., Mathews, A. P., Cohen-Gould, L., Gundersen, D., and Rodriguez-Boulan, E. (1993) immortalization of polarized rat retinal pigment epithelium. *J Cell Sci* **104 (Pt 1)**, 37-49
123. Miller, S. S., Steinberg, R. H., and Oakley, B., 2nd (1978) The electrogenic sodium pump of the frog retinal pigment epithelium. *J Membr Biol* **44**, 259-279
124. Ostwald, T. J., and Steinberg, R. H. (1980) Localization of frog retinal pigment epithelium Na⁺-K⁺ ATPase. *Exp Eye Res* **31**, 351-360

125. Saito, Y., and Wright, E. M. (1982) Kinetics of the sodium pump in the frog choroid plexus. *J Physiol* **328**, 229-243
126. Quinton, P. M., Wright, E. M., and Tormey, J. M. (1973) Localization of sodium pumps in the choroid plexus epithelium. *J Cell Biol* **58**, 724-730
127. Davis, A. A., Bernstein, P. S., Bok, D., Turner, J., Nachtigal, M., and Hunt, R. C. (1995) A human retinal pigment epithelial cell line that retains epithelial characteristics after prolonged culture. *Invest Ophthalmol Vis Sci* **36**, 955-964
128. Mannermaa, E., Vellonen, K. S., Ryhanen, T., Kokkonen, K., Ranta, V. P., Kaarniranta, K., and Urtti, A. (2009) Efflux protein expression in human retinal pigment epithelium cell lines. *Pharm Res* **26**, 1785-1791
129. Bai, L., Zhang, Z., Zhang, H., Li, X., Yu, Q., Lin, H., and Yang, W. (2008) HIV-1 Tat protein alter the tight junction integrity and function of retinal pigment epithelium: an in vitro study. *BMC Infect Dis* **8**, 77
130. Strunnikova, J. B., F. Wang, C Zhi, A. Maminishkis, J. Hammer, J. Munson, S.S. Miller (2008) Analysis of Genetic and Functional Similarities Between Primary Human Fetal RPE (hFRPE) Cultures and Fetal or Adult Native RPE Cells In *ARVO*, E-Abstract 789/A243, Fort Lauderdale, FL.
131. Peng, S., Adelman, R. A., and Rizzolo, L. J. (2010) Minimal effects of VEGF and anti-VEGF drugs on the permeability or selectivity of RPE tight junctions. *Invest Ophthalmol Vis Sci* **51**, 3216-3225
132. Barker, G., and Simmons, N. L. (1981) Identification of two strains of cultured canine renal epithelial cells (MDCK cells) which display entirely different physiological properties. *Q J Exp Physiol* **66**, 61-72
133. Richardson, J. C., Scalera, V., and Simmons, N. L. (1981) Identification of two strains of MDCK cells which resemble separate nephron tubule segments. *Biochim Biophys Acta* **673**, 26-36
134. Tang, V. W., and Goodenough, D. A. (2003) Paracellular ion channel at the tight junction. *Biophys J* **84**, 1660-1673
135. Madara, J. L., and Dharmasathaphorn, K. (1985) Occluding junction structure-function relationships in a cultured epithelial monolayer. *J Cell Biol* **101**, 2124-2133
136. Mankertz, J., Amasheh, M., Krug, S. M., Fromm, A., Amasheh, S., Hillenbrand, B., Tavalali, S., Fromm, M., and Schulzke, J. D. (2009) TNFalpha up-regulates claudin-2 expression in epithelial HT-29/B6 cells via phosphatidylinositol-3-kinase signaling. *Cell Tissue Res* **336**, 67-77
137. Ali, M. H., Schlidt, S. A., Chandel, N. S., Hynes, K. L., Schumacker, P. T., and Gewertz, B. L. (1999) Endothelial permeability and IL-6 production during hypoxia: role of ROS in signal transduction. *Am J Physiol* **277**, L1057-1065
138. Man, S., Ubogu, E. E., Williams, K. A., Tucky, B., Callahan, M. K., and Ransohoff, R. M. (2008) Human brain microvascular endothelial cells and umbilical vein endothelial cells differentially facilitate leukocyte recruitment and utilize chemokines for T cell migration. *Clin Dev Immunol* **2008**, 384982

139. Zhou, J., He, S., Zhang, N., Spee, C., Zhou, P., Ryan, S. J., Kannan, R., and Hinton, D. R. (2010) Neutrophils compromise retinal pigment epithelial barrier integrity. *J Biomed Biotechnol* **2010**, 289360
140. Lara-Castillo, N., Zandi, S., Nakao, S., Ito, Y., Noda, K., She, H., Ahmed, M., Frimmel, S., Ablonczy, Z., and Hafezi-Moghadam, A. (2009) Atrial natriuretic peptide reduces vascular leakage and choroidal neovascularization. *Am J Pathol* **175**, 2343-2350
141. Lammers, K. M., Lu, R., Brownley, J., Lu, B., Gerard, C., Thomas, K., Rallabhandi, P., Shea-Donohue, T., Tamiz, A., Alkan, S., Netzel-Arnett, S., Antalis, T., Vogel, S. N., and Fasano, A. (2008) Gliadin induces an increase in intestinal permeability and zonulin release by binding to the chemokine receptor CXCR3. *Gastroenterology* **135**, 194-204 e193
142. Ghassemifar, R., Lai, C. M., and Rakoczy, P. E. (2006) VEGF differentially regulates transcription and translation of ZO-1alpha+ and ZO-1alpha- and mediates trans-epithelial resistance in cultured endothelial and epithelial cells. *Cell Tissue Res* **323**, 117-125
143. Esumi, N., Kachi, S., Hackler, L., Jr., Masuda, T., Yang, Z., Campochiaro, P. A., and Zack, D. J. (2009) BEST1 expression in the retinal pigment epithelium is modulated by OTX family members. *Hum Mol Genet* **18**, 128-141
144. Ablonczy, Z., Prakasam, A., Fant, J., Fauq, A., Crosson, C., and Sambamurti, K. (2009) Pigment epithelium-derived factor maintains retinal pigment epithelium function by inhibiting vascular endothelial growth factor-R2 signaling through gamma-secretase. *J Biol Chem* **284**, 30177-30186
145. Nakai, K., Tanaka, T., Murai, T., Ohguro, N., Tano, Y., and Miyasaka, M. (2005) Invasive human pancreatic carcinoma cells adhere to endothelial tri-cellular corners and increase endothelial permeability. *Cancer Sci* **96**, 766-773
146. Ussing, H. H., and Zerahn, K. (1951) Active transport of sodium as the source of electric current in the short-circuited isolated frog skin. *Acta Physiol Scand* **23**, 110-127
147. Ussing, H. H. (1980) Life with tracers. *Annu Rev Physiol* **42**, 1-16
148. Hamilton, K. L. (2011) Ussing's "Little Chamber": 60 Years+ Old and Counting. *Front Physiol* **2**, 6
149. Lasansky, A., and De Fisch, F. W. (1966) Potential, current, and ionic fluxes across the isolated retinal pigment epithelium and choroid. *J Gen Physiol* **49**, 913-924
150. Miller, S. S., and Steinberg, R. H. (1977) Passive ionic properties of frog retinal pigment epithelium. *J Membr Biol* **36**, 337-372
151. Frambach, D. A., Weiter, J. J., and Adler, A. J. (1985) A photogrammetric method to measure fluid movement across isolated frog retinal pigment epithelium. *Biophys J* **47**, 547-552
152. Frambach, D. A., and Misfeldt, D. S. (1983) Furosemide-sensitive Cl transport in embryonic chicken retinal pigment epithelium. *Am J Physiol* **244**, F679-685
153. Frambach, D. A., Valentine, J. L., and Weiter, J. J. (1988) Initial observations of rabbit retinal pigment epithelium-choroid-sclera preparations. *Invest Ophthalmol Vis Sci* **29**, 814-817
154. Missel, P., Chastain, J., Mitra, A., Kompella, U., Kansara, V., Duvvuri, S., Amrite, A., and Cheruvu, N. (2010) In vitro transport and partitioning of AL-4940, active metabolite of

- angiostatic agent anecortave acetate, in ocular tissues of the posterior segment. *J Ocul Pharmacol Ther* **26**, 137-146
155. Zhang, N., Kannan, R., Okamoto, C. T., Ryan, S. J., Lee, V. H., and Hinton, D. R. (2006) Characterization of brimonidine transport in retinal pigment epithelium. *Invest Ophthalmol Vis Sci* **47**, 287-294
 156. Linsenmeier, R. A. (1986) Effects of light and darkness on oxygen distribution and consumption in the cat retina. *J Gen Physiol* **88**, 521-542
 157. Winkler, B. S., and Giblin, F. J. (1983) Glutathione oxidation in retina: effects on biochemical and electrical activities. *Exp Eye Res* **36**, 287-297
 158. Dikstein, S., and Maurice, D. M. (1972) The metabolic basis to the fluid pump in the cornea. *J Physiol* **221**, 29-41
 159. Miller, S. S., and Edelman, J. L. (1990) Active ion transport pathways in the bovine retinal pigment epithelium. *J Physiol* **424**, 283-300
 160. Quinn, R. H., and Miller, S. S. (1992) Ion transport mechanisms in native human retinal pigment epithelium. *Invest Ophthalmol Vis Sci* **33**, 3513-3527
 161. Quinn, R. H., Quong, J. N., and Miller, S. S. (2001) Adrenergic receptor activated ion transport in human fetal retinal pigment epithelium. *Invest Ophthalmol Vis Sci* **42**, 255-264
 162. Ban, Y., and Rizzolo, L. J. (2000) Differential regulation of tight junction permeability during development of the retinal pigment epithelium. *Am J Physiol Cell Physiol* **279**, C744-750
 163. Lepe-Zuniga, J. L., Zigler, J. S., Jr., and Gery, I. (1987) Toxicity of light-exposed Hepes media. *J Immunol Methods* **103**, 145
 164. Giddabasappa, A., Bauler, M., Yepuru, M., Chaum, E., Dalton, J. T., and Eswaraka, J. (2010) 17-beta estradiol protects ARPE-19 cells from oxidative stress through estrogen receptor-beta. *Invest Ophthalmol Vis Sci* **51**, 5278-5287
 165. Elliot, S. J., Catanuto, P., Espinosa-Heidmann, D. G., Fernandez, P., Hernandez, E., Saloupi, P., Korach, K., Karl, M., and Cousins, S. W. (2010) Estrogen receptor beta protects against in vivo injury in RPE cells. *Exp Eye Res* **90**, 10-16
 166. Berthois, Y., Katzenellenbogen, J. A., and Katzenellenbogen, B. S. (1986) Phenol red in tissue culture media is a weak estrogen: implications concerning the study of estrogen-responsive cells in culture. *Proc Natl Acad Sci U S A* **83**, 2496-2500
 167. Rosenbaum, J. T., McDevitt, H. O., Guss, R. B., and Egbert, P. R. (1980) Endotoxin-induced uveitis in rats as a model for human disease. *Nature* **286**, 611-613
 168. Kindzelskii, A. L., Elner, V. M., Elner, S. G., Yang, D., Hughes, B. A., and Petty, H. R. (2004) Toll-like receptor 4 (TLR4) of retinal pigment epithelial cells participates in transmembrane signaling in response to photoreceptor outer segments. *J Gen Physiol* **124**, 139-149
 169. Despret, D. D., Bergen, A. A., Merriam, J. E., Zernant, J., Barile, G. R., Smith, R. T., Barbazetto, I. A., van Soest, S., Bakker, A., de Jong, P. T., Allikmets, R., and Klaver, C. C. (2008) Comprehensive analysis of the candidate genes CCL2, CCR2, and TLR4 in age-related macular degeneration. *Invest Ophthalmol Vis Sci* **49**, 364-371

170. Elnér, S. G., Petty, H. R., Elnér, V. M., Yoshida, A., Bian, Z. M., Yang, D., and Kindezelskii, A. L. (2005) TLR4 mediates human retinal pigment epithelial endotoxin binding and cytokine expression. *Trans Am Ophthalmol Soc* **103**, 126-135; discussion 135-127
171. Fujimoto, T., Sonoda, K. H., Hijioka, K., Sato, K., Takeda, A., Hasegawa, E., Oshima, Y., and Ishibashi, T. (2010) Choroidal neovascularization enhanced by Chlamydia pneumoniae via Toll-like receptor 2 in the retinal pigment epithelium. *Invest Ophthalmol Vis Sci* **51**, 4694-4702
172. D'Amico, D. J., Masonson, H. N., Patel, M., Adamis, A. P., Cunningham, E. T., Jr., Guyer, D. R., and Katz, B. (2006) Pegaptanib sodium for neovascular age-related macular degeneration: two-year safety results of the two prospective, multicenter, controlled clinical trials. *Ophthalmology* **113**, 992-1001 e1006
173. Andreoli, C. M., and Miller, J. W. (2007) Anti-vascular endothelial growth factor therapy for ocular neovascular disease. *Curr Opin Ophthalmol* **18**, 502-508
174. Wu, W. C., Hu, D. N., Gao, H. X., Chen, M., Wang, D., Rosen, R., and McCormick, S. A. (2010) Subtoxic levels hydrogen peroxide-induced production of interleukin-6 by retinal pigment epithelial cells. *Mol Vis* **16**, 1864-1873
175. Williams, L. L., Lew, H. M., Shannon, B. T., Singley, C. T., Davidorf, F. H., Jin, R., and Wolinsky, J. S. (1993) Phagocytosis of latex beads is defective in cultured human retinal pigment epithelial cells with persistent rubella virus infection. *Am J Pathol* **142**, 451-461
176. Geisen, P., McColm, J. R., King, B. M., and Hartnett, M. E. (2006) Characterization of barrier properties and inducible VEGF expression of several types of retinal pigment epithelium in medium-term culture. *Curr Eye Res* **31**, 739-748
177. Hughes, B. A., Miller, S. S., and Machen, T. E. (1984) Effects of cyclic AMP on fluid absorption and ion transport across frog retinal pigment epithelium. Measurements in the open-circuit state. *J Gen Physiol* **83**, 875-899
178. Adijanto, J., Banzon, T., Jalickee, S., Wang, N. S., and Miller, S. S. (2009) CO₂-induced ion and fluid transport in human retinal pigment epithelium. *J Gen Physiol* **133**, 603-622
179. Matter, K., and Balda, M. S. (2003) Functional analysis of tight junctions. *Methods* **30**, 228-234
180. Kusaka, S., Inanobe, A., Fujita, A., Makino, Y., Tanemoto, M., Matsushita, K., Tano, Y., and Kurachi, Y. (2001) Functional Kir7.1 channels localized at the root of apical processes in rat retinal pigment epithelium. *J Physiol* **531**, 27-36
181. Shimura, M., Yuan, Y., Chang, J. T., Zhang, S., Campochiaro, P. A., Zack, D. J., and Hughes, B. A. (2001) Expression and permeation properties of the K(+) channel Kir7.1 in the retinal pigment epithelium. *J Physiol* **531**, 329-346
182. Steinberg, R. H. (1985) Interactions between the retinal pigment epithelium and the neural retina. *Doc Ophthalmol* **60**, 327-346
183. Miller, S. S., and Steinberg, R. H. (1977) Active transport of ions across frog retinal pigment epithelium. *Exp Eye Res* **25**, 235-248
184. Hughes, B. A., Gallemore, R. P., and Miller, S. S. (1998) Transport mechanisms in the retinal pigment epithelium. In *The Retinal Pigment Epithelium* (Marmor, M. F., and Wolfenberger, T. J., eds) pp. 103-134, Oxford University Press

185. Bastian, B. L., and Fain, G. L. (1982) The effects of low calcium and background light on the sensitivity of toad rods. *J Physiol* **330**, 307-329
186. Hagins, W. A., and Yoshikami, S. (1975) Ionic mechanisms in excitation of photoreceptors. *Ann N Y Acad Sci* **264**, 314-325
187. Yau, K. W., McNaughton, P. A., and Hodgkin, A. L. (1981) Effect of ions on the light-sensitive current in retinal rods. *Nature* **292**, 502-505
188. McNaughton, P. A. (1990) Light response of vertebrate photoreceptors. *Physiol Rev* **70**, 847-883
189. Lagnado, L., Cervetto, L., and McNaughton, P. A. (1988) Ion transport by the Na-Ca exchange in isolated rod outer segments. *Proc Natl Acad Sci U S A* **85**, 4548-4552
190. Schlingemann, R. O. (2004) Role of growth factors and the wound healing response in age-related macular degeneration. *Graefes Arch Clin Exp Ophthalmol* **242**, 91-101
191. Kalnins, V. I., Sandig, M., Hergott, G. J., and Nagai, H. (1995) Microfilament organization and wound repair in retinal pigment epithelium. *Biochem Cell Biol* **73**, 709-722
192. Yao, X. Y., Hageman, G. S., and Marmor, M. F. (1992) Recovery of retinal adhesion after enzymatic perturbation of the interphotoreceptor matrix. *Invest Ophthalmol Vis Sci* **33**, 498-503
193. Hisatomi, T., Nakazawa, T., Noda, K., Almulki, L., Miyahara, S., Nakao, S., Ito, Y., She, H., Kohno, R., Michaud, N., Ishibashi, T., Hafezi-Moghadam, A., Badley, A. D., Kroemer, G., and Miller, J. W. (2008) HIV protease inhibitors provide neuroprotection through inhibition of mitochondrial apoptosis in mice. *J Clin Invest* **118**, 2025-2038
194. Yoneya, S., Tso, M. O., and Shimizu, K. (1983) Patterns of the choriocapillaris. A method to study the choroidal vasculature of the enucleated human eye. *Int Ophthalmol* **6**, 95-99

6 Appendix

6.1 List of Figures

- Fig. 1-1: Anatomy of the eye
- Fig. 1-2: Model of the retina and underlying tissue
- Fig. 1-3 Macro-anatomy of the choriocapillaris
- Fig. 1-4 Association between RPE microvilli and rod cells
- Fig. 1-5 RPE cell layer from rat
- Fig. 1-6 Association of photo-receptor cells and RPE cells according to their location in the eye
- Fig. 1-7 Diagram of the original Ussing chamber apparatus
-
- Fig. 2-1 The Ussing chamber
- Fig. 2-2 60 Hz frequency during recordings when the heat-block insulation is absent.
- Fig. 2-3 Data recording of the electric pulses using LabChart software
-
- Fig. 3-1 TEER of RPE in Hank's balanced salt solution (HBSS) lacking Ca^{2+}
- Fig. 3-2 Variability in early TEER measurements using Dulbecco's modified Eagle medium (DMEM)
- Fig. 3-3 TEER is dependent on the integrity of the RPE
- Fig. 3-4 Comparison of TEER values using DMEM and HBSS
- Fig. 3-5 The effect of EDTA given to the apical RPE bathing solution
- Fig. 3-6 TEER of RPE without removing the sclera
- Fig. 3-7 Localization of nuclei in RPE cells after Ussing chamber experiment using DMEM as bathing medium
- Fig. 3-8 Staining dead RPE cells after Ussing chamber experiments using *SYTOX Orange*
- Fig. 3-9 TEER values of different materials during the search for a suitable dummy membrane
- Fig. 3-10 Temperature changes of the bathing solution in the Ussing chamber

- Fig. 3-11 TEER and the corresponding short circuit current
- Fig. 3-12 Influence of medium leaking from the Ussing chamber on the TEER
- Fig. 3-13 Effect of the removal of 500 μ l medium from the apical bathing solution
- Fig. 3-14 Apical application of IL-1 β using DMEM to the RPE/choroid explant.
- Fig. 3-15 Use of designated gas channels in the Ussing chamber leads to immediate TEER reduction when gas flow adjustments are required
- Fig. 3-16 TEER values using RPE/choroid explant in RPE-Ringer solution over a period of 100 minutes
- Fig. 3-17 Schematic overview of the Ussing chamber system and associated equipment after the establishing phase.
- Fig. 3-18 Applications into the apical bathing solution of RPE/choroid explants using RPE-Ringer
- Fig. 3-19 Micrograph of RPE and retina individually after retina removal
- Fig. 3-20 TEER values of RPE tissues including retina with or without sclera and individual retina and sclera values
- Fig. 3-21 Comparison of the TEER values of the examined tissues of the eye
- Fig. 3-22 TEER values of the distal eye tissues with an apical sodium-fluorescein concentration of 10 mg/ml in RPE-Ringer
- Fig. 3-23 Fluorescein concentration of the basal bathing medium of RPE-containing tissues
- Fig. 3-24 Fluorescein concentration of the basal bathing medium of retina and sclera

6.2 List of Tables

Table 2-1	Summary of the bathing media components
Table 3-1	Overview of the TEER values of RPE/choroid explants at different time points using DMEM and RPE-Ringer media
Table 3-2:	Overview of the TEER values at different time points using RRS (Retina/RPE/Sclera) and RR (Retina/RPE)
Table 3-3:	Data of TEER values from Retina/RPE/Sclera (RRS) and Retina/RPE (RR) to facilitate data comparison with the values of the application experiments
Table 3-4:	Overview of TEER values during the evaluation of the RPE barrier using 10 mg/ml sodium fluorescein in the apical bathing solution
Table 3-5:	Basal fluorescein concentration of all measured tissues concentration in $\mu\text{g/ml}$

6.3 Publications

List of publications in peer-reviewed journals:

ROCK-Isoform Specific Polarization of Age-Related Macular Degeneration Associated Macrophages: Introducing MaDAMs. *Zandi S, Nakao S, Kim E, Arita R, Schueller O, Schering A, Sun D, Taher M, Melhorn M, Kim Y-B, Schmidt-Ullrich R, Hata Y, Sweetnam P, Ishibashi T, Hafezi-Moghadam A.* in revision

Blood Vessel Endothelial VEGFR-2 Delays Lymphangiogenesis: An Endogenous Trapping Mechanism Links Lymph- and Angiogenesis. *Nakao S, Zandi S, Hata Y, Kawahara S, Arita R, Schering A, Sun D, Melhorn MI, Ito Y, Lara-Castillo N, Ishibashi T, and Hafezi-Moghadam A.* (2011) *Blood* 117 (3):1081-90

An Animal Model of Spontaneous Metabolic Syndrome: Nile Grass Rat. *Noda K, Melhorn MI, Zandi S, Frimmel S, Tayyari F, Hisatomi T, Almulki L, Pronczuk A, Hayes KC and Hafezi-Moghadam A.* (2010) *FASEB J* 24, 2443-53

Lymphangiogenesis and Angiogenesis: Concurrence and/or Dependence? Studies in inbred mouse strains. *Nakao S, Maruyama K, Zandi S, Melhorn MI, Taher M, Noda K, Nusayr E, Doetschman T, and Hafezi-Moghadam A.* (2010) *FASEB J* 24, 504-13

List of poster presentations:

Atrial Natriuretic Peptide Prevents Disruption of RPE Barrier Function by VEGF. *Melhorn MI, Ablonczy Z, Lara-Castillo N, Nakao S, Sambamurti K, Crosson CE, Hafezi-Moghadam A.* (2009) Harvard Medical School, Department of Ophthalmology Annual Meeting, Boston, MA

Depletion of Lyve-1(+) Cells in the Conjunctiva by Clodronate-liposomes. *Melhorn MI, Nakao S, Hafezi-Moghadam A.* (2009) ARVO E-Abstract 5519, Fort Lauderdale, Florida ARVO

Strain-Dependence of Growth Factor-Induced Corneal Lymphangiogenesis. *Nakao S, Zandi S, Melhorn MI, Almulki L, Noda K, Hafezi-Moghadam A.* (2009) ARVO E-Abstract 4970, Fort Lauderdale, Florida ARVO

Non-Invasive Molecular Imaging of MAdCAM-1 in Endotoxin-Induced Uveitis. *Tayyari F, Nakao S, Zandi S, Melhorn MI, Almulki L, Hafezi-Moghadam A.* (2009) ARVO E-Abstract 4278, Fort Lauderdale, Florida ARVO

Impact of IL-1 β on Transepithelial Electrical Resistance on Rodent RPE/Choroid Explants. *Melhorn MI, Yu H-G, Schering AS, Sun D, Nakao S, Thomas KL, Miller JW, Gragoudas ES, Hafezi-Moghadam A.* (2008) Gordon Research Conference: Barriers of the Central Nervous System Tilton School, New Hampshire

Non-Invasive Molecular Imaging of Selectin Ligands During Endotoxin-Induced Uveitis. *Tayyari F, Nakao S, Zandi S, Almulki L, Noda K, Schering A, Frimmel S, Melhorn MI, Thomas KL, Hafezi-Moghadam A.* (2008) ARVO E-Abstract 2864, Fort Lauderdale, Florida ARVO

A Novel Method for Analysis of Leukocyte Infiltration Rate During Inflammatory Corneal Angiogenesis. *Zandi S, Nakao S, Schering A, Melhorn MI, Miyahara S, Noda K, Hisatomi T, Nakazawa T, Thomas KL, Hafezi-Moghadam A.* (2008) ARVO E-Abstract 1490, Fort Lauderdale, Florida ARVO

A Novel model for the study of the outer blood-retinal barrier. *Melhorn MI, Yu H-G, Schering AS, Amini R, Lara-Castillo N, Thomas KL, Miller JW, Gragoudas ES, Hafezi-Moghadam A.* (2007) ARVO E-Abstract, Fort Lauderdale, Florida ARVO

Acknowledgements:

Superior Sensitivity of Novel Molecular Imaging Probe: Simultaneously Targeting Two Types of Endothelial Injury Markers. *Sun D, Nakao S, Xie F, Zandi S, Schering A, Hafezi-Moghadam A.* (2010) *FASEB J* 24, 1532-40

ApoE Deficiency Leads to a Progressive Age-dependent Blood-brain Barrier Leakage. *Hafezi-Moghadam A, Thomas KL, Wagner DD.* (2007) *Am J Physiol Cell Physiol.* 292, C1256-1262

6.4 Curriculum Vitae

Persönliche Angaben:

Name Mark Ivan Melhorn
 Geburtsdatum 8. Dezember 1979
 Geburtsort Hannover
 Nationalität deutsch
 Familienstand verheiratet, zwei Töchter

Ausbildung und Werdegang:

seit 2010 Leibniz Universität Hannover. Institut für Biophysik (Professor Anacllet Ngezahayo).
 Externer Doktorand. Weiterführung der Dissertation.

2006-2010 Massachusetts Eye and Ear Infirmary und Harvard Medical School, Boston, MA.
 Angiogenesis Laboratory (Professor Ali Hafezi-Moghdam). Wissenschaftlicher
 Mitarbeiter. Anfertigung des experimentellen Teils der Dissertation.

2006-2010 Freie Universität Berlin. Institut für Molekularbiologie und Bioinformatik (Professor
 Burghardt Wittig). Doktorand.

2005- 2006 Universität Hannover. Aufnahme eines Zweitstudiums in Technischer Physik.

1999-2005 Universität Hannover. Studium der Biologie. Abschluss: Diplom. Diplomarbeit: Die
 Rolle des Transkriptionsfaktors Gfi1 in der B-Zellen Entwicklung (Professor
 Christoph Klein).

2002-2003 Northeastern University, Boston, MA. DAAD Stipendiat. Mitarbeiter im Labor von
 Professor Rebecca Rosengaus.

1998-1999 Diakonie Sozialstation Laatzen. Zivildienstleistender.

1991-1998 Schillerschule Hannover, Gymnasium. Abschluss: Abitur.

1989-1991 Orientierungsstufe Anderten, Hannover.

1985-1989 Kurt-Schumacher-Schule. Grundschule in Hannover-Anderten.

Preise und Stipendien:

2007-2008 DAAD Doktorandenstipendium

May 2007 Association for Research in Vision and Ophthalmology (ARVO). Foundation for Eye
 Research/Retina Research Foundation/Joseph M. and Eula C. Lawrence. *Travel
 Award*

- 2002-2003 Intercultural Leadership Award. Ausgestellt vom *International Student and Scholar Institute* der Northeastern University, Boston, MA
- 2002-2003 DAAD Stipendium zum Aufenthalt an der Northeastern University, Boston, MA

6.5 Acknowledgements

Meine Dankbarkeit gilt all denjenigen, Menschen, die mich während dieser Zeit auf vielfältiger Art und Weise unterstützt und dieses Werk ermöglicht haben.

Ganz besonders möchte ich mich bei dem Vertrauen von Herrn Professor Hafezi-Moghadam bedanken, der mir die Zeit in seinem Labor, die Konferenzaufenthalte und die Förderung die darüber hinausgeht, ermöglicht hat. Ein herzlicher Dank an Herrn Professor Ngezahayo, der meine Dissertation immer unterstützt hat und trotz der Entfernung immer für Fragen und Diskussionen erreichbar war. Ein weiterer Dank gilt den Herrn Professoren Körber und Wittig, die mir die ersten offiziellen Schritte dieser Dissertation in Berlin ermöglicht haben.

Special thanks to my colleague Shintaro Nakao, M.D., Ph.D., for his support in so many projects inside and outside the lab. You were a true pillar of accessibility, discussions and outlooks. Dr. Alexander Schering, for the many appearances during this educational journey since day one in Hannover. To Dr. Hyeong Gon Yu, for showing me the surgical skills necessary that enabled this work. Dr. Reza Amini, what would the first six months have been without your insightful engineering perspective and time as a friend? Drs. Souska Zandi and Dawei Sun, pillars of hard work and good vibrations in the lab. To all members of the Anigenesis Lab and of the Ophthalmology Department of Harvard Medical School that have crossed my way and that were open for discussions in any direction. Special thanks go to Dr. Chozhavendan Rathinam for encouraging me to go to Boston in 2005.

And of course to my family that has expanded during this time:

Meiner Mutter Carola und Großmutter Giesela, ihr habt mich mit schier unerschöpfbarer und unermüdlicher Liebe unterstützt die sich in so vielen Dingen geäußert hat. Mein bisheriger Weg sind eine Reflexion eurer Liebe und Güte an mir.

Meiner Tochter Johanna Anyika und Noomi Gisela: Eure Präsenz in meinem Leben hat jeden Tag zu einem besondern gemacht. Möget Ihr Euch der Nähe Gottes auf all Euren Wegen bewusst sein.

Maman Marthe et Papa Alidor Beya pour l'aide et support que vous m'avez donner - soyez bénis!

And last but not least, to my wife Carine Ntumba - thank you for your love and support during these years, for your patience and understanding in every moment that you shared with me, for becoming a mother and for knowing when to let go.